Solvatochromic Effects and Photophysical Properties of Metformin Hydrochloride and Its Interaction with Caffeine: Spectroscopic and Computational Approaches

Semahegn Asemare Bitew

A Ph.D. Dissertation Submitted to the Department of Applied Physics

College of Applied Natural Science

Presented in Partial fulfillment of the requirement for the degree of Doctor of Philosophy in Applied Physics (specialization in Laser Spectroscopy)

Adama Science and Technology University

March, 2026

Adama, Ethiopia

Solvatochromic Effects and Photophysical Properties of Metformin Hydrochloride and Its Interaction with Caffeine: Spectroscopic and Computational Approaches

Ph.D. Candidate: Semahegn Asemare Bitew

Supervisor: Abebe Belay Gemta (Professor)

Co-Supervisor: Alemu Kebede Hordofa (PhD)

A Ph.D. dissertation submitted to the Department of Applied Physics

College of Applied Natural Science

Presented in Partial Fulfillment of the requirements for the Degree of Doctor of Philosophy in Applied Physics (specialization in Laser Spectroscopy)

Office of Graduate Studies

Adama Science and Technology University

March, 2026

Adama, Ethiopia

Declaration

I hereby declare that this Ph.D. dissertation entitled "**Solvatochromic Effects and Photophysical Properties of Metformin Hydrochloride and Its Interaction with Caffeine: Spectroscopic and Computational Approaches**" is my original work. It has not been submitted for the award of any academic degree, diploma, or certificate at any other university or institution, and all sources used in this dissertation have been duly acknowledged through proper citation.

Name	Signature	Date

RECOMMENDATION

I/We, the supervisor(s) of this PhD dissertation, hereby certify that I/we have carefully read and revised the dissertation entitled "**Solvatochromic Effects and Photophysical Properties of Metformin Hydrochloride and Its Interaction with Caffeine: Spectroscopic and Computational Approaches**" prepared under my/our guidance by **Semahegn Asemare Bitew** submitted in partial fulfillment of the requirements for the Degree of Doctor of Philosophy in Applied Physics (**Specialization in Laser Spectroscopy**). I/We therefore recommend that the dissertation be submitted to the department for further review and defense.

_____	_____	_____
Major Supervisor	Signature	Date
_____	_____	_____
Co-Supervisor	Signature	Date

APPROVAL SHEET

I/We hereby certify that all recommendations of the Board of Examiners have been duly addressed and incorporated into the final version of the dissertation entitled " **Solvatochromic Effects and Photophysical Properties of Metformin Hydrochloride and Its Interaction with Caffeine: Spectroscopic and Computational Approaches**" by **Semahegn Asemare Bitew.**

Major Supervisor	Signature	Date
Co-Supervisor	Signature	Date

We, the undersigned, members of the Board of Examiners for the open defense of the dissertation submitted by **Semahegn Asemare Bitew** have read and evaluated the dissertation entitled" **Solvatochromic Effects and Photophysical Properties of Metformin Hydrochloride and Its Interaction with Caffeine: Spectroscopic and Computational Approaches**" and examined the candidate during open defense. This certifies that the dissertation is accepted in partial fulfillment of the requirements for the Degree of Doctor of Philosophy in Applied Physics (Specialization in Laser Spectroscopy).

Chairperson	Signature	Date
Internal Examiner 1	Signature	Date
Internal Examiner 2	Signature	Date
External Examiner 1	Signature	Date
External Examiner 2	Signature	Date

Finally, approval and acceptance of the dissertation is contingent upon submission of its final copy to the School of Graduate Studies (SGS) through the candidate's Department Graduate Council (DGC) and College Graduate Committee (SGC).

Department Head	Signature	Date
College Dean	Signature	Date
School of Graduate Studies, Dean	Signature	Date

ACKNOWLEDGEMENTS

The completion of this dissertation has required significant time and dedication, and I am deeply grateful to everyone who contributed to its realization. Above all, I give thanks to Almighty God for His infinite grace and guidance throughout this journey. I extend my profound gratitude to my advisor, Professor Abebe Belay, for his unwavering support, meticulous guidance, consistent follow-up, and generous commitment of time in addressing my questions and ensuring effective supervision. I am equally thankful to my co-advisor, Alemu Kebede (PhD), for his valuable insights and kind support for the completion of this dissertation. I thank Umer Sherefedin (PhD), my classmate, who helped me in commenting, starting from the beginning up to the final work. And also, I thank all ASTU Physics Department Ph.D. students, who contributed their own for me.

I sincerely appreciate the encouragement and assistance provided by the staff members of the Department of Physics at Adama Science and Technology University and Mekdela Amba University, which greatly contributed to my academic and intellectual growth. I also acknowledge with gratitude the financial support received from Adama Science and Technology University and the Ministry of Innovation and Technology.

Finally, I express my deepest appreciation to my families, my mother Birkie Yismaw, my brothers and sister (Birhane, Aschale, Minalu, Bimrew, and Yeshinesh), my wife (Workinesh Abie), and my son, Yared Semahegn, for their immense moral and material support, patience, and encouragement, without which this work would not have been possible. I am forever indebted to them.

Table of Content Page

List of Figures ix

List of Tables xii

List of Acronyms and Abbreviations xiii

1. Introduction 1

1.1. Background 1

1.2. Statement of the Problem 2

1.3. Objectives of the Study 4

1.3.1. General objective 4

1.3.2. Specific Objectives 4

1.4. Significance of the Study 5

1.5. Scope of the Study 6

1.6. Organization of the Document 7

2. Literature Review 8

2.1. Molecular Structure of MF-HCl 8

2.1.1. Pharmacokinetics of MF-HCl and Drug Interactions 9

2.1.2. Protein-Binding and Protein-Target Interactions of MF-HCl 9

2.2. Mechanisms of Caffeine-Drug Interactions and Advanced Delivery Systems 10

2.3. Solvatochromism and Solvent-Drug Interactions 11

2.3.1. General Solvent-Solute Interactions 13

2.3.2. Specific Solvent-solute Interactions 13

2.4. Solvent Polarity Effects on Spectra and Molecular Properties 14

2.4.1. Photophysical and Luminescence Properties of Antidiabetic Drugs 17

2.5. Fluorescence Quenching of Chromophores 23

2.5.1. Static quenching 24

2.5.2. Dynamic quenching 26
2.5.3. Thermodynamic Parameters and Characteristics of Binding Forces 28
2.6. Fluorescence (Forster) resonant energy transfer (FRET) 30
2.7. Computational study of anti-diabetic drugs 32
2.7.1. Density Functional Theory (DFT) 33
2.7.1.1. Multi-Electron System 34
2.7.1.2. Hohenberg-Kohn Variation Theorem 35
2.7.1.3. Density Functional Theory and the Kohn-Sham Equations 37
2.7.1.4. Time-Dependent Density-Functional Theory (TDDFT) 40
2.7.2. Overview of Computer-Aided Drug Design (CADD) 41
2.7.2.1. Structure-Based Drug Design (SBDD) 41
2.7.2.2. Ligand-Based Drug Design (LBDD) 42
2.7.2.3. Molecular Docking 43
2.7.2.4. Classification of Molecular Docking Methods 43
3. Materials and Methods 45
3.1. Solvents and Chemicals 45
3.2. Apparatus, Instruments, and Software 45
3.3. Methods 46
3.3.1. Methods of Studying the Solvatochromic Effects of MF-HCl Drug 46
3.3.2. Methods for Studying the Photophysical Properties of MF-HCl in Solvents 47
3.3.3. Methods of Studying Fluorescence Quenching of MF-HCl with CAF 47
3.3.4. Quantum Chemical Calculations 48
4. Results and Discussions 50
4.1. Solvatochromic Effects 50

4.1.1. Effect of Solvent Polarity on Fluorescence Emission and UV-Vis Absorption Spectra of MF-HCl 50
4.1.2. Determination of Ground and Excited State Dipole Moments of MF-HCl via Solvatochromic Methods 52
4.2. Photophysical Properties of MF-HCl 57
4.2.1. Solvent Polarity Effects 57
4.2.2. Influence of Concentration on the Photophysical Properties of MF-HCl 58
4.2.3. Optical Transition Probability of MF-HCl 60
4.3. Fluorescence Quenching of MF-HCl by CAF 61
4.3.1. Thermodynamic Characteristics and Binding Interactions Between MF-HCl and CAF 63
4.3.2. Determination of Binding Constant and Number of Binding Sites 64
4.3.3. Forester Resonance Energy Transfer Study of MF-HCl-CAF Interactions 66
4.3.4. UV-Vis Absorption Spectroscopic Investigation of MF-HCl-CAF Interactions . 68
4.3.5. Fourier Transforms Infrared Spectroscopy of MF-HCl–CAF Interactions 69
4.3.6. Zeta Potential of MF-HCl–CAF Interactions 70
4.3.7. Dynamic Light Scattering (DLS) of MF-HCl–CAF Interactions 71
4.4. Computational Approaches 73
4.4.1. DFT Analysis of MF-HCl Drug 73
4.4.2. Molecular Docking Analysis of MF-HCl-CAF Interactions 77
5. Conclusion and Recommendations 82
5.1. Conclusion 82
5.2. Future Research and Recommendations 83
References 86

List of Figures

Figure 1: Molecular structure of metformin hydrochloride 8
Figure 2: molecular structure of caffeine 10
Figure 3:The Jablonski diagram of molecular absorbance and fluorescence 19
Figure 4: electronic energy levels of a donor-acceptor pair, used to depict processes like FRET 32
Figure 5: Dependence of energy transfer efficiency (E) as a function of donor-acceptor distance. 32
Figure 6: Categories of computer-aided drug design (CADD): structure-based drug design (SBDD) and ligand-based drug design (LBDD). 41
Figure 7: workflow of structure-based drug design (SBDD) (Iwaloye et al., 2023) 42
Figure 8: Ligand-based drug design (LBDD) 42
Figure 9: molecular docking flow chart (Ferreira et al., 2015) 43
Figure 10: Step-by-step flowchart outlining the docking pipeline. 44
Figure 11: UV/Vis absorption (a), Fluorescence emission (b) spectra of MF-HCl in different solvents 51
Figure 12: Plot of Stokes shift versus solvent polarity parameter for MF-HCl using the Lippert–Mataga model. The solvents used are: (1) 2-Propanol, (2) 1-Propanol, (3) Ethanol, (4) Methanol, (5) Acetonitrile, (6) Glycerol, (7) Water. 54
Figure 13: Plot of Stokes shift versus solvent polarity parameter for MF-HCl using Bakhshiev's model. The solvents used are: (1) 2-Propanol, (2) 1-Propanol, (3) Ethanol, (4) Methanol, (5) Acetonitrile, (6) Glycerol, (7) Water. 55
Figure 14: Plot of Stokes shift versus solvent polarity parameter for MF-HCl using the Kawski-Chamma-Viallet's model. The solvents used are: (1) 2-Propanol, (2) 1-Propanol, (3) Ethanol, (4) Methanol, (5) Acetonitrile, (6) Glycerol, (7) Water. 55
Figure 15: Plot of Stokes shift versus solvent polarity parameter for MF-HCl using the Reichardt's model. The solvents used are: (1) 2-Propanol, (2) 1-Propanol, (3) Ethanol, (4) Methanol, (5) Glycerol, (6) Water. 56
Figure 16: Quantum yield (Φ_f) and fluorescence lifetime (τ_f) of MF-HCl as a function of concentration. 59

Figure 17: Emission spectra versus wavelength variation of metformin hydrochloride in a) (3 × 10-6, b) 6 × 10-6, c) 9 × 10-6, d) 1.2 × 10-5, e) 1.5 × 10-5, f) 1.8 × 10-5, g) 2.1 × 10-5, h) 2.7 × 10-5, and i) 3.3 × 10-5) M concentration..... 60
Figure 18: Fluorescence quenching spectra of MF-HCl in the presence of CAF concentration (a) 0, b) 1 × 10-3, c) 2 × 10-3, d) 3 × 10-3, e) 4 × 10-3, f) 5 × 10-3, g) 6 × 10-3, h) 7 × 10-3, and i) 1 × 10-3)M 62
Figure 19: Stern-Volmer plot of MF-HCl quenched by caffeine via different concentrations at temperatures of 298 K (black), 310 K (red), and 318 K (blue). 63
Figure 20: Graph of logFo-Ff VslogQ-n[D]Fo-FFo when caffeine (1 × 10-3 to 7 × 10-3) M binding to MF-HCl 2 × 10-4M at 298 K (black), 310 K (red), and 318 K (blue) 66
Figure 21: Overlap spectra of UV absorption spectra of CAF (1) and MF-HCl fluorescence emission spectra (2): C of metformin hydrochloride = 1×10^{-5} mol l^{-1}, C of caffeine = 1×10^{-5} mol l^{-1} 68
Figure 22: UV-Vis absorption spectra of metformin hydrochloride in different concentrations of caffeine (1×10^{-3}-7×10^{-3}) M)..... 69
Figure 23: FTIR spectra of 1) MF- HCl+CAF, 2) CAF, and 3) MF- HCl 70
Figure 24: Zeta potential distribution of MF-HCl 71
Figure 25: Zeta potential distribution of MF-HCl-CAF 71
Figure 26: DLS Size distribution of MF-HCl..... 72
Figure 27: DLS Size distribution of MF-HCl-CAF..... 72
Figure 28: Optimized molecular structure of MF-HCl showing the HOMO-LUMO electron distribution, dipole moment vector (indicated by arrow), total density matrix with superimposed electrostatic potential map (TDM-ESP), and corresponding UV/Vis absorption..... 74
Figure 29: Optimized molecular structures and HOMO–LUMO energy gaps of metformin hydrochloride calculated using different DFT levels: A) DFT-B3LYP-3-21+G*, B) DFT-B3LYP-6-31+G (d, p), and C) DFT-B3LYP-6-311+G (d, p). 76
Figure 30: Total electron density map superimposed with the electrostatic potential surface (TDM-ESP) of MF-HCl. 76
Figure 31: Three-dimensional visualization illustrating the binding conformations and interactions of metformin hydrochloride within the active site pocket of AMP-activated protein kinase (AMPK) (PDB ID: 1Z0N). 79

Figure 32: Two-dimensional diagram depicting the binding interactions and poses of metformin hydrochloride within the active site pocket of AMP-activated protein kinase (AMPK) (PDB ID: 1Z0N). 79
Figure 33: Three-dimensional visualization showing the binding conformations and interactions of metformin hydrochloride together with caffeine (dual-ligand docking) within the active site pocket of AMP-activated protein kinase (AMPK) (PDB ID: 1Z0N). 80

List of Tables

Table 1: Calculated values of solvent polarity functions in different solvents 53
Table 2: Peaks of the absorption and emission spectra of metformin hydrochloride in solvents with different polarity 53
Table 3: Statistical correlation of solvent spectral shifts of metformin hydrochloride 56
Table 4: Ground state and excited state dipole moments of metformin hydrochloride 57
Table 5: Photophysical properties of MF-HCl in different solvents 58
Table 6: Optical transition probability of metformin hydrochloride 61
Table 7:Stern-Volmer constant (K_{sv}), and correlation coefficient of MF-HCl with different temperatures 63
Table 9: Thermodynamic parameters (entropy change ΔS, enthalpy change ΔH, free energy change ΔG) at different temperatures 64
Table 11: Theoretical ground state dipole moment (μ_g) in different solvents using B3LYP/6-31+G (d, p) 75
Table 12: Ground state and excited state dipole moments, HOMO-LUMO energy band gap, UV/Vis absorption wavelengths, oscillator strengths employing different basis sets of gas state 77
Table 13: Molecular docking affinities and distance from the best mode of MF-HCl against AMP-activated protein kinase (AMPK) (PDB ID: 1z0n) 80
Table 14: Molecular docking affinities and distance from the best mode of MF-HCl plus CAF (two ligands) against AMP-activated protein kinase (AMPK) (PDB ID: 1z0n) 81

List of Acronyms and Abbreviations

CAF	Caffeine
FRET	Fluorescence Resonance Energy Transfer
FTIR	Fourier Transform Infrared
HOMO	Highest Occupied Molecular Orbital
ICT	Intramolecular Charge Transfer
LUMO	Lowest Unoccupied Molecular Orbital
PLS	Photoluminescence Spectroscopy
QY	Quantum yield
AMPK	AMP-Activated Protein Kinase
DFT	Density Functional Theory
DLS	Dynamic Light Scattering
MF-HCl	Metformin Hydrochloride
TDDFT	Time-Dependent Density Functional Theory
CADD	Computer-Aided Drug Design
SBDD	Structure-Based Drug Design
LBDD	Ligand-based drug design

Abstract

This dissertation provides an investigation of the solvatochromic effect and photophysical properties of metformin hydrochloride (MF-HCl) as well as its interaction with caffeine (CAF), utilizing the integrated spectroscopic and computational approaches. Absorption and fluorescence spectra of MF-HCl were analyzed in solvents of differing polarity, revealing the influence of solvent environment on spectral behavior. For the Solvatochromic effect, Lippert-Mataga, Bakhshiev, Kawski-Chamma-Viallet, and Reichardt models were employed to estimate the ground and excited state dipole moments, with the excited state dipole moment higher than the ground state, suggesting that enhancement might be by intramolecular charge transfer in the excited state. These results were also supported by Density Functional Theory (DFT) using various basis sets. Photophysical properties such as fluorescence quantum yield, lifetime, radiative and non-radiative decay transition dipole moment, and integrated absorption coefficient were found to vary with solvent polarity and MF-HCl concentration. Fluorescence quenching with CAF indicated a predominant static quenching mechanism, forming a ground-state complex. The binding constants, quenching rates, and thermodynamic parameters results obtained indicate the spontaneous, enthalpy-driven interaction, likely mediated by hydrogen bonding and van der Waals forces. The spectral overlap between MF-HCl emission and CAF absorption yields an energy transfer efficiency of 0.72, indicative of Förster resonance energy transfer (FRET). This is substantiated by a Förster radius (R_0) of 1.81 nm and a binding distance (r) of 1.55 nm, consistent with efficient FRET. Molecular docking simulations revealed a notable enhancement in the binding profile of MF-HCl to the AMPK receptor in the presence of caffeine. The binding affinity improved from -5.0 kcal/mol (MF-HCl alone) to -5.9 kcal/mol (MF-HCl + CAF), suggesting a synergistic stabilization of the protein-ligand complex. These computational results complement spectroscopic quenching data, providing molecular-level evidence that caffeine may modulate the pharmacodynamic interaction of metformin with its primary metabolic target. Overall, this work elucidates the solvent-dependent photo physics of MF-HCl and its molecular interaction with CAF, providing valuable implications for understanding drug behavior, potential drug-drug interactions, and pharmacokinetics.

Keywords: Solvatochromic effect; photophysical properties; fluorescence quenching; DFT; molecular docking

1. Introduction

1.1. Background

Metformin hydrochloride (MF-HCl), chemically known as N, N-dimethyl biguanide hydrochloride, is the most widely prescribed oral antidiabetic medication for the management of type 2 diabetes mellitus. It is utilized by over 200 million individuals globally and has been a clinical mainstay since the late 1950s due to its efficacy in lowering blood glucose levels primarily through activation of AMP-activated protein kinase (AMPK) and suppression of hepatic gluconeogenesis (Bailey, 2024; Graham et al., 2011; Catala, 2009).

Solvatochromism refers to the alteration in the peak positions of absorption or emission spectra influenced by the polarity of the surrounding solvent, offering valuable information on modifications in molecular dipole moments during electronic transitions and the specifics of interactions between the solute and solvent (Ansari et al., 2022; Attia et al., 2021). MF-HCl features of multiple sites capable of gaining or losing protons (with PKa values around 12.4 for the biguanide component and 2.8 for its protonated variant) along with numerous groups that can participate in hydrogen bonding as donors or acceptors, positioning it as a prime subject for notable Solvatochromic responses (Somogyi & Muirhead, 1987).

Investigating the photophysical properties of biologically active compounds is of great interest because these properties are crucial for understanding the electronic properties and geometrical structures of drug molecules (Oyola et al., 2005). Since a molecule's biological activity depends on its structure, studying photophysical properties can also help elucidate the biochemical interactions by which a drug exerts its pharmacological effect in various microenvironments (Christina Pires Gonçalves, 2021). The photophysical properties of several drugs have been previously reported, including quinine (Suman et al; 2016), ciprofloxacin and norfloxine (Woldegiorges et al., 2022)], folic acid (Sadigh et al., 2016), naproxen (Miotke & Józefowicz, 2017), and sinapic acid and ferulic (Sherefedin et al., 2025).

Understanding drug-caffeine interactions at the molecular level provides valuable insights for drug design and development. Caffeine can enhance drug effectiveness, such as reducing the adverse effects of antidepressants. However, these interactions can also cause idiosyncratic reactions; for example, a study on rats showed that combining caffeine and ecstasy increased heart rate,

hyperthermia, and mortality (Camarasa et al., 2006). Caffeine may also interfere with the binding of other endogenous or exogenous ligands by competing for binding sites or inducing conformational changes (Chirasani et al., 2021). Given the potential for these interactions to influence drug pharmacodynamics and pharmacokinetic properties by forming complexes (Kokiashvili et al., 2012; Mrkalić et al., 2021), studying drug-caffeine interactions is critical. Previous research has explored the interaction of LVF and NRF with divalent toxic metal ions (Mohd et al., 2010), humic acid and (Ferrie et al., 2017).

Computational approaches, particularly Density Functional Theory (DFT) and molecular docking, have transformed the fields of molecular modeling and pharmaceutical development by delivering rapid, cost-effective predictions of electronic structures, molecular geometries, interaction energies, and ligand-target affinities. These techniques enable researchers to explore vast chemical spaces, prioritize promising candidates, and gain mechanistic insights, thereby streamlining drug discovery pipelines and formulation strategies while cutting down on experimental trial-and-error. Molecular docking and DFT are often combined in practice. Docking-derived poses guide targeted quantum refinements of important interactions, while DFT-refined ligand geometries and electronic descriptors can improve docking accuracy. This synergy helps advance from early hit discovery to lead refining and formulation engineering by boosting confidence in binding strength and specificity predictions (Nivatya et al., 2025; Wu et al., 2023).

1.2. Statement of the Problem

Although a substantial body of work exists examining the pharmacological effectiveness, clinical applications, and analytical determination of metformin hydrochloride encompassing its role in managing type 2 diabetes, interactions mediated by transporters, and methods for measuring it in dosage forms and biological samples relatively little focus has been directed toward its intrinsic photophysical characteristics and solvatochromic responses in different solvent media, or toward its direct molecular associations with everyday dietary substances such as caffeine.

Investigations into solvatochromism yield valuable details regarding conformational modifications in solutes, the organization of surrounding solvent molecules, variations in dipole moments from the ground to excited electronic states, and corresponding energies involved in electronic transitions (Sherefedin et al., 2023; Woldegiorges et al., 2021). Analysis of photophysical attributes supplies broad knowledge about a compound's electronic features, possible risks of light-

induced toxicity, and how surroundings affect its long-term stability (Facciolo et al., 2004). Moreover, exploring interactions between pharmaceuticals and caffeine holds importance for clarifying aspects of drug action, therapeutic outcomes, distribution patterns, and metabolic processing issues especially pertinent in everyday medical practice, where individuals with diabetes often pair metformin treatment with intake of caffeine-rich drinks like coffee (Popovi et al., 2018).

previous research concerning metformin hydrochloride has concentrated mainly on its therapeutic uses, absorption/excretion profiles (characterized by substantial kidney elimination and minimal biotransformation), precise measurement techniques in pharmaceutical preparations and bodily fluids (Polyakova et al., 2022), basic physical-chemical traits (such as aqueous solubility and stability), and broad pharmacological interactions primarily involving organic cation transporters (Bjerregaard et al., 2015; Mohamed et al., 2017). Certain spectroscopic approaches have assessed its association with serum proteins, for instance bovine serum albumin, employing fluorescence quenching to evaluate static binding processes and affinity values (Tanwir et al., 2012). Additional efforts have probed associations within blended solvent environments or alongside auxiliary solutes, aiming to understand intermolecular forces in liquid phases (Kumar et al., 2024).

Nevertheless, to the best of current knowledge, no thorough examinations had previously been published specifically for metformin hydrochloride concerning solvatochromic effects, in-depth photophysical properties. No detailed spectroscopic and theoretical investigations had targeted its precise interplay with caffeine encompassing quenching processes in fluorescence, efficiency of Förster resonance energy transfer, structural alterations evidenced through complementary methods (FTIR shifts in vibrational modes, dynamic light scattering for hydrodynamic diameter, zeta potential for interfacial charge), or computational docking analyses (of binary complexes or multi-ligand binding at sites such as AMPK).

This lack of comprehensive exploration in detailed research highlights a key limitation, because changes in solvent polarity and temperature can substantially alter the drug's dissolution characteristics, its ability to cross biological membranes, its resilience to light-induced breakdown in formulated products, and the pathways through which it may degrade when exposed to illumination during manufacturing, packaging, or long-term storage. Considering how commonly people with diabetes consume caffeine (for instance, through regular intake of coffee or tea),

acquiring precise molecular-level knowledge about interaction strengths, mechanisms of energy-transfer-based quenching, the roles played by hydrogen bonding and van der Waals interactions, and any consequent conformational or structural shifts could help identify subtle modifications in the drug's absorption profile, overall therapeutic impact, or possible additive/synergistic versus opposing effects insights that go beyond the scope of standard pharmacokinetic assessments centered on transporter systems.

Accordingly, the present work seeks to explore the solvatochromic responses, ground- and excited-state dipole moments (via established empirical models alongside density functional theory calculations), and key optical transition features (such as oscillator strengths and integrated absorption intensities) exhibited by metformin hydrochloride across diverse solvent systems. It further evaluates photophysical traits (fluorescence lifetimes, quantum efficiencies, and decay rate constants) as modulated by solvent character and concentration levels. Temperature-variable fluorescence quenching experiments yield thermodynamic descriptors (association constants, quenching efficiencies), supplemented by FTIR analysis to reveal structural modifications during caffeine complexation. Density functional theory computations optimize molecular geometries, assess structural/vibrational/thermodynamic/electronic descriptors (including frontier orbital energies HOMO and LUMO). Molecular docking simulations probe binding interactions at pertinent biological targets (AMPK), encompassing scenarios with single or paired ligands, to clarify possible ramifications for therapeutic performance and safety.

1.3. Objectives of the Study

1.3.1. General objective

The general objective of this research is to investigate the Solvatochromic and photophysical properties of metformin hydrochloride drug and its interaction with caffeine using spectroscopic and computational methods.

1.3.2. Specific Objectives

The specific objectives of this research work were:

- To estimate the ground state and excited state dipole moment of metformin hydrochloride drug in various solvents using different models and DFT

- To determine the photophysical properties (lifetime, fluorescence quantum yield, radiative decay, non-radiative decay, transition dipole moments, absorption cross section, and oscillator strength) of metformin hydrochloride drug measured in various solvents
- To analyze the interaction mechanism of the metformin hydrochloride drug with caffeine using spectroscopic and molecular docking
- To calculate the efficiency rate of energy transfer between the metformin hydrochloride drug and caffeine using the resonance energy transfer mechanism.

1.4. Significance of the Study

This research is significant in that it provides a detailed molecular-level investigation of the solvatochromic, photophysical, and interaction characteristics of MF-HCl using combined experimental spectroscopy and computational techniques. The evaluation of ground and excited-state dipole moments of MF-HCl in solvents of differing polarity offers important insight into how the surrounding medium alters electronic charge distribution and excited-state stabilization. This information is fundamental for interpreting solvent-dependent spectral behavior and for understanding how molecular polarity responds to environmental changes. By determining key photophysical parameters such as fluorescence lifetime, quantum yield, radiative and non-radiative rate constants, transition dipole moments, absorption cross sections, and oscillator strengths, the study establishes a comprehensive description of the excited-state processes of MF-HCl. These findings clarify the pathways of energy relaxation and the role of solvent effects in modulating photophysical behavior.

The spectroscopic and computational analysis of the interaction between MF-HCl and CAF elucidates the nature of complex formation, quenching behavior, and intermolecular forces operating in solution. This contributes to a clearer understanding of how molecular species influence each other's electronic and spectroscopic properties when present together. Furthermore, the estimation of resonance energy transfer efficiency between MF-HCl and CAF quantitatively assesses the feasibility of non-radiative energy transfer and its dependence on spectral overlap and intermolecular separation. This enhances the interpretation of fluorescence quenching mechanisms observed experimentally. Finally, molecular docking simulations provide structural insight into the preferred binding orientations, interaction sites, and relative binding energies of the MF-HCl–CAF complex. When combined with spectroscopic evidence, these simulations strengthen the proposed interaction model and improve the reliability of the conclusions.

Overall, this study delivers an integrated experimental and theoretical framework for analyzing solvent effects, excited-state behavior, and intermolecular interactions of pharmaceutical molecules. The results offer a valuable reference for future spectroscopic and computational investigations involving metformin hydrochloride, caffeine, and related molecular systems.

1.5. Scope of the Study

This dissertation explores how different solvent environments affect the photophysical and solvatochromic properties of MF-HCl, a widely used drug for treating T2DM. The investigation covers the effects of solvent polarity, protic/aprotic nature, and drug concentration on its absorption and fluorescence spectra. This work quantified the ground and excited state dipole moments of MF-HCl using well-established solvatochromic models (Lippert-Mataga, Bakhshiev, Kawski-Chamma-Viallet, and Reichardt), while also examining how the molecule's electronic polarity changes when it gets excited. We also measured important photophysical properties like fluorescence quantum yield, lifetime, and concentration-dependent emission behavior across a range of solvents and concentrations to reveal self-quenching and solvent-induced effects. To support and validate the experimental results, computational studies using Density Functional Theory (DFT) were conducted to determine the optimized molecular geometry, frontier orbital energies (HOMO-LUMO gap), transition dipole moments, and oscillator strengths in various solvent models. The study further investigated the molecular interaction between MF-HCl and CAF through fluorescence quenching experiments, including temperature-dependent measurements to identify the quenching mechanism (static or dynamic), binding stoichiometry, association constants, and thermodynamic parameters ($\Delta H°$, $\Delta S°$, $\Delta G°$). These findings are complemented by molecular docking simulations targeting the AMP-activated protein kinase (AMPK) receptor to evaluate binding modes, affinities, and potential competitive effects in the presence of caffeine. Overall, the scope is limited to spectroscopic characterization, thermodynamic analysis, and computational modeling of MF-HCl's photo physics and its specific interaction with caffeine, without extending it to in vivo/in vitro pharmacokinetic studies or broader clinical trials.

1.6. Organization of the Document

This dissertation is structured into five chapters, beginning with Chapter 1: Introduction, which establishes the research context and objectives. Chapter 2: Literature Review, which comprehensively surveys foundational and contemporary knowledge, and pharmacological examination of metformin hydrochloride. This chapter further delves into cellular metabolism pathways, caffeine-drug interaction mechanisms, stimuli-responsive materials, and the luminescence phenomena relevant to antidiabetic drugs and bioactive compound interactions, covering fundamentals, specific drug properties, and inter-chromophore processes like fluorescence quenching and FRET. It also introduces core photophysical concepts such as solvatochromic, solvent-drug interactions, solvent polarity effects on fluorescence, and the analysis of thermodynamic parameters, binding forces, constants, and sites. The theoretical framework is concluded with an overview of computational methodologies, including Density Functional Theory (DFT) and Computer-Aided Drug Design (CADD). Chapter 3: Materials and Methods detail the experimental and computational protocols, specifying the solvents, chemicals, apparatus, software, and methodologies employed for studying photophysical properties, solvatochromic effects, drug-caffeine interactions, and quantum chemical calculations. Chapter 4: Results and Discussion present and interprets the findings, analyzing how solvent polarity affects the UV-Vis absorption and fluorescence spectra of MF-HCl, estimates dipole moments in ground and excited states using solvatochromic approaches, and shares insights from DFT calculations. The chapter also looks at how concentration influences photophysical behavior and transition probabilities, and dives into CAF's quenching of MF-HCl's fluorescence, covering binding constants, sites, and thermodynamic parameters. These discussions are supported by data from techniques like UV-Vis, fluorescence spectroscopy, FTIR, zeta potential, dynamic light scattering (DLS), FRET studies, DFT, and molecular docking. Finally, Chapter 5: Conclusion, Future Research, and Recommendations is presented.

2. Literature Review

This chapter presents a comprehensive literature review on MF-HCl within the field of antidiabetic research. It starts with an analysis of diabetes mellitus and diabesity: Pharmacology, management challenges, and the central role of metformin hydrochloride (Section 2.1), followed by a discussion on metformin hydrochloride: pharmacological profile, mechanism of action, cellular metabolism pathways, and key pharmacokinetic interactions (Section 2.2). The review then covers Cellular metabolism: key concepts and pathways in antidiabetic drug mechanisms (Section 2.3), and mechanisms of caffeine-drug interactions and advanced delivery systems (Section 2.4). Additional sections address Fluorescence quenching and interactions among chromophores (Section 2.5), fluorescence (Forster) resonant energy transfer (FRET) (Section 2.6), solvatochromism and solvent-drug interactions in antidiabetic drugs (Section 2.7), computational study of anti-diabetic drugs (Section 2.8).

2.1. Molecular Structure of MF-HCl

Metformin hydrochloride (Fig.1), also known as 1, 1-dimethylbiguanide hydrochloride, is established as the preferred first-line agent for type 2 diabetes mellitus (T2DM) worldwide. It is typically considered weight-neutral, though clinical evidence frequently documents modest weight reduction (0.6–2.9 kg), particularly alongside dietary and exercise interventions, alongside consistent HbA1c reductions of approximately 1% (Domecq et al., 2015).

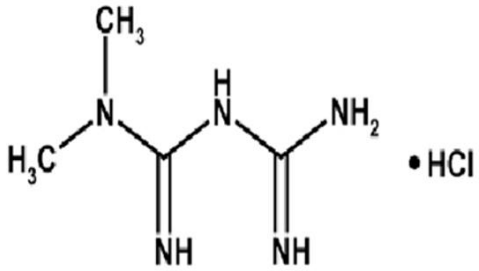

Figure 1: Molecular structure of metformin hydrochloride

MF-HCl's utility in diabesity derives from hepatic glucose production suppression, enhanced muscular insulin sensitivity, and appetite diminution in many patients. Despite intensive study, its precise mechanisms remain partially obscure, currently implicating mitochondrial respiratory chain inhibition, reduced cyclic AMP (lowering protein kinase A activity), mitochondrial

glycerophosphate dehydrogenase blockade, AMP-activated protein kinase (AMPK) activation, and possible gut microbiome alterations (Madiraju et al., 2014; Rena et al., 2013).

2.1.1. Pharmacokinetics of MF-HCl and Drug Interactions

Metformin hydrochloride (MF-HCl), a well-established and safe therapeutic agent for diabetes management, is under investigation for potential applications in supportive cancer therapy, age-related diseases, inflammatory conditions, and COVID-19 (Dutta et al., 2023; Foretz et al., 2023). Metformin hydrochloride has been demonstrated to target various pathways, with the AMPK-signaling pathway being the most extensively researched. Moreover, metformin hydrochloride can exert its effects on cells even in the absence of AMPK, through influencing redox states, mitochondria, and other signaling pathways such as FGF21, PP2A, and mTOR. Furthermore, metformin hydrochloride also indirectly impacts human homeostasis by modulating the gut microbiome (Du et al., 2022).

Most clinically relevant interactions occur via inhibition or competition at renal and hepatic cation transporters, leading to increased MF-HCl plasma concentrations and elevated risk of lactic acidosis, especially in patients with impaired kidney function (Galetin et al., 2024). A thorough understanding of these pharmacokinetic interactions is essential for safe dosing in polypharmacy, which is common in patient populations such as those with cancer or HIV (Kalliokoski & Niemi, 2009).

2.1.2. Protein-Binding and Protein-Target Interactions of MF-HCl

Metformin exhibits minimal plasma protein binding and does not displace highly protein-bound medications (Graham et al., 2011). In vitro analyses suggest that metformin binds non-covalently to albumin ($K \approx 10^4\ M^{-1}$) via hydrophobic, hydrogen bonding, and electrostatic interactions, inducing minor conformational changes (Taylor et al., 2014). Metformin selectively binds to the C-terminal tail of HMGB1, inhibiting HMGB1's cytokine activity, which reduces p38 MAPK phosphorylation and decreases TNF-α release in macrophages ($p < 0.01$). Furthermore, metformin attenuates acetaminophen-induced liver injury in mice, independent of AMPK activation (Horiuchi et al., 2017). The pharmacokinetics of metformin are influenced by transporter proteins (Graham et al., 2011), and interactions with OCT1/2/3 and MATE1/2-K may result in drug-drug interactions (DDIs).

2.2. Mechanisms of Caffeine-Drug Interactions and Advanced Delivery Systems

Caffeine, a commonly consumed methylxanthine, is metabolized by CYP1A2 and used in cocktail probes to assess drug interactions(Kwon et al., 2020; Mumin et al., 2014). It ranks as one of the most common alkaloids present in everyday foods and beverages. Naturally occurring in the leaves, seeds, or fruits of over 60 plant species, its primary dietary sources include coffee beans, cocoa beans, cola nuts, and tea leaves (Belay & Gholap, 2009). With the chemical formula $C_8H_{10}N_4O_2$, pure caffeine appears as a white, odorless powder. It has a molecular weight of 194.19 g/mol, melts at 236 °C, sublimes at around 178 °C, and exhibits a pH between 6 and 9 in solution.

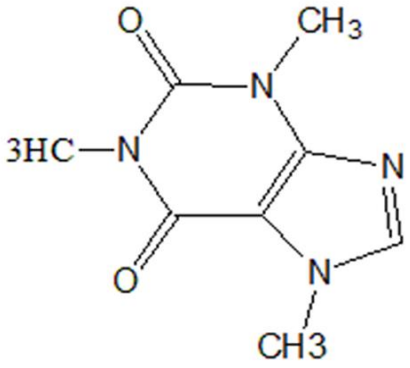

Figure 2: molecular structure of caffeine

Caffeine's interactions occur through pharmacokinetic and pharmacodynamic mechanisms. Pharmacokinetically, competition for CYP1A2 metabolism alters drug clearance, as seen with psychoactive drugs. Pharmacodynamically, caffeine's adenosine receptor antagonism modulates drug effects, enhancing stimulants or counteracting sedatives. Since solvent effects also influence interactions, caffeine's solubility in aqueous biological fluids enhances its rapid absorption, amplifying interaction potential. Additionally, caffeine's weak acid-base properties affect drug dissolution in the gastrointestinal tract, impacting bioavailability (Marcinek et al., 2024, Truong et al., 2025). By antagonizing adenosine receptors (A1 and A2A), caffeine promotes wakefulness, enhances metabolism, and influences cardiovascular and neuroendocrine functions (Cappelletti et al., 2014; Belayneh & Molla, 2020). Its widespread use raises concerns about interactions with prescription drugs, including antidiabetic, psychoactive, cardiovascular, and analgesic medications, which can alter therapeutic efficacy or safety (Reddy et al., 2024, May & Schindler, 2016).

Caffeine reaches peak blood levels within 30–120 minutes, with an elimination half-life of 3–7 hours. Primarily metabolized in the liver by CYP enzymes, especially CYP1A2, it produces paraxanthine, theobromine, and theophylline (Cappelletti et al., 2014; Reddy et al., 2024). Factors like genetics and drugs influence its metabolism. Its solubility in water and ethanol affects bioavailability (Thorn et al., 2012). Caffeine's effects on glucose metabolism can interfere with antidiabetic drugs like metformin and sulfonylureas by reducing insulin sensitivity and potentially decreasing metformin's efficacy. Studies suggest moderate caffeine intake can elevate blood glucose levels, necessitating dose adjustments in type 2 diabetes patients. Caffeine's sympathetic activation may exacerbate hypoglycemia risks in patients on sulfonylureas. Dietary caffeine monitoring is needed in diabetic management (Belayneh & Molla, 2020; Shi et al., 2016). Caffeine interacts with psychoactive drugs primarily via CYP1A2. Fluvoxamine inhibits CYP1A2, increasing caffeine plasma levels, which can lead to toxicity. Conversely, caffeine may enhance the effects of stimulants like methylphenidate through synergistic adenosine receptor antagonism. These interactions require careful monitoring in psychiatric patients consuming caffeine (Faber & Fuhr, 2004; Cappelletti et al., 2014). Caffeine's cardiovascular effects can interfere with antihypertensive drugs. Caffeine's stimulatory effects may counteract beta-blockers ' actions, potentially requiring higher doses. Calcium channel blockers may have altered bioavailability with caffeine. Patients on cardiovascular medications should moderate caffeine intake to optimize therapeutic outcomes (Belayneh & Molla, 2020; Shi et al., 2016).

2.3. Solvatochromism and Solvent-Drug Interactions

Solvatochromism is the change in a molecule's absorption and emission spectra as a function of solvent polarity. This phenomenon arises from the alteration of a molecule's electronic structure due to interactions with surrounding solvent molecules. Solvatochromic probes are therefore valuable tools for assessing both overall and site-specific polarity in complex systems, such as biological membranes, and are useful in studying protein structure and ligand binding. Solvatochromic shifts provide information regarding the microenvironment surrounding a probe molecule, reflecting intermolecular interactions modulated by the dynamics of both the chromophore and the solvent (Welton, 2011).

In fluorescence emission, the local environment influences the energy level of the excited state, which determines the lowest energy state from which emission occurs. Consequently,

solvatochromic effects are closely related to excited-state dynamics and solvent reorganization. Following excitation, the probe may remain localized, reporting properties of its immediate environment, or migrate within the sample, reporting averaged properties. Furthermore, solvent molecules may either maintain their initial ground-state orientation or reorient to achieve solvation equilibrium with the excited state. These factors collectively influence the emission spectrum's peak position, band shape, and intensity (Lakowicz, 2014; Valeur, 2003). In photo physics, electronic state transitions occur upon the absorption of light by a molecule, promoting an electron to a higher energy level. Fluorescence emission subsequently occurs as the excited molecule returns to its ground state, releasing energy in the form of light. Photophysical properties are influenced by factors such as molecular structure, solvent, temperature, and interactions with other molecules. Understanding these principles is essential for applications in fields such as materials science, bioimaging, and photovoltaics, enabling the design of novel materials and the advancement of technologies for energy conversion and storage.

Solvent-drug interactions exert a significant influence on the solubility, stability, bioavailability, and delivery of antidiabetic drugs, including metformin, sulfonylureas, and vanadium-based complexes, thereby affecting drug formulation and efficacy (Dahlén et al., 2022). Solvents such as water, ethanol, and dimethyl sulfoxide (DMSO) interact with drugs via hydrogen bonding, hydrophobic effects, and dipole-dipole interactions, which, in turn, modulate their physicochemical properties (Welton, 2011). Solubility is a critical determinant of bioavailability, particularly for orally administered drugs. Metformin exhibits high aqueous solubility due to its polar structure, which facilitates its dissolution in the gastrointestinal tract (Hohnholt et al., 2017); however, its solubility diminishes in less polar solvents. Generally, dissolution is optimized by matching the polarity of the solvent and solute (Welton, 2011).

Chemical stability is also governed by solvent-drug interactions. While metformin demonstrates stability in aqueous solutions, its degradation is accelerated in organic solvents, leading to the formation of guanyl urea (Hohnholt et al., 2017). Furthermore, solvent-drug interactions influence bioavailability. Metformin's aqueous solubility ensures rapid dissolution, but its bioavailability is limited by first-pass metabolism (Dahlén et al., 2022). Solvents play a crucial role in analytical techniques such as HPLC, where solvents like methanol or acetonitrile are employed to elute antidiabetic drugs (Zhou et al., 2023). Solvents also influence drug-excipient interactions: metformin's compatibility with aqueous excipients enhances tablet dissolution, while gliclazide

requires non-aqueous solvents to prevent degradation (Dahlén et al., 2022). It is important to note that organic solvents like DMSO can present toxicity risks (Welton, 2011). In conclusion, solvent-drug interactions significantly impact the solubility, stability, and bioavailability of antidiabetic drugs.

2.3.1. General Solvent-Solute Interactions

Solvent-solute interactions primarily involve three categories of electrostatic forces: dipole-dipole, dipole-induced dipole, and induced dipole-induced dipole forces. If a molecule's dipole moment becomes larger in the excited state, typically during $n \rightarrow \pi^*$ or $\pi \rightarrow \pi^*$ transitions, a polar or highly polarizable solvent stabilizes the excited state more strongly than the ground state. Consequently, the energy gap between these states narrows, causing a shift of the absorption band toward longer wavelengths (red shift). This behavior is termed positive solvatochromism or bathochromic shift, and its magnitude reflects the extent of dipole moment change upon excitation. Conversely, when the excited state's dipole moment is smaller than that of the ground state, polar solvents preferentially stabilize the ground state, resulting in a higher energy gap and a shift toward shorter wavelengths (blue shift). This effect, called negative solvatochromism or hypsochromic shift, is frequently seen in molecules undergoing $n \rightarrow \pi^*$ transitions (Nigam & Rutan, 2001).

2.3.2. Specific Solvent-solute Interactions

Specific interactions involve targeted chemical associations between the chromophore and solvent molecules, including hydrogen bonding, coordination complex formation, acid-base equilibria, and charge-transfer processes. These can substantially alter the molecule's electronic absorption spectrum. In hydrogen-bond donor (HBD) interactions, the energy of a particular electronic state decreases because of the attractive electrostatic force between a partially positive hydrogen atom in the solvent and a lone electron pair on a basic site (such as oxygen or nitrogen) in the solute. This stabilization can occur in either the ground or excited state.

When excitation causes electron density to shift away from the basic site, hydrogen bond formation opposes this redistribution, requiring additional energy for the transition. As a result, solvents with stronger hydrogen-bond donating ability produce a shift toward shorter wavelengths (blue shift). In contrast, if excitation increases electron density at the basic site, enhanced hydrogen bonding stabilizes the excited state more effectively, lowering the transition energy and causing a shift

toward longer wavelengths (red shift). It is worth emphasizing that these effects arise from true hydrogen bonding rather than full proton transfer (Nigam & Rutan, 2001).

2.4. Solvent Polarity Effects on Spectra and Molecular Properties

Upon absorption of light, a molecule interacts with surrounding solvent molecules, with the strength of this interaction being contingent upon solvent polarity. In fluorescent probes, these excited-state solute-solvent interactions exert a significant influence on the emission spectra. Given that fluorescence occurs on a longer timescale than absorption, solvent molecules have sufficient time to reorient around the altered dipole moment of the excited state. This solvent relaxation is more pronounced in polar solvents, leading to a reduction in the energy of the excited state. By the time the excited molecule emits a photon, the surrounding solvent shell has adopted a configuration optimized for the excited-state dipole. However, the solvent molecules lack sufficient time to revert to their ground-state equilibrium positions during the brief emission event. Consequently, the nascent ground state is at a higher energy level than its fully relaxed counterpart. When the dipole moment of the excited state exceeds that of the ground state, this incomplete solvent reorganization in polar media leads to a substantial decrease in the emission energy, resulting in a red shift.

Fluorescence provides valuable insights into molecular dynamics and interactions in the vicinity of the fluorophore, enabling researchers to assess the polarity of its immediate environment. The excited-state lifetime of a fluorophore is dependent on the rates of various competing deactivation pathways. Excess energy from the excited fluorophore can be transferred to other molecules through quenching. In environments where collisions with quenchers are limited, the fluorophore's lifetime is prolonged. Excimer formation is another key process, occurring when an excited fluorophore collides with an identical ground-state fluorophore, resulting in the formation of an excimer. Excimers exhibit emission spectra that differ from those of isolated monomers, often displaying a broad, red-shifted band. When an excited fluorophore interacts with a different ground-state molecule, the resulting complex is termed an exciplex. Variations in the charge-transfer character of both excimers and exciplexes render them sensitive indicators of the local dielectric environment (Lakowicz, 2014; Nigam & Rutan, 2001). This Solvatochromic technique relies on examining the positions of absorption and fluorescence maxima across a series of solvents with different dielectric constants (ε) and refractive indices (n). Photon absorption triggers electron

redistribution within the molecule, often accompanied by structural rearrangements in the excited state. Consequently, the dipole moment may either increase or decrease relative to the ground state. Fundamentally, the method exploits the polarity-dependent shifts in the wavelengths of maximum absorption and emission observed in solvents of varying polarities (Patil et al., 2012). With increasing solvent polarity, highly polar excited states experience greater stabilization through interactions with surrounding solvent molecules, thereby reducing the energy gap between the ground and excited states. The three key independent equations employed to describe solvent polarity functions are presented below.

Lippert's equation (Lippert, 1955)

$$\overline{\nu}_{\alpha} - \overline{\nu}_{f} = -m_1 f_1(\varepsilon, n) + constant \qquad 2.1$$

Bakshiev's equation (Bakhshiev, 1964)

$$\overline{\nu}_{\alpha} - \overline{\nu}_{f} = -m_2 f_1(\varepsilon, n) + constant \qquad 2.2$$

Kawski-Chamma-Viallet's equation (Chamma & Viallet, 1970)

$$\frac{\overline{\nu}_{\alpha} + \overline{\nu}_{f}}{2} = m_3 f_3(\varepsilon, n) + constant \qquad 2.3$$

The expressions for $f_1(\varepsilon, n)$ [Lippert's polarity function], $f_2(\varepsilon, n)$ [Bakshiev's polarity equation] and $f_3(\varepsilon, n)$[Kawski-Chamma-Viallet's polarity equation] is given as

$$f_1(\varepsilon, n) = \left[\frac{\varepsilon - 1}{2\varepsilon + 1} - \frac{(n^2 - 1)}{(2n^2 + 1)}\right] \qquad 2.4$$

$$f_2\,(\varepsilon, n) = \left[\frac{\varepsilon - 1}{\varepsilon + 2} - \frac{n^2 - 1}{n^2 + 2}\right]\left(\frac{(2n^2 + 1)}{n^2 + 2}\right) \qquad 2.5$$

$$f_3(\varepsilon, n) = \frac{2n^2 + 1}{2(n^2 + 2)}\ \left[\frac{\varepsilon - 1}{\varepsilon + 2} - \frac{n^2 - 1}{n^2 + 2}\right] + \frac{3(n^4 - 1)}{2(n^2 + 2)^2} \qquad 2.6$$

Where $\overline{\nu}_{\alpha}$ and $\overline{\nu}_{f}$ are absorption and fluorescence maxima wavelength in $cm^{-1,}$ respectively. The other symbols ε and *n* are the dielectric constant and refractive index, respectively.

From Eqns. (2.1-2.3) It follows that $(\overline{\nu}_\alpha - \overline{\nu}_f)$ versus$f_1(\varepsilon, n)$, $\left(\overline{\nu}_\alpha - \overline{\nu}_f\right)$ versus $f_2(\varepsilon, n)$ and $\frac{(\overline{\nu}_\alpha + \overline{\nu}_f)}{2}$ versus $f_3(\varepsilon, n)$ should give linear graphs with slopes m_1, m_2 and m_3 respectively and are given as

$$m_1 = 2\left(\frac{\left(\mu_e - \mu_g\right)^2}{hca^3}\right) \quad 2.7$$

$$m_2 = 2\left(\frac{\left(\mu_e - \mu_g\right)^2}{hca^3}\right) \quad 2.8$$

$$m_3 = 2\left(\frac{\mu_e^2 - \mu_g^2}{hca^3}\right) \quad 2.9$$

Where μ_g and μ_e are the ground and excited state dipole moments of the solute molecules. The symbols *h* and *c* are Planck's constant and the velocity of light in vacuum, respectively; *a* is the Onsager radius of the solute molecule. If the ground state and excited states are parallel, the following expressions are obtained based on Eq. (2.7-2.9)

$$\mu_g = \frac{m_3 - m_2}{2}\left(\frac{(hca^3)^{\frac{1}{2}}}{2m_2}\right) \quad 2.10$$

$$\mu_e = \frac{m_3 + m_2}{2}\left(\frac{(hca^3)^{\frac{1}{2}}}{2m_2}\right) \quad 2.11$$

And

$$\mu_e = \frac{m_3 + m_2}{m_3 - m_2}\left(\frac{(hca^3)^{\frac{1}{2}}}{2m_2}\right) \text{ for } m_3 > m_2 \quad 2.12$$

Solvent polarity functions will be calculated using different literature values of the dielectric constant and refractive index of the solvents. The spectroscopic properties correlate with the solvent polarity functions, and from the slope of the Bakhshiev, Kawski–Chamma–Viallet, and

Lippert–Mataga equations, the ground and excited dipole moments are determined to get the Solvatochromic behavior of the compounds (Patil A et al., 2012; Woldegiorges et al., 2021).

The other alternative technique for estimating the dipole moments is the empirical solvent polarity function. Reichardt proposed a solvent polarity to calculate the difference in dipole moment (Δμ) (Reichardt, 1994), and Ravi realized (Ravi et al., 1995). The technique is predicated on the solvatochromic features of betaine dye, along with hydrogen bonding and the polarization effect, given by

$$\nu_\alpha - \nu_f = 11307 \left[\left(\frac{\Delta\mu}{\Delta\mu_B} \right)^2 \left(\frac{\alpha B}{\alpha} \right)^2 \right] E_T^N \qquad 2.13$$

where $\Delta\mu_B$ = 9 D is for change in dipole moment, αB= 6.2 A^o is betaine dye Onsager radius, and are parameters for a compound of interest, and (E_T^N) expressed as

$$E_T^N = \frac{E_T(30)_{solvent} - E_{T(30)_{TMS}}}{E_{T(30)water} - E_{T(30)_{TMS}}} = \frac{E_T(30)_{solvent} - 30.7}{32.4} \qquad 2.14$$

where TM$_S$ symbolizes water as a polar solvent (E_T^N)=1) and using tetramethylsilane as a nonpolar solvent (E_T^N) = 0).

The dipole moments from the slope $\nu_\alpha - \nu_f$ versus E_T^N is expressed as follows:

$$\Delta\mu = \mu_e - \mu_g \left(\sqrt{\frac{\beta \times 81}{\left(\frac{6.2}{\alpha}\right)^3 11307.6}} \right. \qquad 2.15$$

Here, β indicates the slope for the linear plot of E_T^N against Stokes' shift.

2.4.1. Photophysical and Luminescence Properties of Antidiabetic Drugs

Photophysical properties describe how molecules interact with light, encompassing absorption spectra, emission characteristics, and excited-state dynamics. For antidiabetic drugs, these properties influence stability when exposed to light and potential photobiological effects. In contrast to antimalarial drugs, which have well-studied phototoxicity mechanisms, antidiabetic

medications have not been thoroughly investigated (Viola et al., 2007). A deeper understanding of these properties could enhance drug formulation and safety assessments, especially for light-sensitive compounds.

Metformin hydrochloride, the first-line treatment for type 2 diabetes, activates AMP-activated protein kinase (AMPK) to enhance glucose uptake and reduce hepatic gluconeogenesis (Hohnholt et al., 2017). Environmental studies indicate metformin rapidly sorbs in soil matrices (90% within 4–13 hours), yet no significant photodegradation has been observed, suggesting photochemical stability (Hohnholt et al., 2017). Nonetheless, its antioxidant properties may involve weak photophysical interactions, warranting further investigation using techniques such as UV-Vis spectroscopy or fluorescence lifetime imaging.

Sulfonylureas, including gliclazide, stimulate insulin secretion by inhibiting ATP-dependent potassium channels in pancreatic β-cells (S. Zhou et al., 2023). Spectroscopic studies suggest gliclazide may be light-sensitive due to its UV absorption, raising concerns about potential photodegradation during storage (S. Zhou et al., 2023). However, specific data on fluorescence or photoionization are lacking. Compared to antimalarials like chloroquine, which exhibit radical cation formation under UV exposure (Viola et al., 2007), sulfonylureas require additional photophysical characterization to evaluate their stability and safety.

Vanadium-containing complexes, investigated as insulin-mimetic agents, exhibit unique photophysical properties due to their environment-responsive ligand exchange kinetics (Renfrew, 2014). When conjugated to carriers such as vitamin B12, these complexes demonstrate enhanced cellular uptake and glucose-lowering effects in preclinical models (Renfrew, 2014). Their photochemical behavior, including ligand dissociation under visible light, positions them as promising candidates for light-activated drug delivery systems.

2.4.1.1. Fundamentals of Luminescence in Pharmaceutical Molecules

Luminescence, including fluorescence and phosphorescence, involves light emission following photon absorption. The Jablonski diagram (fig. 4) illustrates electronic transitions: absorption elevates electrons from the ground state (S_0) to excited singlet states (S_1 or higher), followed by vibrational relaxation, fluorescence ($S_1 \rightarrow S_0$), or intersystem crossing to triplet states and phosphorescence (Lakowicz, 2006). In pharmaceutical compounds, native luminescence is often subdued due to limited π-conjugation; however, solvent polarity can induce Solvatochromic shifts,

reflecting dipole moment changes upon excitation (C. R. and T. Welton, 2011). Luminescence spectroscopy is a sensitive analytical tool in pharmaceutical research for detecting trace concentrations, studying molecular interactions, and probing drug molecule microenvironments. Understanding antidiabetic drug photophysical behavior is crucial for developing assays, investigating stability, and elucidating mechanisms of action (Sina et al., 2021). Key photophysical parameters, including absorption/emission profiles, Stokes shift, transition dipole moments, fluorescence quantum yield, and energy bandgap, are sensitive to intramolecular charge transfer (ICT) (Asiri et al., 2022). Fluorescence quantum yield, the ratio of emitted to absorbed photons, is a critical parameter for any fluorophore.

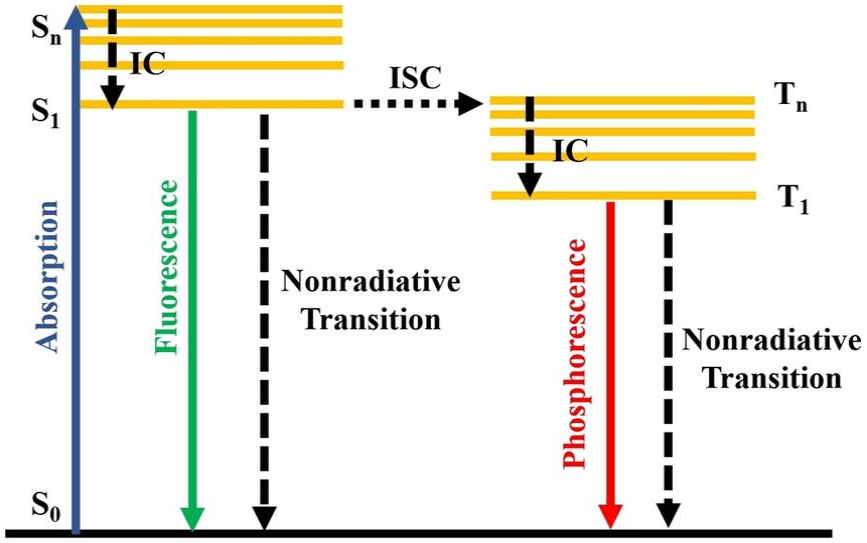

Figure 3:The Jablonski diagram of molecular absorbance and fluorescence

To ensure accurate measurement, fluorescence spectra of both the sample and a reference standard are recorded under identical conditions, using solutions adjusted to the same absorbance at the excitation wavelength. Before spectral integration, both datasets are corrected by subtracting the solvent blank background (Suhina, 2017). The quantum yield of the target compound is subsequently determined using the standard comparative method as described in Eqn. (2.16) (Lakowicz, 2000).

$$\Phi_{f,x} = \Phi_{f,st} \frac{F_x \cdot f_{st}}{F_{st} \cdot f_x} \left(\frac{n_x}{n_{st}}\right)^2 \qquad 2.16$$

In this equation, $\Phi_{f,x}$ represents the fluorescence quantum yield of the target compound, while $\Phi_{f,st}$ denotes the quantum yield of the reference standard. F_x and F_{st} correspond to the integrated fluorescence intensities of the sample and standard, respectively. The terms f_x and f_{st} are the absorption correction factors (calculated as $f = 1 - 10^{A}$, where A is the absorbance at the excitation wavelength) for the sample and standard, respectively. Finally, n_x and n_{st} are the refractive indices of the solvents used for the sample and the standard solutions.

Following photoexcitation, molecules persist in the excited state for a brief period before relaxing back to the ground state. The duration they spend in this excited state, on average, defines the excited-state lifetime, which is commonly referred to as the fluorescence lifetime. This lifetime typically spans from picoseconds (10^{-12} s) to nanoseconds (10^{-9} s). The fluorescence lifetime, denoted as $\tau_{f,}$ is given by Eqn. (2.17) (Sauer et al., 2011):

$$\tau = \frac{1}{K} = \frac{1}{Kr + Knr} \qquad 2.17$$

The rate of radiative decay exhibits a notable dependence on the surrounding medium, specifically increasing with greater polarizability of the environment. This behavior can be quantitatively anticipated using the established Strickler–Berg Eqn. (2.18) (Strickler & Berg, 1962).

$$K_r = \frac{1}{\tau_o} = 2.88X10^{-9}n^2\left(\frac{\int f(\overline{\nu})d\overline{\nu}}{\left(\int f(\overline{\nu})\overline{\nu}^{-3}\right)d\overline{\nu}}\right)\int\left(\frac{\epsilon(\overline{\nu})}{\overline{\nu}}\right)d\overline{\nu} \qquad 2.18$$

Here, $f(\overline{\nu})$ denotes the fluorescence intensity, $\overline{\nu}$ represents the wavenumber, and $\epsilon(\overline{\nu})$ is the molar decadic absorption coefficient. The term n stands for the refractive index of the medium, while τ_0 corresponds to the natural (radiative) lifetime.

In the idealized scenario where the Stokes shift is minimal, and the absorption and emission spectra exhibit near-perfect mirror symmetry, Eqn. (2.18) reduces to the simplified form presented below (Suhina, 2017):

$$\kappa_r = 2.88X10^{-9}n^2(\overline{\nu})_{av}^2\int\epsilon(\overline{\nu})d\overline{\nu} \qquad 2.19$$

And

$$\tau_f = \tau_o\phi_f \qquad 2.20$$

The intensity of an absorption band provides key insights into the type of electronic transition involved. A quantitative experimental indicator of this transition strength is the oscillator strength, which represents one of the core parameters in spectroscopic analysis. In practical applications, it governs the detection sensitivity of a specific absorption feature and must be precisely determined when correlating the absorption signal amplitude with analyte concentration. Oscillator strength can be obtained directly from measurements of absolute emission rates, absorption intensities, or dispersion properties. It is connected to the molar decadic absorption coefficient through the relation given below (Belay, 2010).

$$f = 4.32X10^{-9} mol\ cm^2 L^{-1} \int \epsilon dv \qquad 2.21$$

And

$$\epsilon = \frac{A}{lc} \qquad 2.22$$

Where A absorption intensity, l is the length of the cuvette ϵ is the molar decadic absorption coefficient carrying the unit Lmol $^{-1}$ cm$^{-1,}$ and wave number ν in cm^{-1}.

The absorption coefficient can alternatively be expressed as the product of either the molar absorption coefficient (ε) of the absorbing species and its concentration (c), or the absorption cross-section (σ) and the number density (N) of the absorbers. In the context of liquid solutions, these relationships are typically formulated as follows:

$$T = \frac{I}{I_o} = 10^{-\alpha l} = 10^{-\varepsilon c l} \qquad 2.23$$

Here, I_0 and I represent the intensities of the incident and transmitted light, respectively.

For liquid samples, transmittance can be related to absorbance through the following expression:

$$A = log\left(\frac{I_o}{I}\right) = \varepsilon c l \qquad 2.24$$

The absorption cross-section (σ), which represents the effective photon-capture area per molecule, is connected to the absorption coefficient (α) at a specific frequency through the following expression, where N denotes the number density of absorbing molecules per unit volume:

$$\alpha(\nu) = N\sigma(\nu) \quad 2.25$$

In practice, UV-Vis spectroscopy of molecules in solution reveals absorption bands spanning a broad range of wavelengths rather than sharp lines at discrete frequencies. As a result, the absorption coefficient measured at any individual wavelength may not accurately reflect the overall strength of the electronic transition. A more reliable approach involves using the integrated absorption coefficient, which represents the total area under the absorption band across all contributing wavelengths. This integrated value provides a better measure of transition intensity and finds wide application because it remains unaffected by factors that alter band shape, such as temperature, pressure, solute concentration, and solute–solvent interactions (Liptay, 1969; Thorne, 1988). Furthermore, this method proves particularly valuable when high-resolution instrumentation is unavailable (Ramsay, 1951). Consequently, for liquid samples and solutions where broadening effects are prominent, the true band intensity is appropriately expressed by the integrated absorption through the following equation:

$$\alpha_t = \int \alpha d\nu \quad 2.26$$

Using Eqn. (2.24) into (2.26) yields

$$\alpha_t = \frac{1}{l}\int log\left(\frac{I_o}{I}\right) d\nu \quad 2.27$$

The integrated absorption cross-section can be derived from the integrated absorption coefficient through the relation provided below (Milonni & Eberly, 2010).

$$\sigma_t = \frac{1}{Nl} log \int \left(\frac{I_o}{I}\right) d\nu \quad 2.28$$

Here, σ_t denotes the integrated absorption cross-section, α_t represents the integrated absorption coefficient, and $N$is the number density of the absorbing species. The transition dipole moment is connected to the molar decadic absorption coefficient through the following relation (Liptay, 1969).

$$\frac{1}{3}S|\mu|^2 = \frac{\int \epsilon(\nu)}{\nu}\, d\nu \qquad 2.29$$

Where $S = 2.9352\times10^{60}C^{-2}mol^{-1}$ μ is the transition dipole moment.

2.5. Fluorescence Quenching of Chromophores

In fluorescence spectroscopy, the number of photons emitted by a molecule is usually fewer than the number of photons it absorbs, resulting in a quantum yield below one. This reduction occurs because some of the absorbed energy is lost through non-radiative pathways rather than being released as light. These non-radiative processes include internal conversion (vibrational relaxation without emission) and intersystem crossing, where the excited molecule shifts to a triplet state from which phosphorescence or further energy dissipation is more likely. Certain structural features in the fluorophore itself can promote such energy loss, leading to internal or intramolecular quenching. For instance, heavy atoms (like iodine or bromine) attached to the molecule increase intersystem crossing via the heavy-atom effect, while specifically designed quenching groups covalently linked to the fluorophore, such as those used in molecular beacon probes, can dramatically suppress emission (Setiawan et al., 2010). In contrast, external quenching happens when emission is reduced by molecules or ions in the surrounding environment that are not part of the fluorophore structure.

Quenching can also arise in concentrated solutions from the formation of molecular aggregates, where excited states undergo rapid internal conversion or intersystem crossing. Overall, fluorescence intensity can be lowered by several mechanisms, many of which are valuable in biochemical studies. These include conformational changes in molecules, resonance energy transfer, formation of non-fluorescent ground-state complexes, and dynamic collisions between the excited fluorophore and quencher species. The extent of quenching is also affected by factors such as the polarity of mixed solvent systems and the concentration of quenching agents (Koppal et al., 2018). The effectiveness of a quencher is commonly measured using the Stern–Volmer constant (K_{sv}), a parameter that reflects the strength of the quenching process and can change depending on temperature, viscosity, or other experimental variables. It is defined according to the Stern-Volmer Eqn. (2.30):

$$\frac{F_o}{F} = 1 + \tau_{o\kappa_o[Q]} = 1 + \kappa_{sv}[Q] \qquad 2.30$$

In the Stern-Volmer equation, K_{sv} represents the quenching constant, K_q is the bimolecular rate constant for the quenching process, τ_o denotes the fluorescence lifetime of the fluorophore in the absence of quencher, and [Q] is the concentration of the quencher species. The value of K_{sv} reflects how readily the fluorophore's emission is suppressed by the quencher. Fluorophores deeply embedded within a protein or other large macromolecule are often shielded from soluble quenchers in the surrounding medium, resulting in a relatively small K_{sv}. In contrast, higher K_{sv} values are observed when the fluorophore is freely dissolved or positioned on the exterior surface of a biomolecule, making it more accessible.

It is important to recognize that fluorescence emission is highly sensitive to temperature changes, with elevated temperatures generally leading to reduced quantum yields due to enhanced non-radiative decay pathways. This effect can be particularly pronounced for indole-based fluorophores, such as tryptophan residues in proteins. Consequently, accurate quenching studies require precise and consistent temperature regulation throughout experiments. External quenching processes are broadly classified into two main types: dynamic (also called collisional) and static.

2.5.1. Static quenching

occurs when the quencher forms a non-fluorescent ground-state complex with the fluorophore before excitation. In this case, the complex does not emit light, so the overall fluorescence intensity decreases proportionally to the fraction of fluorophores bound to quenchers. For instance, if half of the fluorophore population is complexed, the emission intensity drops to about half of its original value compared to a quencher-free sample. This type of quenching is governed by an association or binding constant (K_α) and does not involve diffusion-limited collisions in the excited state.

Static quenching arises from ground-state interactions and is independent of molecular diffusion. Other mechanisms that can reduce fluorescence intensity include excited-state reactions, energy transfer processes, conformational changes in molecules, collisional encounters, and direct disruption of the emitting chromophore (Song et al., 2014).

When fluorophores bind independently to identical sites on a macromolecule, the equilibrium between unbound and bound forms can be analyzed to determine the binding constant and the location of binding sites. This relationship is expressed through a modified form of the Stern-Volmer equation tailored for such systems:

$$log\left(\frac{F_o - F}{F}\right) = log\ \kappa_\alpha \ \ + nlog[Q] \qquad 2.31$$

In this equation, Ka represents the association (binding) constant for complex formation, while **n** denotes the number of equivalent and independent binding sites per macromolecule. The parameters Ka and n can be obtained from the slope and y-intercept of a linear plot constructed by fitting the experimental data to Eqn. (2.31) (typically a double-logarithmic or modified Stern-Volmer form used for site-specific binding).

Consider a solution containing a total concentration of fluorophores **[**No**]**. When some of these fluorophores form non-fluorescent complexes with quenchers, the concentration of complexed fluorophores is $[N_c]$, leaving the concentration of free (unquenched) fluorophores as $[N]$ (where $[N] = [N_o] - [N_c]$). The formation of these ground-state complexes depends on the availability of both free fluorophores and quencher molecules. Consequently, the concentration of complexes $[N_c]$ is proportional to the product of the free fluorophore concentration $[N]$ and the quencher concentration $[Q]$, reflecting the equilibrium nature of the binding process:

$$N_c = N_O - N = K_\alpha N[Q] \qquad 2.32$$

These leads

$$\frac{N_O}{N} = 1 + K\alpha[Q] \qquad 2.33$$

The observed fluorescence intensity is directly proportional to the concentration of free fluorophores in the solution. As a result, the relationship can be expressed as follows:

$$\frac{I_O}{I} = 1 + K_\alpha[Q] \qquad 2.34$$

The ratio $\frac{I}{I_o}$ depends linearly on the quencher concentration.

In static quenching, the uncomplexed (free) fluorophores emit fluorescence with the same characteristic intensity per molecule, lifetime, and polarization as they would in a quencher-free environment. The only apparent effect is a reduction in the total number of emitting species, making the solution appear to contain a lower overall concentration of fluorophores. Complex formation responsible for static quenching is temperature-dependent: elevated temperatures weaken the binding interactions, leading to fewer non-fluorescent ground-state complexes and, consequently, reduced effectiveness of static quenching. When external quenchers do not interact with fluorophores in their ground state, meaning they do not form non-fluorescent ground-state complexes, they can still suppress emission by encountering the fluorophore during its excited-state lifetime. For this to occur, the quencher must physically collide with the excited fluorophore molecule. In solution, molecular diffusion brings excited fluorophores and quencher species into transient contact, enabling these deactivating collisions. This mechanism is known as dynamic quenching or collisional quenching.

2.5.2. Dynamic quenching

also referred to as collisional quenching, depends on both the effectiveness of the deactivation encounter described by the bimolecular rate constant (K_q) and the quencher concentration $[Q]$. The overall rate of this quenching process is therefore expressed as $K_q \times [Q]$. Collisional quenching takes place when a molecule in its excited state briefly contacts a quencher species in solution, leading to the rapid return of the fluorophore to the ground state without emitting light or undergoing any permanent chemical change. Many different substances can act as effective collisional quenchers, such as dissolved oxygen, halide ions, amines, and electron-accepting compounds like acrylamide.

The precise mechanism of deactivation varies with the particular fluorophore-quencher combination. For example, acrylamide quenches indole fluorescence primarily through electron transfer from the excited indole to acrylamide, a process that cannot occur in the ground state. In contrast, heavy atoms and halides promote quenching mainly by enhancing spin-orbit coupling, which facilitates intersystem crossing to the triplet state. These molecular events are commonly visualized using a Jablonski diagram. Dynamic quenching appears as a concentration-dependent non-radiative pathway from the first excited singlet state (S_1) back to the ground state (S_0), with a rate constant of $K_q \times [Q]$.

Other key processes shown include: Light absorption (Abs), Radiative emission (fluorescence) with rate constant Γ, Quencher-independent non-radiative decay with rate constant k_{nr}, Intersystem crossing to the triplet state with rate constant k_{isc}. Each rate constant (k_i) reflects the probability per unit time of the corresponding deactivation pathway and has units of s^{-1}. The characteristic time for a process is simply the reciprocal, $\frac{1}{K_i}$. For fluorescence specifically, the intrinsic (radiative) lifetime is defined as $\tau_n = \frac{1}{\Gamma}$.

$$\tau = \frac{1}{\Gamma + \sum K_i} \tag{2.35}$$

$$\tau_o = \frac{1}{\Gamma + K_{nr} + K_{isc}} \tag{2.36}$$

And in the presence of the quencher:

$$\tau = \frac{1}{\Gamma + K_{nr} + K_{isc} + K_q[Q]} \tag{2.37}$$

The efficiency of a specific deactivation process is determined by the fraction of excited molecules that follow that pathway, calculated as the ratio of its rate constant to the total sum of all competing rate constants for deactivation:

$$E = \frac{K_i}{\Gamma + \sum K_i} \tag{2.38}$$

The efficiency of the fluorescence (fluorescence intensity) in the absence of the quencher is:

$$E_o = I_o = \frac{\Gamma}{\Gamma + K_{nr} + K_{isc}} \tag{2.39}$$

And in the presence of the quencher:

$$E_f = I_f = \frac{\Gamma}{\Gamma + K_{nr} + K_{isc} + K_q[Q]} \tag{2.40}$$

Equations 2.36 through 2.40 give:

$$\frac{\tau_o}{\tau} = \frac{I_o}{I_f} = \frac{\Gamma + K_{nr} + K_{isc} + K_q[Q]}{\Gamma + K_{nr} + K_{isc}} = 1 + \tau_o K_q[Q] = 1 + K_{sv}[Q] \tag{2.41}$$

This equation is recognized as the Stern–Volmer relationship, where K_{SV} serves as the Stern-Volmer quenching constant. Plotting the data according to this equation produces a graph known as a Stern-Volmer plot. A key distinction between quenching mechanisms lies in their effects on observable parameters: dynamic quenching reduces both the fluorescence lifetime and the emission intensity proportionally, while static quenching affects only the intensity, leaving the lifetime of the remaining emitting fluorophores unchanged.

Temperature dependence provides another diagnostic tool. Dynamic quenching becomes more efficient at higher temperatures due to faster molecular diffusion and increased collision rates. In contrast, static quenching weakens as temperature rises because ground-state complex formation is typically less favored under those conditions. In many real systems, a single quencher can operate through both static and dynamic mechanisms simultaneously. When this occurs, the overall reduction in fluorescence intensity is described by the combined contribution of the two processes, expressed as the product of their individual quenching factors.

$$\frac{I_O}{I} = (1 + K_\alpha[Q]).(1 + K_{sv}[Q]) \qquad 2.42$$

The fluorescence lifetime is influenced solely by dynamic quenching processes, as static quenching does not alter the excited-state duration of the remaining free fluorophores. Consequently, time-resolved lifetime measurements provide a direct and unambiguous way to determine the Stern–Volmer constant (K_{SV}) specifically for the dynamic component. Several theoretical frameworks have been developed to describe quenching mechanisms in greater detail. These include the sphere-of-action model (assuming instantaneous quenching within a certain volume around the fluorophore), models incorporating transient diffusion effects, and the Collins–Kimball approach, which accounts for distance-dependent quenching rates. Despite these advanced treatments, the majority of experimental quenching data can be adequately analyzed using the straightforward Stern-Volmer formalism.

2.5.3. Thermodynamic Parameters and Characteristics of Binding Forces

Examination of the thermodynamic parameters associated with the decomposition process was conducted to gain a deeper understanding of the underlying complexation mechanism. The Van't Hoff equation serves as a key tool for calculating these thermodynamic parameters. Complex

formation is characterized by various biophysical quantities, including the association constant and related thermodynamic properties such as enthalpy, entropy, and Gibbs free energy changes. To elucidate the nature of the weak intermolecular forces involved in the binding of lamivudine and dolutegravir with caffeine, thermodynamic parameters were derived through application of the Van't Hoff equation. Provided that the enthalpy change (ΔH) remains relatively constant across the investigated temperature range, these parameters can be reliably obtained from the Van't Hoff relationship as follows (Belay, Kim, et al., 2016):

$$ln\,\kappa_{\alpha} = -\frac{\Delta H}{RT} + \frac{\Delta S}{R} \qquad 2.43$$

The Gibbs free energy change (ΔG) and the entropy change (ΔS) can be obtained from the equations listed below:

$$\Delta G = -RT\ ln\kappa_{\alpha} = \Delta H - T\Delta S \qquad 2.44$$

$$\Delta S = \frac{\Delta H - \Delta G}{T} \qquad 2.45$$

Here, K_{α} represents the binding constant at the given temperature, R is the universal gas constant, and T denotes the absolute temperature used in the experiment. The symbols ΔH, ΔS, and ΔG correspond to the changes in enthalpy, entropy, and Gibbs free energy, respectively.

On the assumption that there are n substantive binding sites the drug molecule has on the antiviral, the quenching reaction can be shown as follows

$$nQ + B \leftrightharpoons Q_n B \qquad 2.46$$

The binding constant κ_a can be calculated as Eqn. (2.47)

$$\kappa_a = \frac{|Q_n B|}{|Q|^n |B|} \qquad 2.47$$

Where |B| and |Q| are the antiviral drugs and quencher concentration, respectively, $|Q|^n|B|$ is the concentration of the non-fluorescent fluorophore-quencher complex. Given the total antiviral drug concentration is$|B_o|$; then $|Q_nB| = |B_o| - |B|$ and then Eqn. (2.47) is

$$\kappa_a = \frac{(|B_O| - |B|)}{|Q|^n|B|} \quad 2.48$$

The fluorescence intensity is proportional to the concentration of antiviral drugs, which is described as Eqn. (2.49)

$$\frac{|B|}{|B_o|} = \frac{F}{F_o} \quad 2.49$$

From Eqns. (2.48) and (2.49), it follows that.

$$log\left(\frac{F_o - F}{F}\right) = log\kappa_a + nlog[Q] \quad 2.50$$

Where, κ_a is the binding constant of antiviral drugs with Caffeine, and n is the number of binding sites per Caffeine molecule. The values of κ_a and n will be determined from the slope and intercept of the linear fit of eqn. (2.50) to the experimental data (Belay et al., 2017).

2.6. Fluorescence (Forster) resonant energy transfer (FRET)

Another significant process occurring in the excited state is Förster resonance energy transfer (FRET), a non-radiative mechanism through which excitation energy is transferred from an excited fluorophore (the donor) to a nearby molecule (the acceptor) via long-range dipole-dipole coupling (Mokashi et al., 2014). Unlike trivial reabsorption, where emitted photons from the donor are subsequently absorbed by the acceptor. a process influenced by concentration, sample geometry, and path length. FRET does not involve light emission or reabsorption and is independent of such external factors.

The efficiency of FRET depends on several key parameters: (1) the distance (r) between donor and acceptor, (2) the extent of spectral overlap between the donor's emission spectrum and the acceptor's absorption spectrum, (3) the relative orientation of the transition dipoles of donor and

acceptor, (4) the fluorescence quantum yield of the donor in the absence of acceptor, (5) the refractive index of the medium, and (6) the donor's excited-state lifetime.

The rate of energy transfer, $K_T(r)$, is expressed as:

$$K_T(r) = \frac{1}{\tau_D}\left(\frac{R_o}{r}\right)^6 \quad 2.51$$

where τ_D is the donor lifetime without acceptor, and R0 is the Förster critical distance at which the transfer efficiency is 50%. The transfer efficiency E for a donor-acceptor pair separated by distance r is given by:

$$E = \frac{1-F}{F_o} = \frac{R_o^6}{R_o^6 + R^6} \quad 2.52$$

The Förster distance R_o (typically in Ångströms) is calculated using:

$$R_o = 8.79 \times 10^{-25} K^2 N^{-4} \Phi J \quad 2.53$$

here κ^2 κ^2 is the dipole orientation factor (commonly assumed as $\frac{2}{3}$ for random orientation in fluid solutions), Φ_D is the donor quantum yield, n is the refractive index of the medium, N_A is Avogadro's number, and J is the spectral overlap integral defined as:

$$J(\lambda) = \frac{\sum F(\lambda)\varepsilon A(\lambda)\lambda^4 \Delta\lambda}{\sum F(\lambda)\Delta\lambda} \quad 2.54$$

Here, F(λ) is the normalized donor emission intensity at wavelength λ, and εA(λ) is the molar extinction coefficient of the acceptor.

Fig. 4 illustrates the electronic energy levels of an interacting donor–acceptor system, showing how the donor's excited-state energy overlaps with the acceptor's absorption, enabling efficient transfer when the acceptor's excited state lies energetically below that of the donor. When donor and acceptor are different species, the process is termed hetero-FRET, distinct from homo-FRET (energy migration) between identical chromophores.

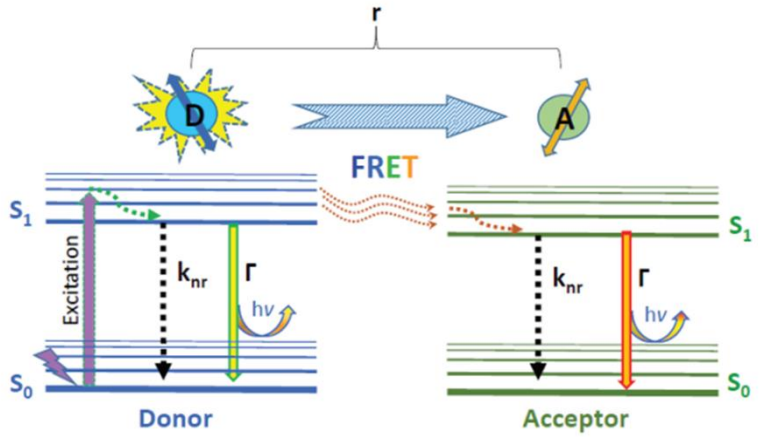

Figure 4: electronic energy levels of a donor-acceptor pair, used to depict processes like FRET

The strong sixth-power dependence of FRET efficiency on distance ($\frac{1}{r^6}$) results in a sharp sensitivity near R0: for example, at $r = 0.5R_O$, E ≈ 98.5%, while at $r = 2R_o$, E drops to ~1.5% (Figure 6). This remarkable distance dependence allows FRET to function as a highly precise "molecular ruler" for measuring separations typically in the 1–10 nm range, making it an invaluable tool for studying molecular interactions, conformational changes, and binding events in biological and chemical systems.

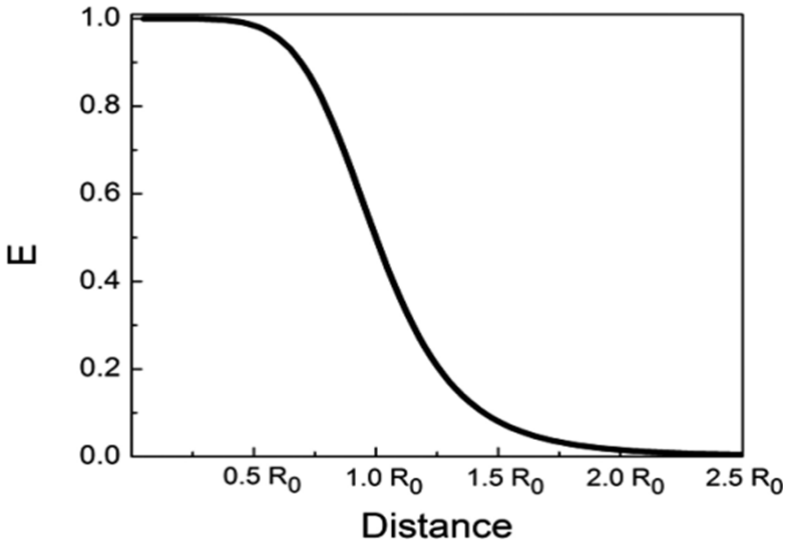

Figure 5: Dependence of energy transfer efficiency (E) as a function of donor-acceptor distance.

2.7. Computational study of anti-diabetic drugs

Computational chemistry has significantly transformed the study of molecular systems by providing sophisticated tools for modeling electronic structures, spectroscopic properties, and

intermolecular interactions with exceptional precision. These computational methods complement experimental techniques, enabling a thorough exploration of complex phenomena such as Solvatochromic (solvent-induced shifts in molecular absorption or emission spectra), photophysical processes (e.g., absorption, fluorescence, phosphorescence), and molecular binding interactions. Two principal approaches in this domain are Density Functional Theory (DFT) and molecular docking. DFT offers a quantum mechanical framework for calculating electronic properties, including molecular orbital's, dipole moments, polarizability, vibrational frequencies, and excitation energies, which are critical for understanding Solvatochromic and photophysical behavior.

Conversely, molecular docking predicts the optimal binding orientations and affinities of ligands with receptors such as proteins, enzymes, or small molecules, thereby facilitating the investigation of molecular interactions in biochemical, pharmaceutical, and materials science contexts. This section aims to establish a comprehensive theoretical foundation for these methods by providing detailed derivations, extensive explanations of their mathematical underpinnings, and practical applications in chemical and biochemical research. By examining the principles, computational tools, and validation strategies, this thesis establishes a robust framework for investigating molecular properties and interactions across various chemical systems (Bacilieri & Moro, 2007; Kapetanovic, 2008).

2.7.1. Density Functional Theory (DFT)

Density Functional Theory (DFT) is an essential tool in contemporary computational chemistry, providing a computationally efficient alternative to traditional wave function-based methods for the study of many-electron systems. Unlike methods that depend on the complete many-body wave function, which escalates exponentially with the number of electrons, DFT concentrates on the electron density, $\rho(r)$, a function defined by only three spatial coordinates. This reduction in dimensionality renders DFT particularly suitable for the analysis of large molecules and complex systems, including those exhibiting Solvatochromic and photophysical properties. The subsequent subsections will delve into the theoretical foundations of DFT, its mathematical derivations, and various applications, supported by rigorous proofs and additional citations to enhance comprehension.

2.7.1.1. Multi-Electron System

The quantum mechanical treatment of molecules with multiple electrons is inherently complex due to the intricate interactions among electrons and between electrons and nuclei. The time-independent Schrödinger equation for a system of *N* electrons is given by (Cramer, 2004; Gey, 1995) :

$$\widehat{H}\Psi = E\Psi \qquad 2.55$$

Where E is the electronic energy, $\Psi = \Psi(r_1, r_2, r_3 \dots \dots . r_n)$ is the many- electron wave function dependent on the spatial coordinates r_i of each electron, and $\widehat{H}$ is the Hamiltonian operator,

$$\widehat{H} = \sum_{i=1}^{n}\left(-\frac{1}{2}\nabla_i^2\right) + \sum_{i=1}^{n} v(r_i) + \sum_{i=1}^{n}\frac{1}{r_{ij}} \qquad 2.56$$

In which

$$v(r_{ij}) = -\sum_{\alpha}\frac{Z_\alpha}{r_{i\alpha}} \qquad 2.57$$

Is the "external" potential acting on electron i, the potential due to nuclei of charges $Z\alpha$.

The Hamiltonian consists of three components: (1) the kinetic energy of the electrons, $\sum_{i=1}^{n}\left(-\frac{1}{2}\nabla_i^2\right)$, where ∇_i^2 is the Laplacian operator for electron *i*; (2) the electron-nuclear attraction, $\sum_{i=1}^{n} v(r_i)$, and (3) the electron-electron repulsion, $\sum_{i=1}^{n}\frac{1}{r_{ij}}$, which accounts for Coulomb interactions between electron pairs. The wave functions' dependence on 3*N* spatial coordinates (plus spin) results in an exponential increase in computational complexity, making direct solutions impractical for systems beyond a few electrons. For instance, a molecule with 10 electrons requires handling a wave function with approximately 10^{18} degrees of freedom, far exceeding the capabilities of modern computational resources (DeRocco, 1967). This computational bottleneck necessitates approximations, and DFT addresses this by reformulating the problem in terms of the electron density, $\rho(r) = \sum_i |\psi_i(r)|^2$, which depends only on three spatial coordinates, drastically reducing the computational cost (Gey, 1995).

2.7.1.2. Hohenberg-Kohn Variation Theorem

Density functional theory (DFT) rests on the foundational theorems established by Hohenberg and Kohn. For a system comprising N electrons confined within a large volume and subject to a static, local external potential v(r), the first Hohenberg-Kohn theorem asserts that this external potential is uniquely defined up to an unimportant constant solely by the ground-state electron density n(r). To prove this uniqueness, assume the existence of a different external potential v'(r) ≠ v(r) + constant that yields the identical ground-state density n(r). This would imply two distinct Hamiltonians, Ĥ and Ĥ', each with its own ground-state wave functions Ψ and Ψ' (non-degenerate), and corresponding ground-state energies E and E'. The many-electron Hamiltonian takes the general form (Cramer, 2004):

$$\hat{H} = \hat{T} + \hat{v}_{ee} + \sum_{i=1}^{n} v(r_i) \qquad 2.58$$

Where $\hat{T} + \hat{v}$ are the kinetic and electron-electron repulsion operators

$$\hat{T} = -\frac{1}{2}\sum_{i=1}^{n} \nabla_i^2 \qquad 2.59$$

$$\hat{v}_{ee} = \sum_{i<1}^{n} \frac{1}{r_{ij}} \qquad 2.60$$

$$\hat{v} = \sum_{i=1}^{n} v(r_i) \qquad 2.61$$

Atomic units are used everywhere. From the Rayleigh—Ritz variational principle, it follows that (Nagy, 1998)

$$E_o = \langle \psi | H | \psi \rangle < \langle \psi' | H | \psi' \rangle = \langle \psi' | H | \psi' \rangle + \langle \psi' | H - H' | \psi' \rangle \qquad 2.62$$

$$= E'_o + \int n(r)[v(r) - v'(r)]dr \qquad 2.63$$

Similarly, using the variational principle for the Hamiltonian H' With the trial function ψ, we have

$$E'_o = \langle\psi'|H'|\psi'\rangle < \langle\psi|H'|\psi\rangle = \langle\psi|H|\psi\rangle + \langle\psi|H' - H|\psi\rangle \qquad 2.64$$

$$= E_o + \int n(r)[v'(r) - v(r)]dr \qquad 2.65$$

Adding Eqns. (2.60) and (2.62) produce a strict mathematical contradiction, which rigorously demonstrates that the ground-state electron density n(r) uniquely determines the external potential v(r) (up to an additive constant). As a result, the density fully specifies the Hamiltonian operator and, therefore, all electronic properties of the system, both for the ground state and excited states. The total energy of the system can then be expressed as

$$E_v[n] = \int n(r)v(r)dr + F_{HK}[n], \qquad 2.66$$

The functional $F_{HK}[n]$ is the sum of the kinetic and electron-electron repulsion energies. The second Hohenberg-Kohn theorem states that for any trial density n'

$$E_o \leq E[n'] \qquad 2.67$$

If $n'(r) \geq 0$ and $N = \int n'(r)dr$ the proof is based on the variational principle, as for any trial wave function ψ

$$\langle\psi|H|\psi\rangle = \int n'(r)v(r)dr + F[n'] = E_v[n'] \geq E_v[n] \qquad 2.68$$

The variation of the total energy at constant number of electrons

$$\delta\{E_v[n] - \mu[\int n(r)dr - N]\} \qquad 2.69$$

Leads to the Euler equation

$$\mu = \frac{\delta E_v[n]}{\delta n} = v(r) + \frac{\delta F_{HK}[n]}{\delta n} \qquad 2.70$$

where μ is the Lagrange multiplier corresponding to the chemical potential (equivalent to the negative of the electronegativity).

The functional $F_{HK}[n]$ is defined exclusively for trial densities n(r) that are classified as v-representable. A density is considered v-representable if it corresponds to the ground-state electron density derived from a many-electron wave function of a Hamiltonian featuring a local (multiplicative) external potential.

2.7.1.3. Density Functional Theory and the Kohn-Sham Equations

DFT is a computational method employed to model molecular systems by utilizing energy density rather than the wave function. The Hohenberg-Kohn theorem establishes that the observables of a system are functionals of the ground state density, $\rho_{gs}(r)$. Consequently, it is essential to identify methods for solving for this density, which can be achieved through the Kohn-Sham equations. Consider a system of non-interacting particles characterized by the following Hamiltonian (Cramer, 2004; Kless, 1996):

$$\widehat{H}_s = \hat{T} + \hat{v}_s = \sum_{i=1}^{n} -\frac{\nabla_i^2}{2} + v_s(r_i) \qquad 2.71$$

Where v_s is an arbitrary external potential. We can write the associated total energy of the system as a functional given by:

$$E_{vs}[\rho] = T_s[\rho] + \int d^3 r \rho(r) v_s(r) \qquad 2.72$$

While $\rho(r)$ is the system electron density. Since the particles are non-interacting, a Slater determinant can be used to approximate the ground state wave function. $\psi_{gs}(r)$ of the N particle system (Cramer, 2004; Skoromnik et al., 2017).

$$\psi_{gs}(r) = \frac{1}{\sqrt{N!}} \begin{vmatrix} \phi_1(r_1) & \phi_1(r_2) & \phi_1(r_3) & \dots & \phi_N(r_N) \\ \phi_2(r_1) & \phi_2(r_2) & \phi_2(r_3) & \dots & \phi_N(r_N) \\ \phi_3(r_1) & \phi_3(r_2) & \phi_3(r_3) & \dots & \phi_N(r_N) \\ \vdots & \vdots & \vdots & \dots & \vdots \\ \phi_N(r_1) & \phi_N(r_2) & \phi_N(r_3) & \dots & \phi_N(r_N) \end{vmatrix} \qquad 2.73$$

Where the orbitals ϕ_i are solutions to the single-particle Schrödinger equation

$$-\frac{1}{2} \nabla^2 \phi_i(r_i) + v_s(r_i) \phi_i(r_i) = \epsilon_i \phi_i(r_i) \qquad 2.74$$

The ground state density of the N-electron system is given by

$$\rho_{gs}(r) = \sum_{i=1}^{n} \left|\phi_{i(r_i)}\right|^2 \qquad 2.75$$

In this case, the HK theorem applies, and there exists a one-to-one mapping between the ground state density $\rho(r)$ and the potential $v_s(r)$. The energy of the system is given by

$$E_{s,gs}[\rho] = T_s[\rho_{gs}] + \int dr\rho(r)v_s(r) = \sum\int dr\phi_i^*(r) + \int dr\rho(r)v_s(r) \qquad 2.76$$

Consider a system of interacting electrons subjected to an external potential v(r). The ground-state electron density ($\rho(r)$) of this interacting system can be exactly reproduced by those of a fictitious auxiliary system of non-interacting particles placed under an appropriately chosen effective potential, v(r). This key insight allows the intricate many-electron Schrödinger equation to be replaced by a set of independent single-particle equations, which are far easier to solve. As a result, the computational effort required for the accurate numerical treatment of many-body systems is dramatically lowered. For the real interacting system, the total energy functional takes the form (Cramer, 2004).

$$E[\rho_{gs}] = T_s[\rho_{gs}] + v_H[\rho_{gs}] + E_{xc}[\rho_{gs}] + v[\rho_{gs}] \qquad 2.77$$

The second term $v_H[\rho_{gs}]$ is the Hartree energy (classical Coulomb energy), which is given by

$$v_H[\rho_{gs}] = \frac{1}{2}\int dr\int dr'\left(\frac{\rho_{gs}(r)\rho_{gs}(r')}{|r-r'|}\right) \qquad 2.78$$

The exchange correlation energy $E_{xc}[\rho_{gs}]$

$$E_{xc}[\rho_{gs}] = T[\rho_{gs}] - T_s[\rho_{gs}] + U[\rho_{gs}] - \frac{1}{2}\int dr\int dr'\frac{\rho_{gs}(r)\rho_{gs}(r')}{|r-r'|} \qquad 2.79$$

Differentiating the exchange-correlation energy functional with respect to the electron density yields the corresponding exchange-correlation potential.

$$v_{xc}[\rho_{gs}] = \left(\frac{\delta E_{xc}}{d\rho_{gs}}\right) \qquad 2.80$$

Although the exact form of this potential remains unknown, it can be effectively approximated in various ways tailored to specific systems. Applying the variational principle to the electron density for a system of interacting electrons yields the following relation [162], [165].

$$\frac{\delta E_{xc}}{d\rho_{gs}} + \frac{\delta v[\rho_{gs}]}{\delta \rho_{gs}} + \frac{\delta v_H[\rho_{gs}]}{\delta \rho_{gs}} + \frac{\delta E_{xc}}{d\rho_{gs}} = 0 \qquad 2.81$$

Similarly, for a system of non-interacting particles, the variation principle with respect to density yields

$$\frac{\delta E_{xc}}{d\rho_{gs}} = 0 = \frac{\delta T_s[\rho_{gs}]}{\delta \rho_{gs}} + \frac{\delta v[\rho_{gs}]}{\delta \rho_{gs}} \qquad 2.82$$

Comparing the variation principle for both interacting and non-interacting systems, we get

$$v_s(r) = v_{ext}(r) + v_H(r) + v_xc(r) \qquad 2.83$$

To attain both minimizations that result in the same electron density $\rho_s\,(r) = \rho(r)$It is established that the density of an interacting electron system subjected to an external potential $v_{ext}(r)$ can be exactly reproduced by solving the Schrödinger equation for a system of non-interacting particles in a potential $\psi_{gs}\,(r)$, contingent upon the knowledge of the exchange-correlation potential. Based on this premise, the orbitals of the non-interacting system can be derived by solving the Kohn-Sham equation, which is expressed as (Cramer, 2004; Nagy, 1998):

$$-\frac{1}{2}\,\nabla^2\phi_i(r) + v_s(r)\phi_i(r) = \epsilon_i\phi_i(r) \qquad 2.84$$

The electron density of the actual interacting system is subsequently constructed as follows:

$$\rho(r) = \sum_{i=1}^{n} |\phi_i(r)|^2 \qquad 2.85$$

The Kohn-Sham (KS) equations must be solved self-consistently, as both the Hartree potential (vH(r)) and the exchange-correlation potential. $v_{xc}\,(r)$ are dependent on the electron density $\rho(r)$. This density, in turn, is influenced by the orbitals. $\phi_i(r)$, which are determined by the effective potential $v_s(r)$. To initiate the calculation, an initial estimate of the electron density $\rho(r)$ is made. Based on this estimate, the effective potential $v_s(r)$ is computed, which leads to a solution for the KS equations $\phi_i(r)$. This solution subsequently yields a new electron density $\rho(r)$ (Capaz, 2014;

Nagy, 1998). This iterative process continues until the system converges to the correct ground state density. Upon achieving convergence, the relevant observables for the system can be calculated.

2.7.1.4. Time-Dependent Density-Functional Theory (TDDFT)

Time-Dependent Density Functional Theory (TDDFT) represents a natural extension of standard DFT, designed to describe electronic systems subjected to time-varying external potentials. This approach finds widespread application in investigations of molecule-laser interactions and excited-state dynamics. The formalism relies on several key approximations:

- The electromagnetic field is modeled classically, an assumption justified at high intensities where the photon occupation number is large.
- The dipole approximation is employed, valid when the laser wavelength significantly exceeds the spatial extent of the molecular system.

Within the typical frequency and intensity ranges considered, the magnetic component of the field is negligible, allowing the interaction to be represented solely by a time-dependent electric field.

For systems under time-dependent potentials, the Runge-Gross theorem establishes a unique (up to a purely time-dependent additive function) correspondence between the time-evolving electron density ρ (r, t) and the external potential v (r, t). Consequently, rather than tackling the full many-body time-dependent Schrödinger equation, the density evolution can be obtained by solving a set of auxiliary time-dependent Kohn–Sham equations, as expressed in Eqn. (2.95).

$$-\frac{1}{2}\nabla^2\phi_i(r,t) + v_{ks}(r,t)\phi_{i(r,t)} = i\frac{\partial}{\partial t}\phi_i(r,t) \qquad 2.86$$

In the time-dependent case, the external potential incorporates the contribution from the laser field and assumes the following form:

$$\rho v_{ks}(r,t) = v_{ext}(r) + v_H(r) + v_{xc}(r) + v_{laser}(r,t) \qquad 2.87$$

The electron density of the interacting system is constructed from the occupied time-dependent Kohn–Sham orbitals according to Eqn. (2.97):

$$\rho(r,t) = \sum_{i=1}^{n} |\phi_i(r,t)|^2 \qquad 2.88$$

The function given in Eqn. (2.97) is the density of all interacting electrons and nuclei that is used in density functional theory to determine computational parameters such as the dipole moments, HOMO energy, LUMO energy, oscillator strength, and many others.

2.7.2. Overview of Computer-Aided Drug Design (CADD)

Developing novel therapeutic agents is fundamental to modern healthcare, helping combat various diseases and improve patient outcomes worldwide. Historically, drug discovery involved lengthy and resource-intensive processes, sometimes lasting over a decade. The advent of computer-aided drug design (CADD), often termed in silico drug discovery, has dramatically accelerated these efforts by applying computational methods to enhance efficiency across multiple phases (Baldi, 2010; Hassan Baig et al., 2016). CADD integrates diverse computational approaches in drug development (Bassani & Moro, 2023). It primarily divides into structure-based drug design (SBDD), which uses known target structures, and ligand-based drug design (LBDD), which relies on properties of active compounds.

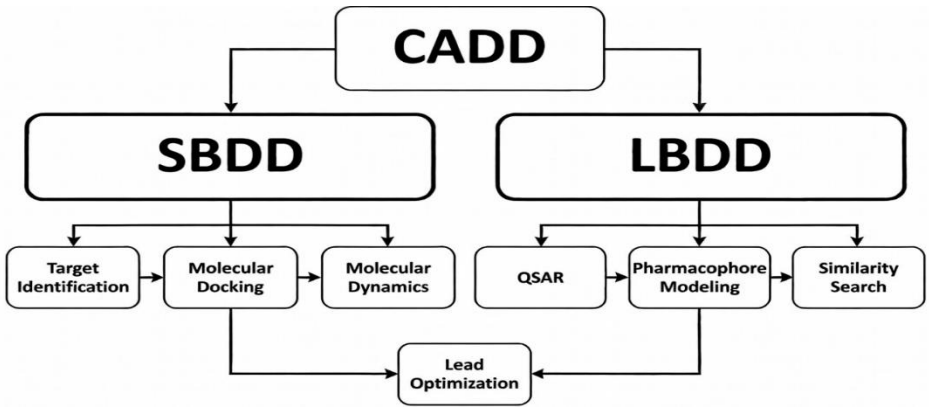

Figure 6: Categories of computer-aided drug design (CADD): structure-based drug design (SBDD) and ligand-based drug design (LBDD).

2.7.2.1. Structure-Based Drug Design (SBDD)

SBDD utilizes the 3D structure of a biological target to inform compound design (Batool et al., 2019). Prominent methods encompass: predicting interaction patterns, assessing complex stability over time, and pharmacophore modeling to define key binding features. These tools enable the precise tailoring of molecules to fit target sites effectively.

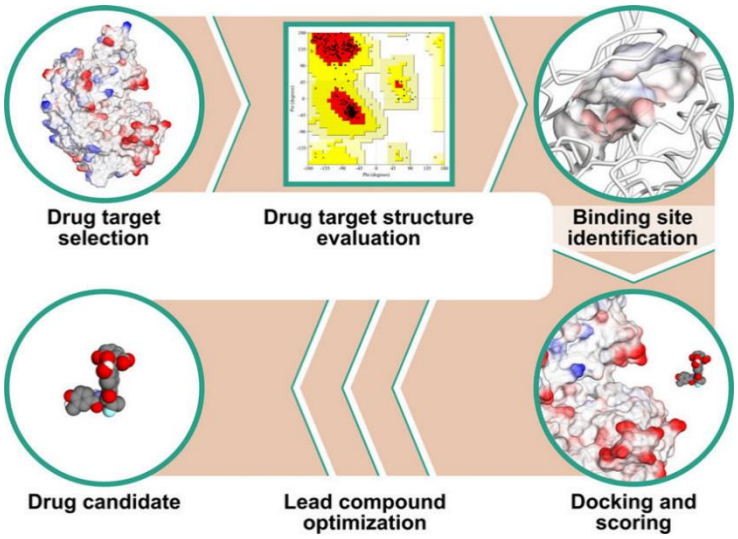

Figure 7: workflow of structure-based drug design (SBDD) (Iwaloye et al., 2023)

2.7.2.2. Ligand-Based Drug Design (LBDD)

When target structures are unavailable, LBDD draws from known ligands active against a target (Kapetanovic, 2008). Techniques include quantitative structure-activity relationships (QSAR) in 2D or 3D forms, alongside pharmacophore derivation from ligand sets. These predict activity for novel structures and support refinement (Bacilieri & Moro, 2007; Sliwoski et al., 2014).

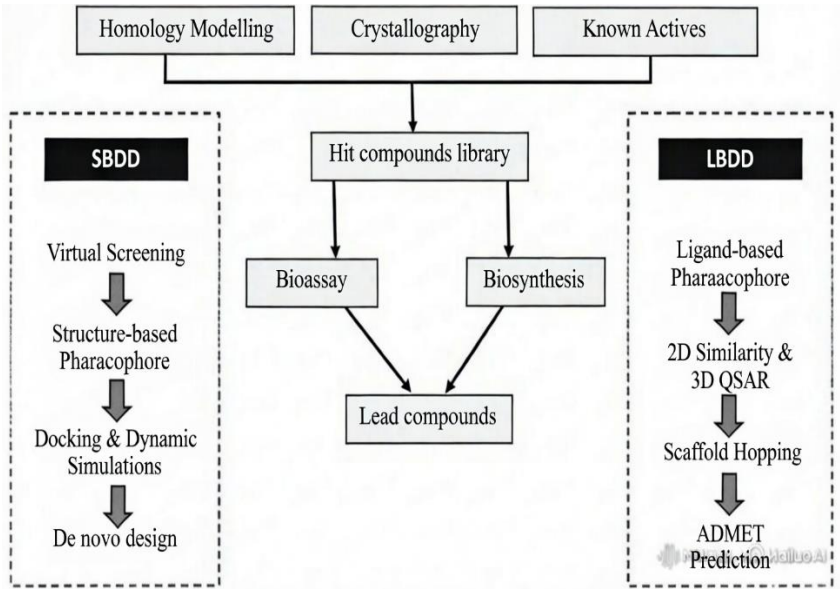

Figure 8: Ligand-based drug design (LBDD)

2.7.2.3. Molecular Docking

Molecular docking, a cornerstone of SBDD, computationally forecasts the most favorable orientation of a small molecule (ligand) binding to a macromolecule (typically a protein), resulting in a stable complex. It emulates biological recognition by seeking configurations with minimal binding free energy, accounting for various non-covalent interactions like hydrogen bonds, hydrophobic effects, and electrostatic forces (Agarwal & Mehrotra, 2016).

This approach is indispensable for rational design, allowing atomic-level insight into binding requirements and aiding creation of compounds with optimized efficacy and reduced off-target effects (Dastmalchi et al., 2016).

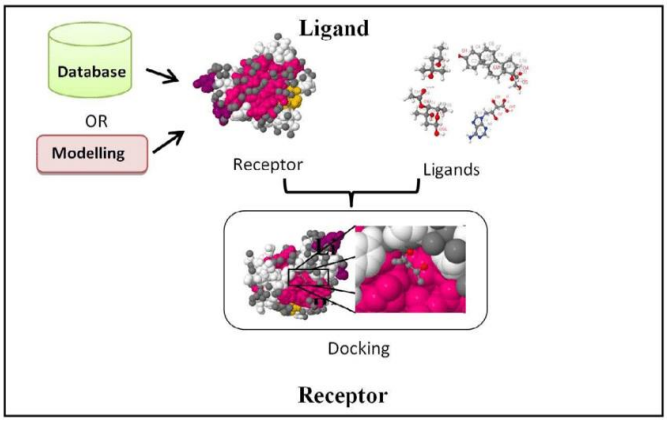

Figure 9: molecular docking flow chart (Ferreira et al., 2015)

2.7.2.4. Classification of Molecular Docking Methods

Docking approaches are classified according to the level of structural flexibility they accommodate. In rigid docking, both the receptor and ligand are treated as fixed, inflexible entities, with optimization limited to their translational and rotational alignment. Semi-flexible docking, which represents the most widely used method, allows the ligand to explore different conformations while keeping the receptor rigid, thereby achieving a favorable compromise between predictive accuracy and computational speed. Fully flexible docking, by contrast, incorporates conformational freedom for both the receptor and ligand, delivering the highest realism but requiring substantially greater computational resources (Chaudhary & Mishra, 2016; Mani et al., 2016).

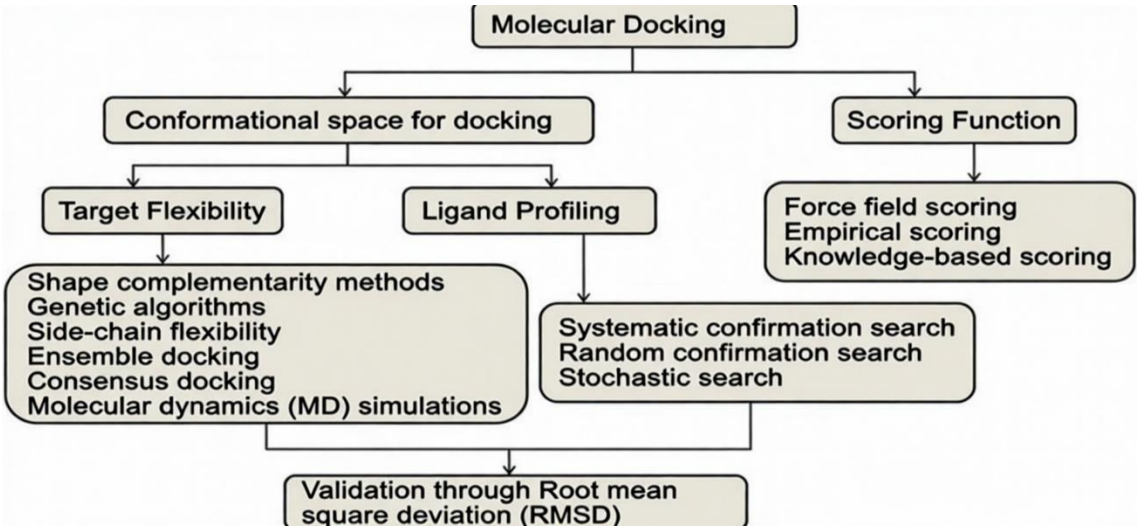

Figure 10: Step-by-step flowchart outlining the docking pipeline.

Docking plays a pivotal role in:

- Virtual high-throughput screening to pinpoint promising hits from vast libraries.
- Refinement of leads by exploring binding variants for improved properties.
- Environmental applications, such as predicting pollutant degradation by enzymes.
- Additional roles in site mapping, mechanism studies, and toxicity assessment [160] [162].

Docking begins with a resolved protein structure (often from crystallography or NMR) and ligand collections. Core elements are the sampling algorithm, which probes possible poses, and the scoring function, which estimates binding strength. The process aims to locate the energetically favored native-like conformation amid numerous alternatives (Sousa et al., 2013).

3. Materials and Methods

This chapter outlines the materials and methodologies applied throughout the research. Section 3.1 details the chemicals and solvents utilized in the experiments. Section 3.2 presents the apparatus and instruments employed. Section 3.3 describes the overall experimental approaches, including specific subsections: the techniques used to examine Solvatochromic effects on the drugs (Section 3.3.1), investigation of the photophysical properties of drugs in various solvents (Section 3.3.2), the methods for studying interactions between the drugs and caffeine (Section 3.3.3), and the quantum chemical computation protocols (Section 3.3.4).

3.1. Solvents and Chemicals

All chemicals and solvents used in this study were of analytical grade or higher purity and were employed without further purification. Methylene blue (molecular weight: 285.14 g/mol, 95% purity) was used to calculate the fluorescence quantum yield of MF-HCl. MF-HCl (molecular weight: 162.63 g/mol) and caffeine were procured from reputable local and international suppliers. Metformin hydrochloride served as the primary compound for investigating Solvatochromic behavior, photophysical properties, and its molecular interactions with caffeine. Various solvents: acetonitrile, methanol, ethanol, 2-propanol, 1-propanol, glycerol, and deionized water were used to examine the influence of solvent polarity on the absorption and emission characteristics of metformin hydrochloride.

3.2. Apparatus, Instruments, and Software

The experimental work in this dissertation required several apparatus and specialized instruments for the physicochemical characterization of metformin hydrochloride, its Solvatochromic behavior, photophysical properties, and its interaction with caffeine.

Volumetric flasks, measuring cylinders, pipettes, a magnetic stirrer with a hot plate, spatula, beakers, aluminum foil, and a cuvette are some of them. The masses of MF-HCl, methylene blue, and CAF were measured by a digital balance with an accuracy of 0.0001g.

UV-Visible Spectrophotometer (An ISO 9001): used to record absorption spectra from which molar absorptivity determination, investigation of Solvatochromic shifts, and evaluation of

ground-state interactions between metformin hydrochloride and caffeine in various solvents were performed. Fluorescence Spectrophotometer (Agilent, Malaysia): Employed to acquire excitation and emission spectra from which fluorescence intensity, fluorescence quantum yields, fluorescence lifetimes, and parameters such as radiative and non-radiative decay rates, oscillator strength, transition dipole moments, and absorption cross-sections were determined. Fourier Transform Infrared (FTIR) Spectrometer (Nicolet ISO50): Utilized to obtain vibrational spectra of metformin hydrochloride and its mixtures with caffeine, providing insights into potential intermolecular interactions through changes in characteristic IR bands. Dynamic Light Scattering (DLS) (Malvern Panalytical) Instrument and Zeta Potential Capability (Zetasizer Ver. 8.02, Serial Number: MAL1149420): applied to measure particle size distribution and surface charge (zeta potential) of MF-HCl in solution, particularly to examine any aggregation behavior influenced by CAF addition.

Computational and data analysis tasks were supported by the following software packages: Gaussian 09: Employed for density functional theory (DFT) calculations to optimize molecular geometries of metformin hydrochloride in different solvent environments (using polarizable continuum model, PCM), predict frontier molecular orbital energies (HOMO and LUMO), calculate energy band gaps, dipole moments, electron density distributions, and theoretical oscillator strengths. Molecular Docking Software (Auto Dock Vina and associated tools such as Auto Dock Tools and PyMOL): applied to perform computational docking studies to explore the binding mode, binding affinity, and potential interaction sites between metformin hydrochloride and caffeine, complementing the experimental spectroscopic findings. Origin Pro 2021: Used for comprehensive data processing, spectral analysis, curve fitting, statistical evaluation, and graphical representation of experimental results, including Solvatochromic correlations and photophysical parameter calculations.

3.3. Methods

3.3.1. Solvatochromic Effects of MF-HCl Drug

The Stock solutions of metformin hydrochloride were prepared and stored in darkness in the refrigerator for steady state fluorescence and UV/vis absorption measurements. To investigate the Solvatochromic effects of the antidiabetic drugs metformin hydrochloride, the maximum emission and excitation wavelength, fluorescence, and absorbance intensity observed at room temperature of each solvent (Acetonitrile, Methanol, deionized Water, Ethanol, 2-Propanol, 1-Propanol,

Glycerol) were recorded using UV–vis and fluorescence spectroscopy. Solvent polarity functions were calculated using different literature values of the dielectric constant and refractive index of the solvents. The Solvatochromic effects were investigated by the Lippert-Mataga equation (2.1), Bakhshiev equation (2.2), and Kawski Chamma-Viallet equation (2.3). From the slope of the graph of solvent polarity functions and Bakhshiev, Kawski-Chamma Viallet, and Lippert-Mataga equations, ground and excited dipole moments were determined (Woldegiorges et al., 2021).

3.3.2. Photophysical Properties of MF-HCl in Solvents

Photophysical properties of the antiviral drug metformin hydrochloride were investigated from the recorded maximum absorption and emission wavelength observed in polar solvents (Acetonitrile, Methanol, deionized Water, Ethanol, 2-Propanol) and non-polar solvents (Benzene, Toluene, Chloroform, dichloromethane) using UV-vis spectroscopy and fluorescence spectroscopy. The photophysical properties such as quantum yield, fluorescence lifetime, radiative decay, oscillator strength, absorption cross section, and transition dipole moments in different solvents were determined using Eqns. (2.13), (2.14), (2.15), (2.18), (2.25), and (2.26), respectively.

3.3.3. Fluorescence Quenching of MF-HCl with CAF

Stock solutions of MF-HCl solution and CAF were prepared in deionized water for fluorescence emission, UV/Vis absorption, FTIR, DLS, and Zeta potential measurements. Fluorescence emission spectra measurements were carried out by successive addition of CAF solution to a fixed amount of MF-HCl solution. The mixed solutions were subjected to ultrasonic vibration for 30 min, and fluorescence spectral measurements were carried out at various temperatures by setting emission slit widths (10) and the scan speed medium. Similarly, the UV/vis absorption spectra of the MF-HCl were recorded by successive addition of CAF solution to the fixed amount of MF-HCl solution by setting excitation slit widths (10) and the scan speed to medium. For FTIR, DLS, and Zeta potential measurements, MF-HCl and MF-HCl –CAF were prepared in powder form by evaporating water using a hot magnetic stirrer and recording the spectra of powder samples at 298 K temperature.

To investigate quenching efficiency of drug-Caffeine interactions, the well-known Stern-Volmer Eqn. (2.41) was used. The binding site and binding constant values were derived from the slope and y-intercept of the linear fit. This linear fit was obtained by applying the equilibrium equation between free and bound molecules, Eqn. (2.47) to the experimental data. The values of the binding

site and binding constant were determined from the slope and y-intercept of the linear fit of the equation of the equilibrium between free and bound molecules, Eqn. (2.47) to the experimental data. The thermodynamic parameters were determined from the slope and intercept of the linear fit of the Van't Hoff Eqn. (2.43-2.45). The resonance energy transfer efficiency of molecules was determined by FRET theory using the data recorded from fluorescence spectra of pure and caffeine mixed drugs by applying Eqn. (2.52). In addition, the critical distance, the effect of the spectral overlap between the excitation spectrum of the acceptor and the emission spectra of the donor, was determined by using Eqns. (2.53) and (2.54), respectively. To analyze the steady-state data for all measurements, Origin software was deployed.

3.3.4. Quantum Chemical Calculations

Theoretical calculations were conducted utilizing the Gaussian 09 program to investigate the structural and electronic characteristics of metformin hydrochloride. The molecular geometry in the ground state was optimized without imposing symmetry restrictions, applying Density Functional Theory (DFT) with the B3LYP exchange-correlation functional and the 6-31G+(d,p) basis set.

The influence of solvation was accounted for through the Integral Equation Formalism variant of the Polarizable Continuum Model (IEFPCM), which effectively mimicked the diverse solvent environments used experimentally, ranging from highly polar protic solvents (such as water, methanol, ethanol, and 2-propanol) and polar aprotic (acetonitrile) to non-polar ones (benzene, toluene, chloroform, and dichloromethane). Harmonic vibrational frequency computations were performed on all optimized geometries to ensure they represented genuine potential energy minima, as evidenced by the lack of imaginary frequencies.

To gain a deeper understanding of intermolecular associations, docking simulations were executed to model the binding of metformin hydrochloride with caffeine and their interactions with the AMP-activated protein kinase (AMPK) target. The crystal structure of AMPK was downloaded from the Protein Data Bank (PDB entry appropriate for the subunit of interest). Initial coordinates for metformin hydrochloride (in protonated form) and caffeine were sourced from chemical databases and subsequently refined via DFT optimization at the B3LYP/6-31G+(d,p) level within Gaussian 09.

Docking was performed employing Auto Dock Vina, with molecular preparation handled through Auto Dock Tools. Standard procedures involved the removal of crystallographic waters, addition of polar hydrogens, and assignment of Gasteiger partial charges. For unbiased screening, blind docking was implemented by setting grid dimensions to cover the full extent of the smaller molecule or the known binding pocket of AMPK. Individual and combined docking scenarios included:

- Metformin hydrochloride binds to caffeine.
- Metformin hydrochloride docking into AMPK.
- Caffeine docks into AMPK.
- Simultaneous presence of both molecules as ligands at the AMPK site.

Each docking experiment consisted of 100 genetic algorithm runs to ensure thorough conformational sampling. The most favorable binding conformation was identified based on the lowest predicted binding free energy (expressed in kcal/mol).

Resulting complexes were examined in detail using PyMOL and Discovery Studio software to characterize specific non-covalent contributions, such as conventional and carbon-hydrogen bonds, π-π stacking, amide-π interactions, hydrophobic contacts, and electrostatic forces. These theoretical binding models supported the interpretation of experimental fluorescence quenching phenomena and offered potential mechanistic explanations for synergistic effects on AMPK modulation.

4. Results and Discussions

This chapter discusses the key findings and their interpretation of the dissertation work. The first subsection, Section 4.1, examines the influence of solvent polarity, including fluorescence emission and UV-visible absorption spectra of metformin hydrochloride, estimation of ground and excited-state dipole moments of metformin hydrochloride based on Solvatochromic data, and density functional theory (DFT) computations. Section 4.3 explores how solvent polarity affects the overall photophysical behavior of MF-HCl, and Section 4.4 presents the calculation of optical transition probabilities. Section 4.5 analyzes the fluorescence quenching of MF-HCl induced by CAF including binding constants and number of binding sites, thermodynamic parameters and nature of binding forces in the interaction between metformin hydrochloride and caffeine, UV-visible absorption spectroscopy results for the MF-HCl-caffeine system, Fourier-transform infrared (FTIR) spectroscopy spectra, results of zeta potential and dynamic light scattering (DLS) experiments, and Förster resonance energy transfer (FRET) observations. While section 4.6 discusses DFT Analysis of MF-HCl Drug, section 4.7 outlines the results of molecular docking simulations.

4.1. Solvatochromic Effects

4.1.1. Effect of Solvent Polarity on Fluorescence Emission and UV-Vis Absorption Spectra of MF-HCl

Fig. 11a and 11b show the UV-Vis absorption and fluorescence emission spectra, respectively, of metformin hydrochloride in solvents of varying polarity. These measurements were performed using different solvents with dielectric constants spanning the range of 18.2 to 80.1 and refractive indices between 1.332 and 1.472.

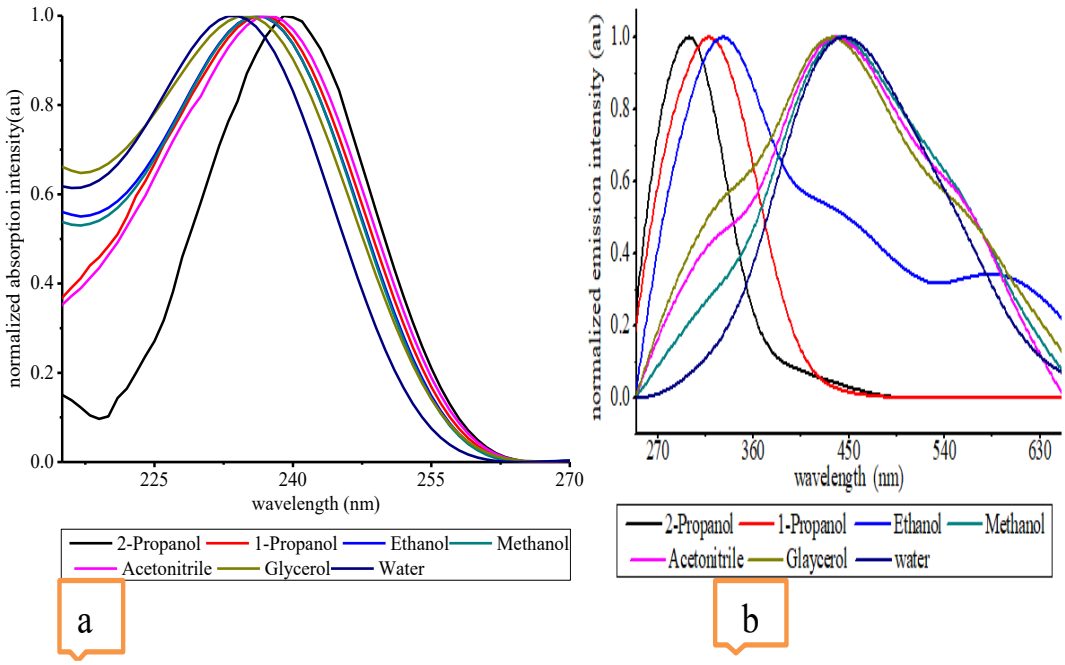

Figure 11: UV/Vis absorption (a), Fluorescence emission (b) spectra of MF-HCl in different solvents

The UV-Vis absorption maximum peak of MF-HCl appeared in the wavelength range of 220–260 nm. As shown in Fig. 11a, increasing the solvent polarity resulted in a noticeable blue shift. This hypsochromic shift with rising solvent polarity suggests an n → π* electronic transition associated with the nitro group (Design, 2023; Domecq et al., 2015; Sola & Vuj, 2024). The blue shift observed upon transitioning from less polar to more polar solvents arises because the non-bonding orbital is more effectively stabilized in polar environments through mechanisms such as hydrogen bonding. Similar observation was reported for nitro-substituted pyridine[3,4-c] coumarins, where the observed effects were attributed to n → π* transitions (Sıdır, 2015).

In contrast, the fluorescence emission spectra (Fig. 11b) exhibited a red shift with increasing solvent polarity. This bathochromic shift indicates that the excited state of metformin hydrochloride is more strongly stabilized in polar solvents compared to non-polar ones (Domecq et al., 2015; Sola & Vuj, 2024). The substantial shift in the emission spectrum highlights a significant difference in molecular geometry between the ground and excited states. The absorption maxima, expressed in wavenumbers, shifted from 42,194 cm^{-1} in 2-propanol to 42,725 cm^{-1} in more polar solvents. Correspondingly, a pronounced emission shift of 531 cm^{-1} was recorded between 2-propanol and water.

4.1.2. Determination of Ground and Excited State Dipole Moments of MF-HCl via Solvatochromic Methods

Measuring the UV-Vis absorption and fluorescence emission spectra in a variety of solvents provides reliable results to estimate the ground (μ_g) and excited (μ_e) states dipole moment (Bozkurt et al., 2017). The dipole moments of MF-HCl in its ground and excited states were calculated based on plots of absorption and emission maxima against solvent polarity parameters, as illustrated in Figs. 12–15. Results showed that the excited-state dipole moment (μ_e) is substantially larger than the ground-state value (μ_g). This marked difference between the two states can be attributed to intramolecular charge transfer, specific solute–solvent interactions, and hydrogen bonding effects (Woldegiorges et al., 2021). Furthermore, the excited-state dipole moments obtained from the Lippert–Mataga, Bakhshiev, Kawski–Chamma–Viallet, and solvent polarity parameter models vary from one another. These discrepancies arise from the distinct approximations and assumptions inherent to each theoretical approach (Woldegiorges et al., 2021).

In the Lippert–Mataga approach, solute polarizability is disregarded, leading to higher estimated dipole moments compared to other methods. This overestimation stems from the equation's omission of the polarizability contribution from the solute molecule (Krawczyk et al., 2020). Previous studies have similarly noted that the Lippert–Mataga model tends to yield larger changes in dipole moment than those derived from other techniques (Meneses et al., 2015; Sola & Vuj, 2024). The excited-state dipole moment obtained via the solvent polarity parameter method is typically lower than values from the Lippert–Mataga or Bakhshiev models. This difference likely arises because the former two approaches overlook specific solvation effects, such as hydrogen bonding and other molecular interactions, which are explicitly incorporated in the solvent polarity parameter treatment (Patil et al., 2019).

Tables 1 and 2 list the spectral shifts of $(\nu_\alpha - \nu_f)$ and $\left(\frac{\nu_\alpha + \nu_f}{2}\right)$ of MF-HCl, along with the corresponding solvent polarity parameters: $f(\varepsilon, n)$, $f_1(\varepsilon, n)$, $F_2(\varepsilon, n)$, and E_T^N, for various solvents. Seven solvents of differing polarity were employed, with dielectric constants ranging from 18.2 to 80.1.

Table 1: Calculated values of solvent polarity functions in different solvents

solvents	n	ε_r	F_{LM}	F_{BAC}	F_{KCV}	E^N_T
2-Propanol	1.377	18.2	0.273	0.764	0.639	0.546
1-Propanol	1.384	20.33	0.225	0.780	0.651	0.617
Ethanol	1.361	24.5	0.289	0.813	0.653	0.654
Methanol	1.328	32.7	0.309	0.855	0.651	0.762
Acetonitrile	1.344	37.5	0.306	0.863	0.666	0.460
Glycerol	1.472	46.5	0.265	0.842	0.741	0.812
Water	1.332	80.1	0.320	0.914	0.683	1.000

Table 2: Peaks of the absorption and emission spectra of metformin hydrochloride in solvents with different polarity

solvents	$V_a(cm^{-1})$	$V_f(cm^{-1})$	v_a-v_f (cm^{-1})	v_a+v_f (cm^{-1})	$(v_a+v_f)/2(cm^{-1})$
2-Propanol	41841.0043	33112.5828	8728.42140	74953.5870	37476.7935
1-Propanol	42194.0928	30769.2308	11424.8620	72963.324	36481.662
Ethanol	42194.0928	29850.7463	12343.3466	72044.839	36022.4196
Methanol	42372.8814	22371.3647	20001.517	64744.2460	32372.1230
Acetonitrile	42016.8067	22624.4344	19392.3723	64641.2411	32320.6206
Glycerol	42553.1915	22779.0433	19774.1482	65332.2348	32666.1174
Water	42735.0427	22371.3647	20363.6781	65106.4074	32553.2037

Fig. 12 shows the graphs of $(\nu_\alpha - \nu_f)$ versus $f(\varepsilon, n)$, Fig. 13 shows the graphs of $(\nu_\alpha - \nu_f)$ versus $f_1(\varepsilon, n)$, and Fig. 14 shows the graphs of $\left(\frac{\nu_\alpha + \nu_f}{2}\right)$ versus $F_2(\varepsilon, n)$ of MF-HCl. Another effective approach for determining dipole moments relies on the empirical solvent polarity parameter. E_T^N. Compared to conventional bulk polarity functions, this parameter demonstrates superior correlation with solvatochromic shifts (Hospital et al., 2015; Rena et al., 2013). The E_T^N scale accounts for a broader range of intermolecular forces beyond simple dielectric effects and reduces uncertainties associated with estimating the Onsager cavity radius. Fig. 15 presents the linear plot of Stokes shift $(\bar{\nu}_a - \bar{\nu}_f)$ versus E_T^N for MF-HCl. The analysis yielded a high correlation coefficient $(R^2 = 0.89)$, indicating excellent linearity. This strong relationship confirms that E_T^N parameter effectively captures both general solute-solvent interactions and specific contributions from hydrogen bonding.

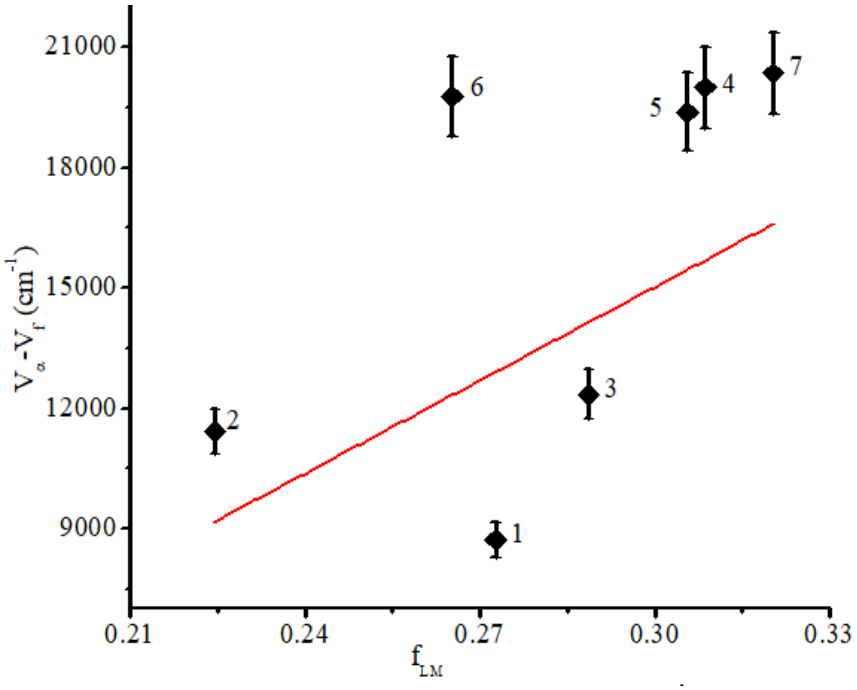

Figure 12: Plot of Stokes shift versus solvent polarity parameter for MF-HCl using the Lippert–Mataga model. The solvents used are: (1) 2-Propanol, (2) 1-Propanol, (3) Ethanol, (4) Methanol, (5) Acetonitrile, (6) Glycerol, (7) Water.

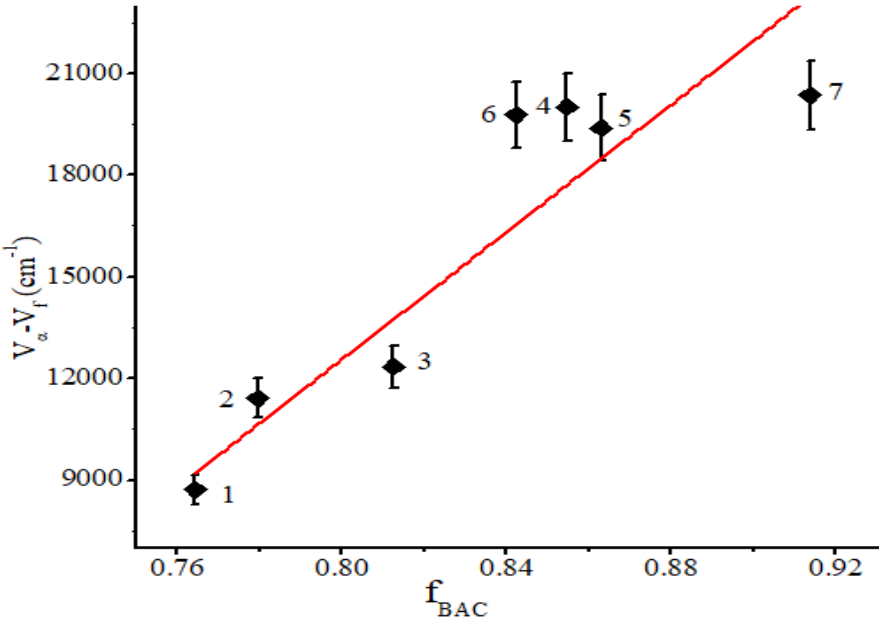

Figure 13: Plot of Stokes shift versus solvent polarity parameter for MF-HCl using Bakhshiev's model. The solvents used are: (1) 2-Propanol, (2) 1-Propanol, (3) Ethanol, (4) Methanol, (5) Acetonitrile, (6) Glycerol, (7) Water.

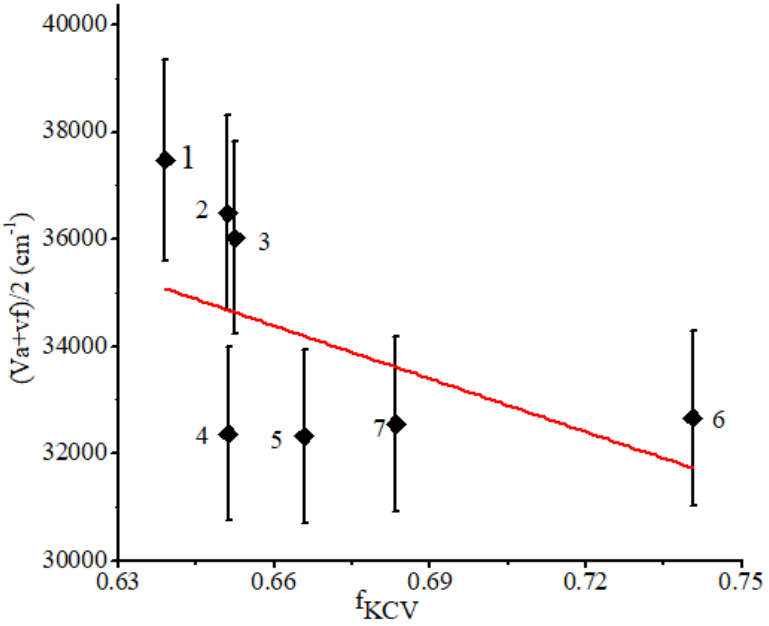

Figure 14: Plot of Stokes shift versus solvent polarity parameter for MF-HCl using the Kawski- Chamma-Viallet's model. The solvents used are: (1) 2-Propanol, (2) 1-Propanol, (3) Ethanol, (4) Methanol, (5) Acetonitrile, (6) Glycerol, (7) Water.

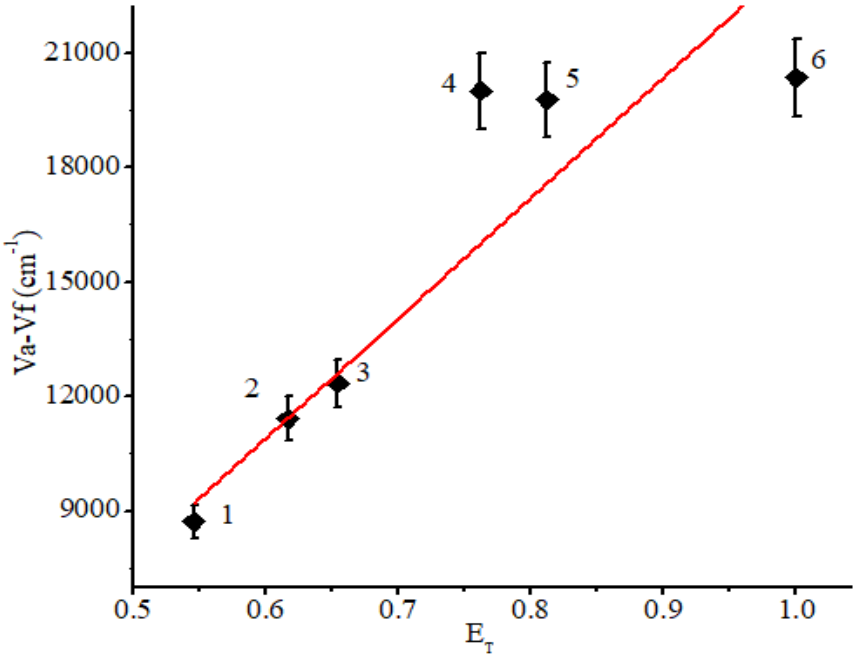

Figure 15: Plot of Stokes shift versus solvent polarity parameter for MF-HCl using the Reichardt's model. The solvents used are: (1) 2-Propanol, (2) 1-Propanol, (3) Ethanol, (4) Methanol, (5) Glycerol, (6) Water.

Linear regression analysis was performed on the Solvatochromic data, yielding straight-line fits. The resulting slopes, intercepts, and correlation coefficients are summarized in Table 3. Though the maximum feasible number of solvents was employed to achieve satisfactory linear correlations, resulting in correlation coefficients (R^2) ranging from 0.56 to 0.91, deviations were observed in the results. These deviations from perfect linearity can be attributed to specific short-range interactions between the solute and solvent molecules (Painagoni & Patil, 2013).

Table 3: Statistical correlation of solvent spectral shifts of metformin hydrochloride

Correlation Model	Slope (cm^{-1})	Intercept (cm^{-1})	Correlation coefficient (R^2)
Lippert- Mataga	9280.77	1032.90	0.61
Bakhshiev	8731.97	5671.34	0.91
Kawski-Chamma-Viallet	3695.31	5899.49	0.56
Reichardt	2823.13	5216.76	0.89

The calculated ground and excited state dipole moment using Eqn. (2.27) and Eq. (2.28) are (μ_g = 1.87 D) and (μ_e = 4.61 D), respectively. Similarly, the dipole moments calculated using Lippert-Mataga's equation (2.1), Bakhshiev's equation (2.2), Kawaski Chamma-Viallet's equation (2.3) and Reichardt's equation (2.14) are shown in Table 4.

Table 4: Ground state and excited state dipole moments of metformin hydrochloride

$a^a(A^o)$	$\mu_g{}^b$(D)	$\mu_e{}^c$(D)	$\mu_e{}^d$(D)	$\Delta\mu_g{}^e$(D)	$\mu_e{}^h$(D)	$\mu_e{}^i$(D)	$\mu_e{}^j$(D)	$\Delta\mu^k$(D)	$(\mu e/\mu g)^l$(D)
3.642	1.87	4.61	8.27	2.74	8.55	8.34	6.08	6.4	2.47

a Calculated value of Onsager cavity radius in angstrom, b experimental μ_g value calculated by (2.10), c experimental μ_e value calculated by (2.11), d experimental μ_e calculated from empirical solvent polarity function, e $\Delta\mu$ calculated from (2.10)and (2.11), h μ_e calculated from (2.7), i μ_e calculated from (2.8), j μ_e calculated from (2.9), k $\Delta\mu$ calculated from (2.15), and l μ_e/μ_g ratio of excited and ground states dipole moments calculated from (2.12).

4.2. Photophysical Properties of MF-HCl

4.2.1. Solvent Polarity Effects

The photophysical properties of MF-HCl are markedly influenced by solvent polarity. The fluorescence quantum yield (Φ_f), determined according to Eqn. (2.16) demonstrates a clear dependence on the polarity of the solvent. As solvent polarity increases, the quantum yield generally decreases. This trend is largely due to the reorganization of solvent molecules surrounding the solute, which modifies both the absorption and fluorescence spectra of the compound (Woldegiorges et al., 2021). Polar solvents are known to quench fluorophores through hydrogen bonding interactions (Bozkurt et al., 2017). Consequently, less polar (low-polarity) solvents yield higher quantum efficiencies compared to highly polar ones. The elevated quantum yield observed in low-polarity solvents can be explained by the reduced solute–solvent interactions, which favor faster radiative decay processes (Nad & Pal, 2001).

The fluorescence lifetime (τ_f) of MF-HCl, calculated using Eqn. (2.20), also exhibits significant variation with changing solvent polarity. These differences reflect the sensitivity of the excited-state dynamics to the local microscopic environment provided by the solvent. Distinct solute-solvent interactions in different media lead to noticeable changes in fluorescence lifetime values

(Panja, 2021). Furthermore, the rates of radiative (κ_r) and non-radiative (κ_{nr}) decay processes evaluated using Eqns. (2.17) and (2.18) show distinct behavior depending on solvent polarity. The non-radiative decay rate tends to be lower in low-polarity solvents compared to high-polarity ones. In contrast, highly polar solvents are associated with a reduced radiative decay rate, which is likely attributable to emission originating predominantly from a locally excited electronic state (Lakowicz, 2000). This comprehensive solvent-dependent behavior highlights the important role of the surrounding medium in modulating the excited-state properties of MF-HCl.

Table 5: Photophysical properties of MF-HCl in different solvents

Solvents	solvent polarity (Δf)	ϕ_f	$\kappa_r \times 10^8 (s^{-1})$	$\kappa_{nr} \times 10^8$ (s^{-1})	$\tau_o\ (ns)$	$\tau\ (ns)$
2-Propanol	0.546	0.35	10.3	19.9	0.97	0.50
1-Propanol	0.617	0.34	8.55	22.2	1.17	0.45
Ethanol	0.654	0.33	6.10	25.1	1.64	0.40
Methanol	0.762	0.33	3.67	9.65	2.73	1.04
Acetonitrile	0.46	0.30	2.85	6.92	3.51	1.45
Glycerol	0.812	0.28	10.9	12.8	0.92	0.78
Water	1.00	0.24	3.91	7.53	2.55	0.13

4.2.2. Influence of Concentration on the Photophysical Properties of MF-HCl

Fig. 16 illustrates the concentration-dependent photophysical properties of MF-HCl. As the concentration of the drug increases, a clear reduction in the fluorescence quantum yield is observed. Within the studied concentration range, the radiative decay rate also shows a substantial decrease. This behavior is primarily attributed to the formation of molecular aggregates, particularly dimers, which significantly alter the photophysical characteristics of the compound.

Conversely, the fluorescence lifetime (τ_f) increases with rising concentration. The extended lifetime suggests that the excited state of MF-HCl persists for a longer duration under these

conditions. At the same time, the non-radiative decay rate becomes more pronounced as concentration increases. These changes are most likely caused by the formation of dimers along with other intermolecular interactions occurring within the molecular assemblies (Panja, 2021). The dimerization process plays a key role in reducing the quantum yield, rather than directly inducing classical self-quenching of the fluorescence emission. Overall, the photophysical response of MF-HCl is governed by the intricate equilibrium and interactions between monomeric and dimeric species in solution.

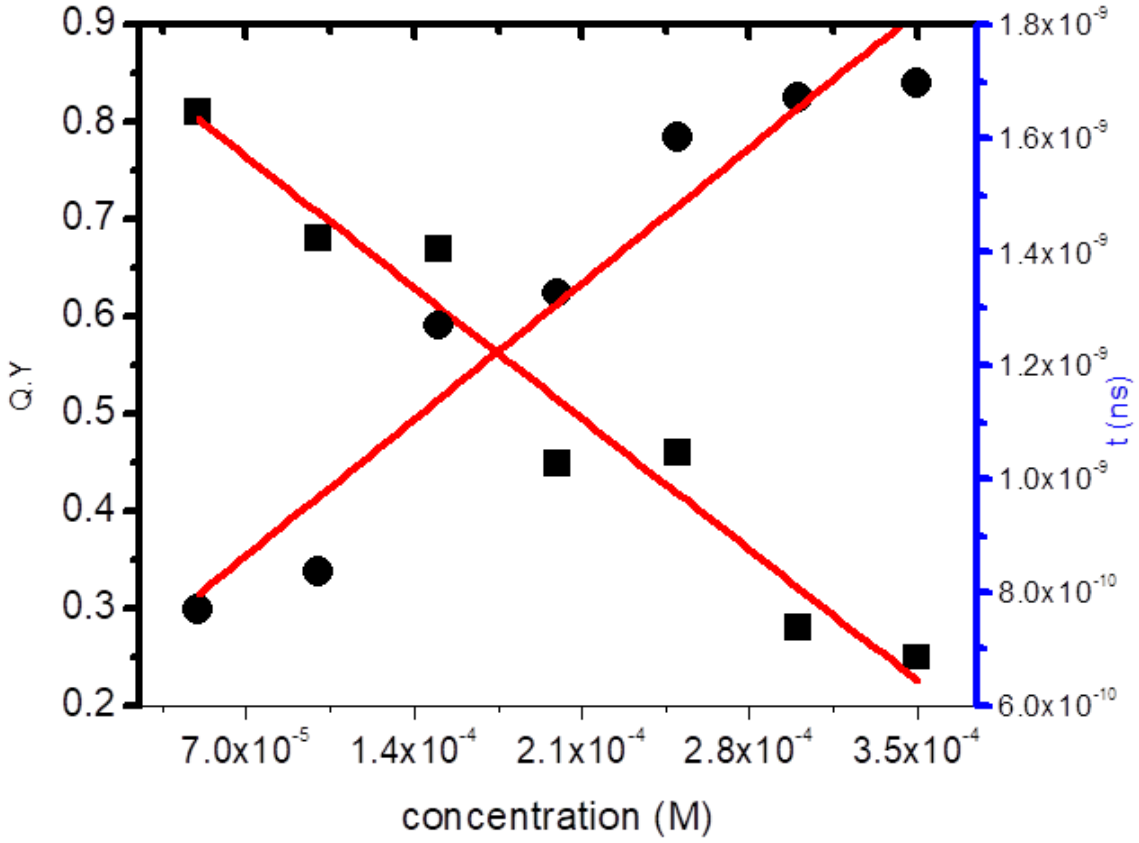

Figure 16: Quantum yield (Φ_f) and fluorescence lifetime (τ_f) of MF-HCl as a function of concentration.

Fig. 17 demonstrates that, at low concentrations, the fluorescence intensity of MF-HCl increases in a linear fashion with concentration. This linear dependence confirms that the emitted fluorescence arises primarily from isolated, individual MF-HCl molecules. However, as the concentration is further increased, the emission intensity concentration relationship deviates from linearity, accompanied by a noticeable bathochromic (red) shift in the emission spectrum. These changes are indicative of the formation of molecular aggregates. The aggregation process promotes self-quenching of the fluorescence, resulting in a progressive reduction in emission intensity at

higher concentrations. The inset plot in Fig. 18 highlights this behavior more clearly: the fluorescence intensity of MF-HCl rises linearly up to approximately 2.1×10^{-5} M, beyond which it begins to decline. This decrease at elevated concentrations is likely due to inner filter effects and dynamic quenching (Woldegiorges et al., 2022).

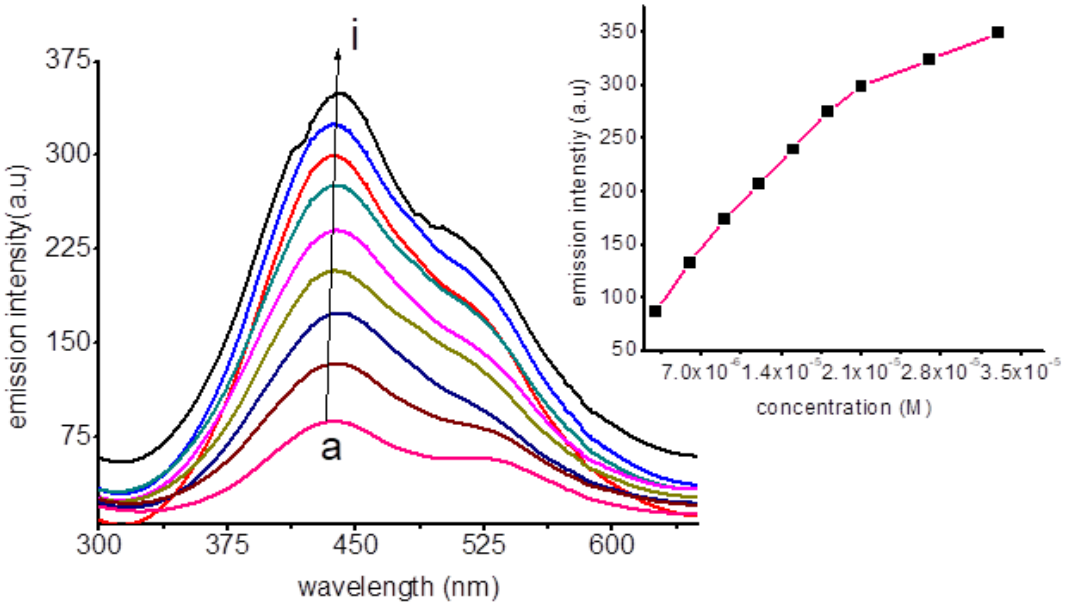

Figure 17: Emission spectra versus wavelength variation of metformin hydrochloride in a) $(3 \times 10^{-6}$, b) 6×10^{-6}, c) 9×10^{-6}, d) 1.2×10^{-5}, e) 1.5×10^{-5}, f) 1.8×10^{-5}, g) 2.1×10^{-5}, h) 2.7×10^{-5}, and i) 3.3×10^{-5}) M concentration

4.2.3. Optical Transition Probability of MF-HCl

Understanding the integrated absorption cross-section, oscillator strength, and transition dipole moment is fundamental to elucidating the nature of electronic transitions in molecules. These parameters, derived from the analysis of absorption spectra using Eqns. (2.21–2.29), serve as key indicators for evaluating and comparing the intensity of electronic transitions across different solvent environments (Belay, 2010).

This work's results indicate that the oscillator strength of MF-HCl reaches its highest value in glycerol as compared to the other solvents examined (Table 6). This notable enhancement can be explained by the accelerated absorption process of MF-HCl in highly polar media. Since oscillator strength reflects the probability of photon absorption, it is strongly influenced by the polarity of the surrounding solvent. This finding is consistent with results from spectra observations, in which

the absorption spectra of MF-HCl displayed a progressive blue shift with increasing solvent polarity (Asemare et al., 2023; Sherefedin et al., 2023).

In solvents of low polarity, MF-HCl exhibits relatively lower transition probabilities, whereas in highly polar solvents, these probabilities are markedly increased at ambient temperature. Such solvent-dependent trends underscore the significant role of the medium's polarity in modulating the electronic transitions of MF-HCl. It is worth noting that similar behavior, namely, absorption coefficients and larger transition dipole moments in polar solvents, has been reported in investigations of coumarin and anthracene derivatives (Fahmy et al., 2018).

Table 6: Optical transition probability of metformin hydrochloride

solvents	Concentration (mol/L)	Abs_{max}	f	α (cm^{-1})	$\sigma_t \times 10^{-18}$ (cm/molecule)	$\mu_{km} \times 10^{-31}$ (C.m)
2-Propanol	2×10^{-4}	0.92	0.103	10968.09	2.2384	2.388
1-Propanol	2×10^{-4}	0.81	0.098	10489.4	2.1407	2.32938
Ethanol	2×10^{-4}	0.9	0.138	14746.23	3.0094	2.715
Methanol	2×10^{-4}	0.77	0.115	12272.71	2.5046	2.47967
Acetonitrile	2×10^{-4}	0.65	0.104	8480.219	1.7307	2.08418
Glycerol	2×10^{-4}	0.51	0.254	27058.11	5.5221	3.70368
Water	2×10^{-4}	0.86	0.133	14152.12	2.8882	2.65279

A: absorbance at maximum; f: oscillator strength; α: absorption coefficient; σ_t: absorption cross section; μ_{km}: transition dipole moment; kg: kilogram; C: Coulomb; m: meter; L: Littre; cm: centimeter; s: second.

4.3. Fluorescence Quenching of MF-HCl by CAF

Fluorescence quenching refers to the reduction in emission intensity caused by various mechanisms, including energy transfer, formation of ground state complexes, excited state reactions, and collisional deactivation (Lakowicz, 2014). In the present study, the influence of CAF on the fluorescence of MF-HCl was investigated. Fig. 18 presents the fluorescence emission spectra of MF-HCl recorded in the absence and presence of increasing concentrations of CAF. The results clearly demonstrate a progressive and substantial decrease in the intrinsic fluorescence intensity of MF-HCl as the concentration of CAF was raised. This marked reduction in emission intensity indicates the occurrence of a strong interaction between MF-HCl and caffeine within the

system. Notably, the shape and position of the fluorescence spectrum of MF-HCl remained essentially unchanged upon addition of CAF, with no observable spectral shift (bathochromic or hypsochromic). This suggests that the quenching process does not involve significant alteration of the emitting species' electronic environment.

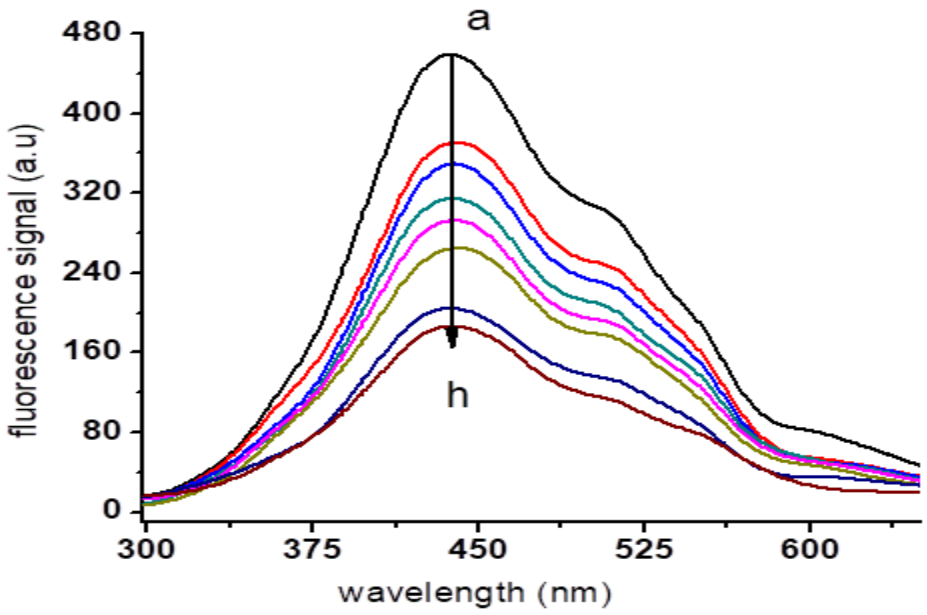

Figure 18: Fluorescence quenching spectra of MF-HCl in the presence of CAF concentration $(a)\ 0, b)\ 1\times10^{-3}, c)\ 2\times10^{-3}, d)\ 3\times10^{-3}, e)\ 4\times10^{-3}, f)\ 5\times10^{-3}, g)\ 6\times10^{-3}, h)\ 7\times10^{-3}, and\ i)\ 1\times10^{-3})M$

Furthermore, the fluorescence quenching of MF-HCl in the presence of CAF was investigated at different temperatures using Eqn. (2.43) to determine the Stern–Volmer constant (K_{SV}). The corresponding Stern–Volmer plots, presented in Fig. 19, exhibited strong linearity (with correlation coefficients of 0.98) and yielded substantial K_{SV} values, such as 534.51 ± 57 M^{-1} at 298 K. The relatively large magnitude of K_{SV} reflects a strong binding interaction between MF-HCl and CAF. The temperature dependence of the Stern–Volmer constant provides key mechanistic insight: K_{SV} decreased as temperature increased. This inverse relationship is characteristic of static quenching, where the formation of a ground-state complex is primarily responsible for the observed fluorescence reduction, rather than dynamic (collisional) quenching (Woldegiorges et al., 2022). The bimolecular quenching rate constants derived from the Stern–Volmer analysis at three different temperatures are summarized in Table 7.

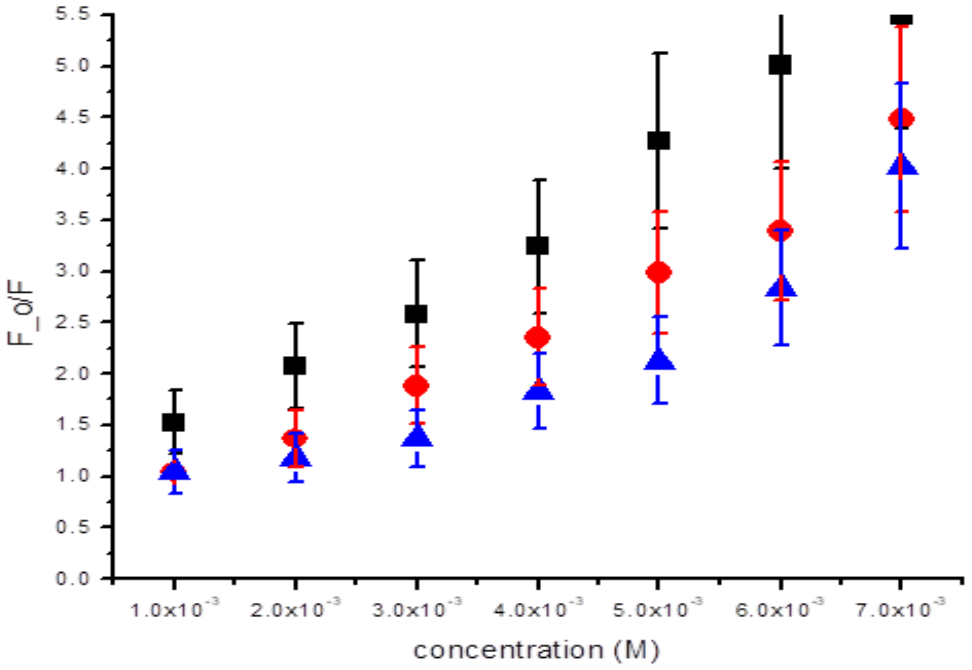

Figure 19: Stern-Volmer plot of MF-HCl quenched by caffeine via different concentrations at temperatures of 298 K (black), 310 K (red), and 318 K (blue).

Table 7:Stern-Volmer constant (K_{sv}), and correlation coefficient of MF-HCl with different temperatures

Temperature (K)	k_{sv} (M^{-1})	Regression (R)
298	534.51±57	0.98
310	526.41±29	0.93
318	395.15±70	0.84

4.3.1. Thermodynamic Characteristics and Binding Interactions Between MF-HCl and CAF

To further elucidate the nature of the interaction between MF-HCl and CAF, the thermodynamic parameters such as standard enthalpy change (ΔH°), standard entropy change (ΔS°), and standard Gibbs free energy change (ΔG°) were determined using the van't Hoff equation (Eqn. 2.43) (Gemta, 2015). These parameters were evaluated from the linear plot of ln(K) versus 1/T at three different temperatures, with the corresponding results summarized in Table 9. The calculated ΔG°

values were negative across the temperature range studied, confirming that the binding process between MF-HCl and CAF is spontaneous and thermodynamically favorable. The negative sign of ΔH° indicates that the binding reaction is exothermic, which also describes the detected decrease in the binding constant (Ka) with increasing temperature. Moreover, both ΔH° and ΔS° were found to be negative, which is the characteristic of binding interactions driven predominantly by hydrogen bonding and van der Waals forces (Table 9) (Sherefedin et al., 2025; Woldegiorges et al., 2022).

These intermolecular forces arise from specific functional groups present in both molecules:

- In metformin hydrochloride: amino (–NH_2) groups, guanidine-like nitrogen atoms, and protonated sites capable of forming hydrogen bonds.
- In caffeine: carbonyl (C=O) groups, nitrogen atoms within the purine ring system, and nonpolar aliphatic and aromatic regions that support van der Waals interactions.

The combined contribution of hydrogen bonding (between polar groups such as –NH, –NH_2, and C=O) and van der Waals contacts (involving hydrophobic and π-stacking regions) accounts for the stability of the MF-HCl–CAF complex and the overall favorable thermodynamic profile. This interpretation is consistent with previous reports, which have established that negative values of both ΔH° and ΔS° typically indicate that hydrogen bonding and van der Waals interactions are the dominant forces governing the association (Woldegiorges et al., 2022).

Table 8: Thermodynamic parameters (entropy change ΔS, enthalpy change ΔH, free energy change ΔG) at different temperatures

Temperature (K)	lnKa	ΔH($molL^{-1}$)	ΔS($molL^{-1}$)	ΔG($molL^{-1}$) × 10^4
298	6.28±4.04	- 7.74±1.03× 10^4	-2.34±0.33× 10^2	-1.77±0.15
310	6.26±3.37			-0.49±0.01
318	5.98±4.25			-0.30±0.01

4.3.2. Determination of Binding Constant and Number of Binding Sites

The binding constant (K) and the number of binding sites (n) can be derived from fluorescence titration data. Knowledge of these parameters for the interaction between MF-HCl and CAF is essential for understanding the drug's distribution in plasma, as well as its implications for

pharmacodynamics and pharmacokinetics (Mrkalić et al., 2021; Weiser & Weigmann, 2019). As discussed in the section on fluorescence quenching of MF-HCl, the observed quenching by CAF occurs via a static mechanism, involving the formation of a non-fluorescent ground-state complex. For static quenching systems, the binding constant and the number of binding sites can be reliably determined from a plot of $\log(\mathrm{F_o} - \mathrm{F})\,/\mathrm{F}$ vs $\log([\mathrm{Q}] - [\mathrm{D}]\frac{\mathrm{F_o}-\mathrm{F}}{\mathrm{F}})$ (where F_0 and F represent the fluorescence intensities in the absence and presence of quencher, respectively).

While Fig. 20 presents the binding plots, the corresponding calculated values of K and n are summarized in Table 10. The results indicate that approximately one caffeine molecule binds to one molecule of MF-HCl, consistent with a 1:1 stoichiometric binding ratio. The relatively high magnitude of the binding constant reflects a strong interaction between MF-HCl and CAF under the studied conditions. Such drug–ligand associations can significantly modulate the pharmacokinetic behavior of the drug. Similar studies, such as those examining the interaction between caffeine and clozapine, have highlighted the potential for increased toxicity arising from similar binding phenomena (Yartsev & Peisah, 2021). Additionally, the observed decrease in the binding constant with rising temperature further supports the static quenching model, as it indicates the formation of relatively unstable complexes that become partially dissociated at elevated temperatures (Belay et al., 2016a).

Table 10: Binding parameters of MF-HCl at various temperatures

Temperature (K)	Log (Ka)	$\kappa_\alpha(M^{-1}) \times 10^5$	N	Regression (R)
298	5.04±0.41	1.10 ± 2.57	1.96±0.16	0.96
310	5.55±0.17	3.55 ± 1.48	2.28±0.07	0.99
318	5.11±0.32	1.29 ± 2.09	2.18±0.13	0.98

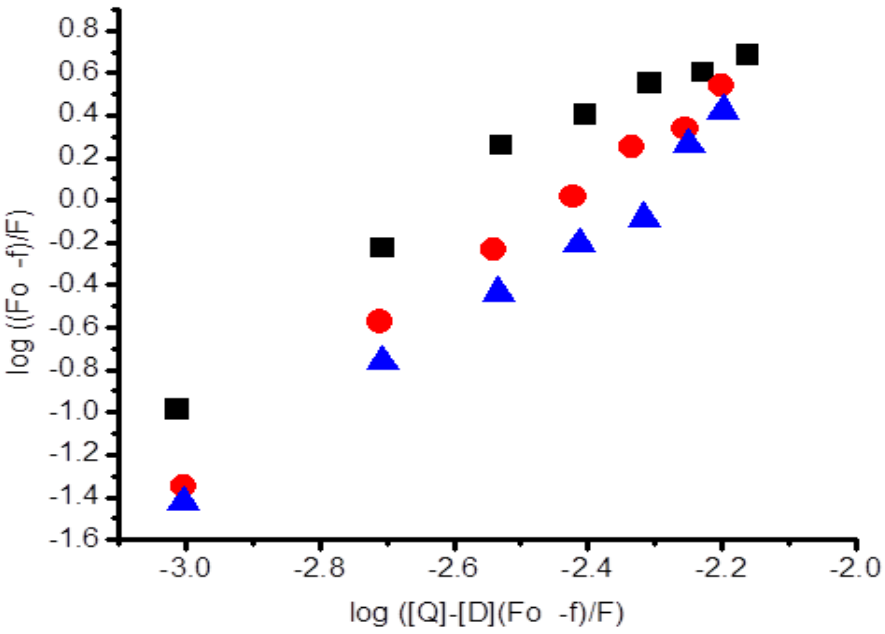

Figure 20: Graph of $\log\frac{F_o-F}{f}$ Vs $\log\left([Q]-n[D]\frac{(F_o-F)}{F_o}\right)$ when caffeine $(1\times10^{-3}$ to $7\times10^{-3})$ M binding to MF-HCl $2\times10^{-4}M$ at 298 K (black), 310 K (red), and 318 K (blue)

4.3.3. Forester Resonance Energy Transfer Study of MF-HCl-CAF Interactions

In Förster's theory of non-radiative energy transfer (FRET), the efficiency of energy transfer depends on both the distance between donor and acceptor and the critical transfer distance R_0 as:

$$E=\frac{R_o^6}{R_o^6+r^6} \tag{4.1}$$

$$E=1-\frac{F}{F_O} \tag{4.2}$$

where E represents the energy transfer efficiency, R_0 is the Förster critical distance (at which the transfer efficiency equals 50%), and r is the actual distance between the donor and acceptor.

$$R_O^6=8.8\times10^{-25}K^2N^{-4}\Phi J \tag{4.3}$$

where κ^2 is the orientation factor between the donor and acceptor dipoles, N is the refractive index of the surrounding medium, Φ is the fluorescence quantum yield of the donor, and J represents the

spectral overlap integral between the donor's emission spectrum and the acceptor's absorption spectrum. Therefore,

$$J = \frac{(\sum IP(\lambda)\varepsilon A(\lambda)\lambda^4 \Delta\lambda)}{(\sum IP(\lambda)\Delta\lambda)} \quad (4.4)$$

Here, IP(λ) represents the fluorescence intensity of the donor at wavelength λ, and εA(λ) is the molar extinction coefficient (absorptivity) of the acceptor at wavelength λ.

Fig. 21 illustrates the significant spectral overlap between the fluorescence emission spectrum of MF-HCl (serving as the donor) and the absorption spectrum of CAF (the acceptor). Using Equation (4.2), the calculated energy transfer efficiency is 0.72. By integrating the relevant spectral data over the wavelength range of 200–600 nm, as shown in Fig. 21, the spectral overlap integral J was determined to be 3.972×10^9 nm⁴ / (M.cm) under ambient conditions.

Eqn. (4.3) yields the Förster critical distance R_0, the separation at which energy transfer efficiency reaches 50%, as 1.81 nm for the transfer from MF-HCl to CAF. The orientation factor κ^2 for the donor-acceptor dipoles was taken as 2/3, which corresponds to dynamic random orientation averaging (Melle et al., 2018). The donor quantum yield, Φ, was 0.5, and the refractive index of the medium, N, was 1.35.

The computed binding distance r between caffeine and the amino acid residue in metformin hydrochloride is 1.55 nm. This value is considerably smaller than the typical upper limit of ~7 nm required for efficient FRET to occur. Consequently, the proximity strongly favors non-radiative energy transfer from the donor to the acceptor. These results demonstrate that the donor and acceptor are favorably positioned for effective Förster Resonance Energy Transfer (FRET). When $R_0 > r$, the molecular arrangement is optimal for high-efficiency energy transfer, which supports a reliable and sensitive FRET mechanism. This configuration enhances the applicability of FRET-based approaches for investigating various biological and chemical interactions.

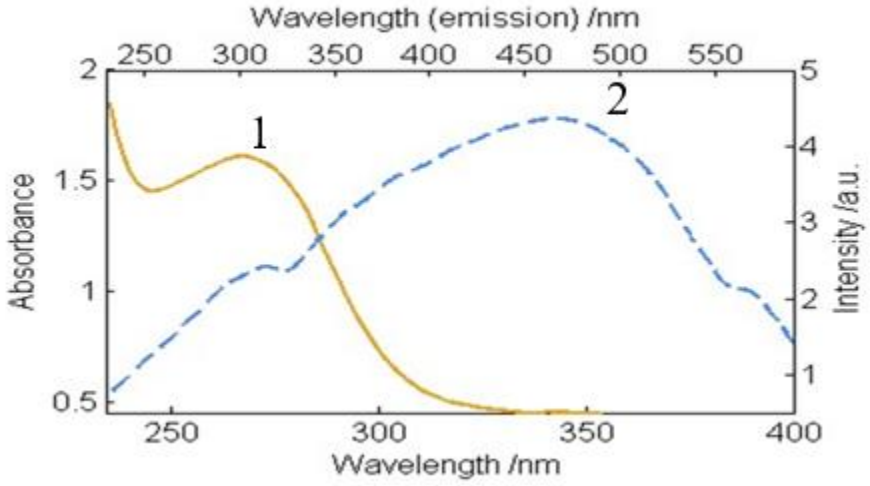

Figure 21: Overlap spectra of UV absorption spectra of CAF (1) and MF-HCl fluorescence emission spectra (2): C of metformin hydrochloride = 1×10^{-5} mol l^{-1}, C of caffeine = 1×10^{-5} mol l^{-1}

4.3.4. UV-Vis Absorption Spectroscopic Investigation of MF-HCl-CAF Interactions

UV/Vis absorption spectroscopy provides a straightforward and intuitive method for exploring both the interaction mechanism and any structural changes arising from molecular interactions involving bioactive compounds (Mrkalić et al., 2021). In this study, the UV–Vis absorption spectra of MF-HCl were recorded at various concentrations of CAF, as illustrated in Fig. 22. Upon addition of CAF, the absorption spectra of MF-HCl exhibit a clear blue shift (hypsochromic shift). Furthermore, an isosbestic point is observed at 251 nm in the series of spectra, which is a strong indicator of the formation of a ground-state complex between MF-HCl and CAF. This spectroscopic evidence is fully consistent with the conclusion drawn from the fluorescence quenching experiments in this work, confirming that the quenching process is predominantly static in nature (i.e., involving the formation of a non-fluorescent ground-state complex rather than dynamic collisional quenching). The present findings are in good agreement with previously reported studies describing the binding interactions of CAF with structurally related phenolic compounds, such as chlorogenic acid and caffeic acid (Belay et al., 2016a).

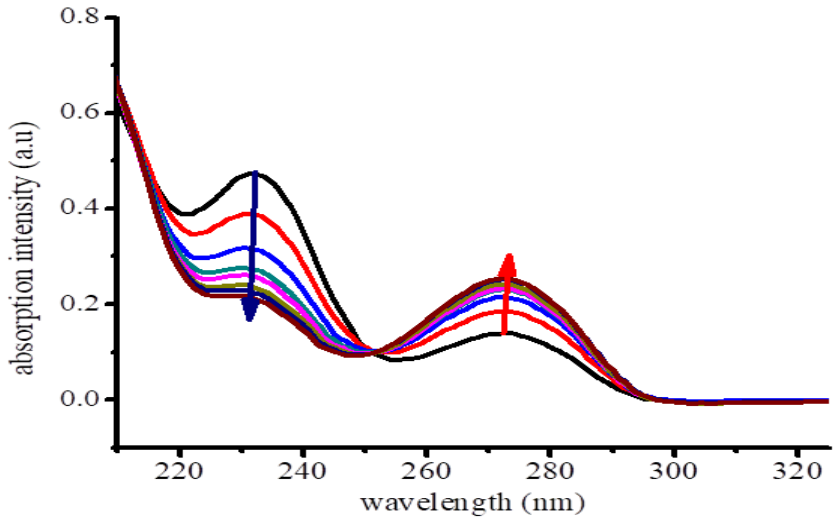

Figure 22: UV-Vis absorption spectra of metformin hydrochloride in different concentrations of caffeine (1×10^{-3}-7×10^{-3}) M)

4.3.5. Fourier Transforms Infrared Spectroscopy of MF-HCl–CAF Interactions

Fourier Transform Infrared (FTIR) spectroscopy was employed to examine the molecular interactions and possible conformational changes between MF-HCl and CAF. MF-HCl contains characteristic functional groups, including imine, enamine, amine, and methyl moieties, which contribute to its distinctive vibrational signature. The FTIR spectrum of pure MF-HCl (Fig. 23(3)) displays prominent absorption bands at: 3333 cm^{-1} (N–H stretching vibrations), 2916 cm^{-1} (C–H stretching vibrations), 1016 cm^{-1} (C–N stretching vibrations) (Sahoo et al., 2012). For pure CAF(Fig. 23(2)), the key bands are observed at: 3107 cm^{-1} (N–H stretching), 2949 cm^{-1} (C–H stretching), 1644 cm^{-1} (C=C stretching), 1225 cm^{-1} (C–N stretching) (Gunasekaran et al., 2005).

Upon interaction between MF-HCl and CAF (Fig. 23(1)), noticeable shifts and intensity changes occur in the spectrum of MF-HCl. Specifically: The N–H stretching band at 3333 cm^{-1} shifts to 3328 cm^{-1}, the C–H stretching band at 2916 cm^{-1} moves to 2908 cm^{-1}. In addition to these wavenumber shifts, a reduction in peak intensities is observed in the presence of CAF. Such perturbations in the FTIR absorption bands, shifts in position, combined with decreased intensity, are commonly interpreted as evidence of conformational changes and intermolecular interactions resulting from the association between MF-HCl and CAF molecules (Alsaif et al., 2020). The observed alterations, including the weakening or partial disappearance of certain characteristic bands, further support the formation of a molecular complex through binding between MF-HCl and CAF.

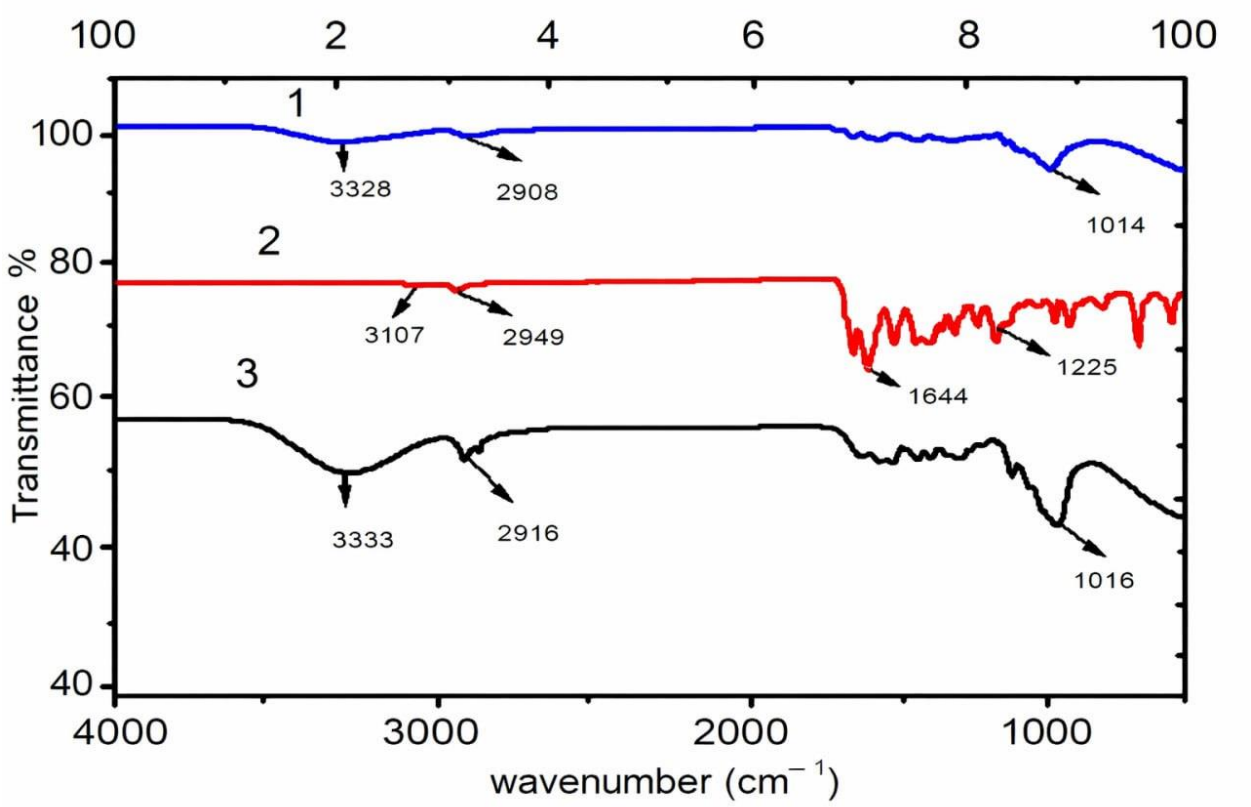

Figure 23: FTIR spectra of 1) MF- HCl+CAF, 2) CAF, and 3) MF- HCl

4.3.6. Zeta Potential of MF-HCl–CAF Interactions

Fig. 24 presents the zeta potential distribution for MF-HCl, which exhibits a peak value of –7.79 mV. This negative charge on the particle surface indicates moderate colloidal stability. The negative zeta potential provides a degree of electrostatic repulsion between particles, which helps to reduce the likelihood of aggregation to some extent. In contrast, Fig. 25 shows the zeta potential profile of the MF-HCl–CAF system, with a significantly more negative peak at –31.6 mV. This larger magnitude of negative charge suggests strong electrostatic repulsion among the particles, resulting in markedly improved colloidal stability and a more uniform, stable dispersion.

It is well established that zeta potential values with absolute magnitudes exceeding ±30 mV generally correspond to good stability, whereas values closer to zero increase the risk of particle aggregation due to insufficient repulsive forces (Bhattacharjee, 2016; Ullah et al., 2022). The substantial increase in the absolute zeta potential value upon addition of CAF (from –7.79 mV to –31.6 mV) indicates that the MF-HCl–CAF system possesses considerably higher stability compared to MF-HCl alone. This enhancement is most likely due to the adsorption of CAF

molecules onto the surface of MF-HCl particles, leading to the formation of a complex with increased surface charge density.

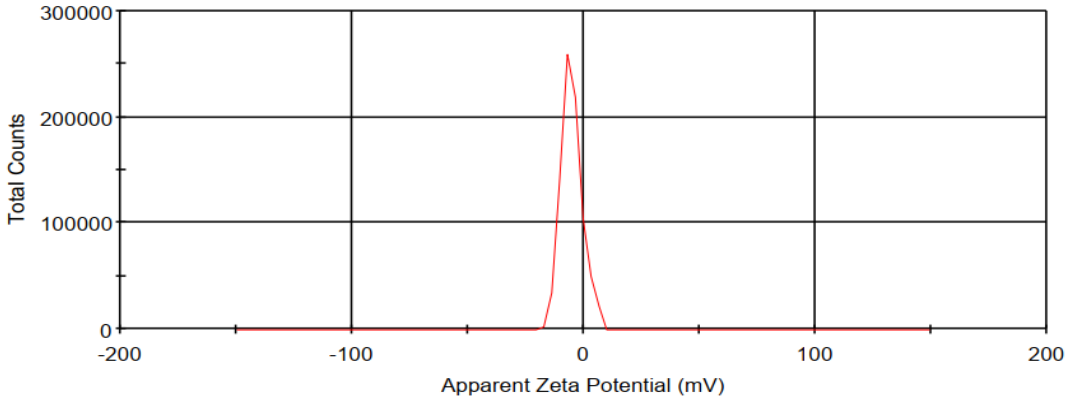

Figure 24: Zeta potential distribution of MF-HCl

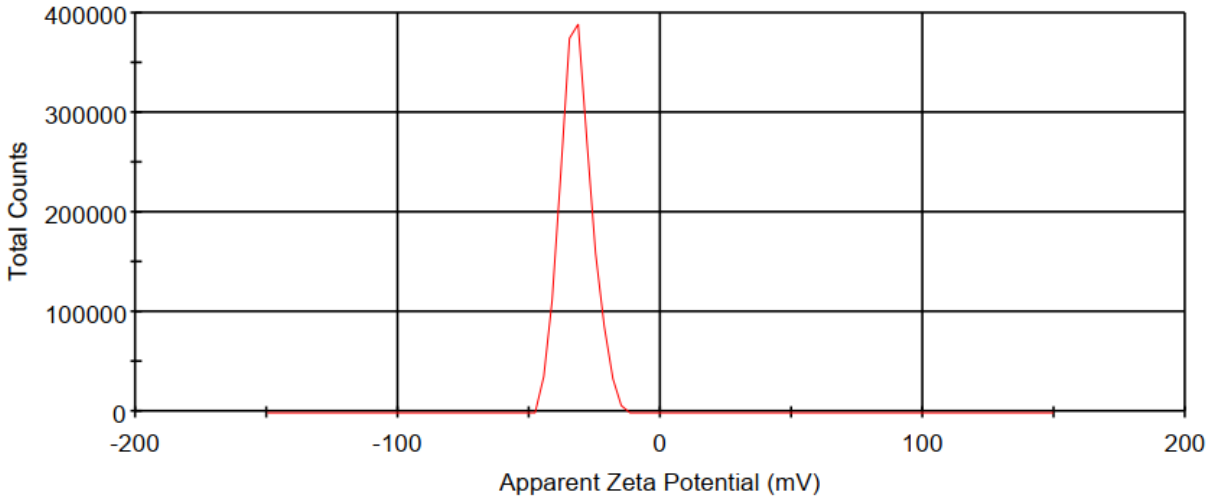

Figure 25: Zeta potential distribution of MF-HCl-CAF

4.3.7. Dynamic Light Scattering (DLS) of MF-HCl–CAF Interactions

Fig. 26 and Fig. 27 present the dynamic light scattering (DLS) size distribution profiles for MF-HCl alone and in the presence of CAF (MF-HCl–CAF), respectively. For pure MF-HCl, the DLS measurement reveals two distinct populations: Peak 1 at 16.80 nm (corresponding to smaller, likely monomeric or small oligomeric species), Peak 2 at 564.5 nm (indicative of larger aggregates).

In the MF-HCl–CAF system, the size distribution shifts noticeably: Peak 1 increases slightly to 20.79 nm, and Peak 2 shifts significantly to 1274 nm. These changes demonstrate that the addition of caffeine substantially alters the aggregation behavior of metformin hydrochloride particles,

promoting the formation of larger assemblies (Henderson et al., 2013; Kramar, 2021). The presence of bigger, more loosely associated clusters in the MF-HCl–CAF mixture suggests that these aggregates are less tightly packed compared to those in pure MF-HCl. Such larger particles tend to sediment more slowly from solution and may be more prone to irreversible aggregation, primarily driven by van der Waals interactions. Overall, the results suggest that caffeine molecules likely function as bridging agents, facilitating intermolecular interactions between metformin hydrochloride particles and thereby leading to the development of significantly larger aggregates.

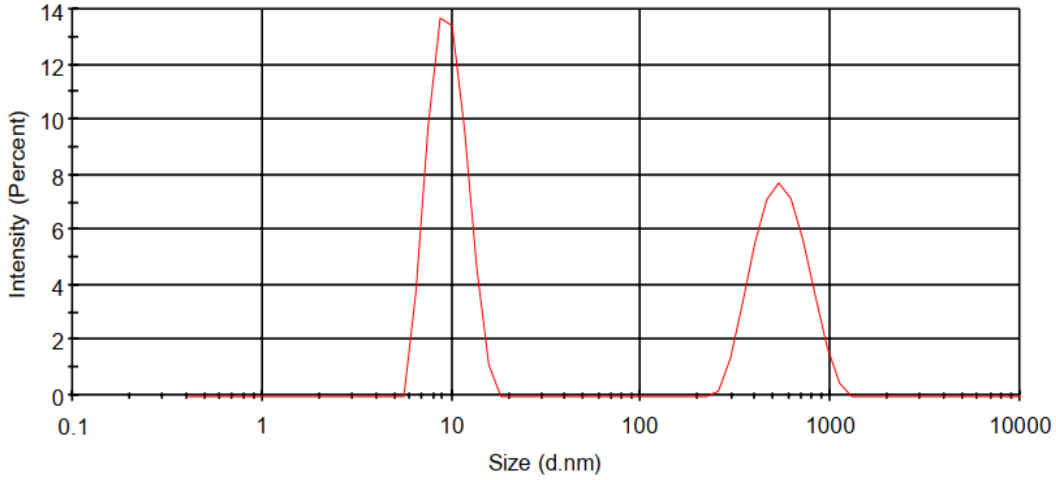

Figure 26: DLS Size distribution of MF-HCl

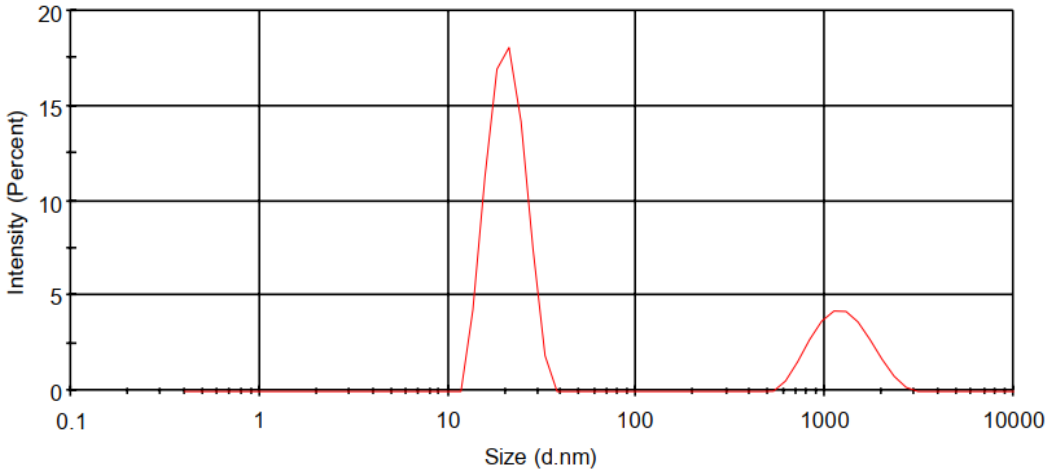

Figure 27: DLS Size distribution of MF-HCl-CAF

4.4. Computational Approaches

4.4.1. DFT Analysis of MF-HCl Drug

Quantum chemical calculations were performed using Gaussian 09W to determine the dipole moments of MF-HCl, allowing direct comparison with experimentally derived values. The molecular structure was fully optimized to reach its lowest energy conformation. The DFT-calculated dipole moment in the ground state (μ_g) was found to be smaller than that in the excited state (μ_e). This result confirms that the excited state of MF-HCl exhibits greater polarity than the ground state (Gülseven Sidir & Sidir, 2013). Ground and excited state dipole moments in the gas phase were evaluated using the B3LYP functional with various basis sets: 3-21+G*, 6-31+G(d,p), 6-311+G(d,p), and 6-31+G(d,p). Fig. 28 illustrates the optimized geometry of MF-HCl, including the direction of the dipole moment vector (indicated by an arrow), the total density matrix overlaid with the electrostatic potential map (TDM-ESP), the HOMO and LUMO orbital distributions, and the simulated UV-Vis spectrum. As the basis set size increased, the computed ground state dipole moment decreased. Additional calculations of the ground-state dipole moment in different solvents were carried out using DFT and TD-DFT with the B3LYP/6-31+G (d,p) level, incorporating the IEFPCM (Integral Equation Formalism Polarizable Continuum Model) solvation approach. The results, summarized in Table 11, reveal that the ground-state dipole moment (μ_g) in each solvent is larger than the corresponding gas-phase value.

optimized structure		**direction of the dipole moment**	
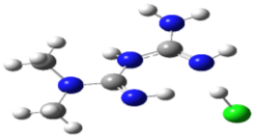		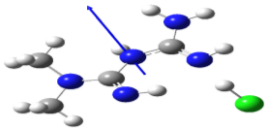	
HOMO-3-21+G*	LUMO-3-21+G*	3-21+G*-TD-ESP	
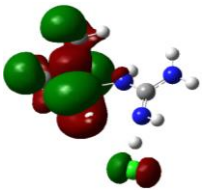	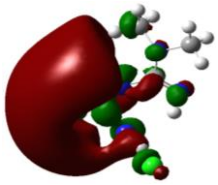	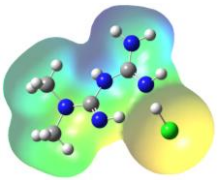	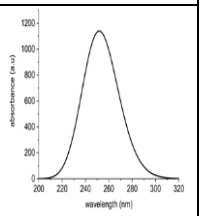
HOMO-6-31+G(d, p)	LUMO-6-31+G(d, p)	6-31+G(d, p)-TD-ESP	
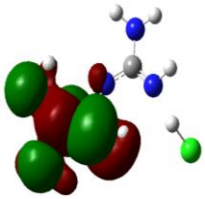	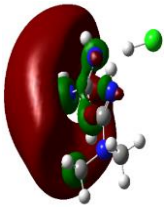	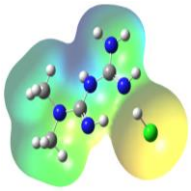	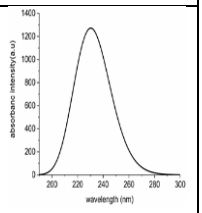
HOMO-6-311+G(d, p)	LUMO-6-311 +G(d, p)	6-31+G(d, p)1-TD-ESP	
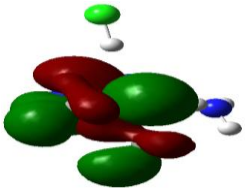	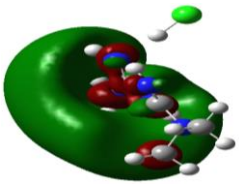	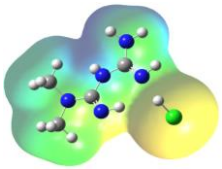	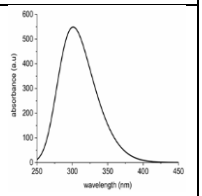

Figure 28: Optimized molecular structure of MF-HCl showing the HOMO-LUMO electron distribution, dipole moment vector (indicated by arrow), total density matrix with superimposed electrostatic potential map (TDM-ESP), and corresponding UV/Vis absorption

Table 91: Theoretical ground state dipole moment (μ_g) in different solvents using B3LYP/6-31+G (d, p)

solvents	μ_g (D)	HOMO (ev)	LUMO (ev)
2-Propanol	19.43	-6.634	-1.082
1-Propanol	19.47	-6.635	-1.080
Ethanol	19.60	-6.634	-1.073
Methanol	19.77	-6.629	-1.062
Acetonitrile	19.80	-6.629	-1.060
Water	20.05	-6.627	-1.046

DFT calculations showed good agreement with the experimental findings overall. Nevertheless, the computed dipole moments for both the ground and excited states were found to be higher than the corresponding experimental values. This difference can be attributed primarily to the fact that quantum chemical computations typically model the molecule in the gas phase (isolated), whereas experimental measurements reflect the influence of the surrounding solvent environment, including solute-solvent interactions and other environmental effects (Galetin et al., 2024).

The electrostatic potential (ESP) maps provide valuable insights for identifying preferred sites for nucleophilic and electrophilic attacks, as well as potential regions involved in hydrogen bonding with solvents. Fig.29 presents the HOMO and LUMO energy levels, the corresponding energy gap (band gap), and the optimized molecular structure of MF-HCl obtained from DFT calculations using various basis sets. The surface is color-coded to represent the electrostatic potential distribution, with blue and grey regions indicating positive and negative potentials, respectively. In this scheme, the blue areas correspond to electrophilic (electron-deficient) regions, while the grey areas represent nucleophilic (electron-rich) regions (Sola & Vuj, 2024; Taylor et al., 2014). The presence of the chlorine atom contributes to an electron-rich (negative potential) region in the MF-HCl molecule, whereas certain nitrogen atoms exhibit relatively electron-deficient (positive potential) characteristics. Fig. 30 illustrates the electrostatic potential map of MF-HCl. While theoretical ground-state dipole moments (μ_g) of MF-HCl in different solvents, calculated using the B3LYP/6-31+G(d,p) level of theory, are summarized in Table 11 and Table 12 lists the ground-state and excited-state dipole moments, HOMO–LUMO energy gaps, UV/Vis absorption wavelengths, and oscillator strengths for MF-HCl in the gas phase, computed with various basis sets.

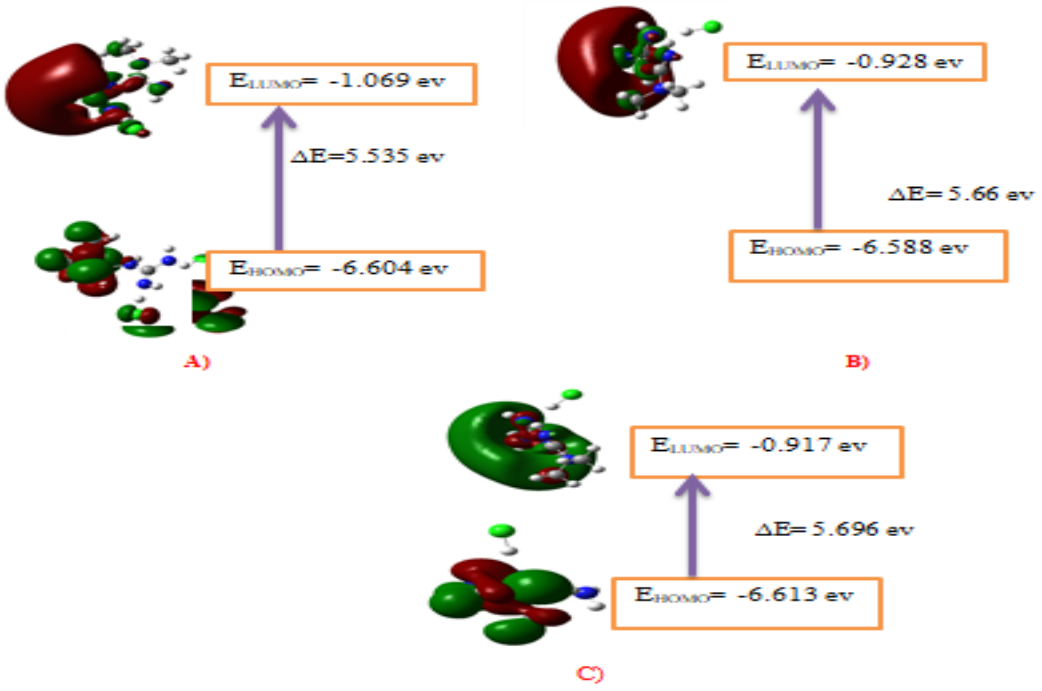

Figure 29: Optimized molecular structures and HOMO–LUMO energy gaps of metformin hydrochloride calculated using different DFT levels: A) DFT-B3LYP-3-21+G*, B) DFT-B3LYP-6-31+G (d, p), and C) DFT-B3LYP-6-311+G (d, p).

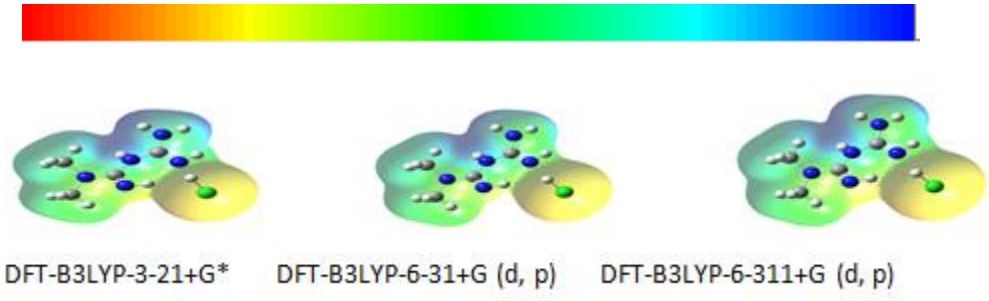

Figure 30: Total electron density map superimposed with the electrostatic potential surface (TDM-ESP) of MF-HCl.

Table 102: Ground state and excited state dipole moments, HOMO-LUMO energy band gap, UV/Vis absorption wavelengths, oscillator strengths employing different basis sets of gas state

Basis set	μ_g (D)	μ_e (D)	Band gap (eV)	λ(nm)	Oscillatory strength
DFT-B3LYP-3-21+G*	10.02	11.94	5.51	252.59	0.0198
DFT-B3LYP-6-31+G (d, p)	8.44	10.87	5.66	233.98	0.0209
DFT-B3LYP-6-311+G (d, p)	8.24	18.74	5.7	306.23	0.0035

4.4.2. Molecular Docking Analysis of MF-HCl-CAF Interactions

AMP-activated protein kinase (AMPK) serves as a central regulator of cellular energy homeostasis, responding to various metabolic stresses and energy fluctuations by modulating key pathways, including those related to glycogen metabolism (Polekhina et al., 2005). As a member of the Ca^{2+}/calmodulin-dependent protein kinase family within the kinome, AMPK, along with phosphorylase kinase, functions as a sensor of metabolic stress (Manning, 2012). Recent research has highlighted AMPK's significance due to its activation by antidiabetic agents such as MF-HCl and rosiglitazone, which are commonly prescribed for type 2 diabetes (Aljofan, 2019; Fryer et al., 2002; G. Zhou et al., 2001). Upon activation, AMPK suppresses anabolic processes like fatty acid, triglyceride, and cholesterol synthesis (Meeting et al., 2003) while promoting catabolic pathways, including fatty acid β-oxidation (Chen et al., 2024; Park et al., 2024), glycolysis (Marsin et al., n.d.), glucose uptake (Xi et al., 2001), and, in some contexts, increased food intake (Hardie, 2004).

Before performing molecular docking simulations, the 3D structures of MF-HCl (the ligand) and caffeine were energy minimized and optimized using Discovery Studio software, then converted to PDB format. Docking calculations were conducted with Auto Dock Vina version 1.5.7 (Eberhardt et al., 2021; Trott & Olson, 2009). The crystal structure of the AMPK glycogen-binding domain (PDB ID: 1Z0N, corresponding to the β-subunit from rat) was retrieved from the Protein Data Bank. Using MGL Tools 1.5.6, co-crystallized ligands (such as β-cyclodextrin) and water molecules were removed, polar hydrogens were added, and Kollman united atom charges were assigned to the receptor. A cubic grid box of dimensions 70 × 70 × 70 Å was defined, centered at

coordinates (0.860727, -20.437701, 2.478026) Å in the x, y, and z directions, respectively, to encompass the potential binding region. The interactions between MF-HCl and AMPK (PDB ID: 1Z0N) are illustrated in Figs. 31–33, detailing key interacting amino acid residues and the computed binding affinity (in kcal/mol). Molecular docking analysis of MF-HCl revealed unfavorable steric clashes, conventional hydrogen bonds, and carbon-hydrogen bond interactions primarily involving residues such as Phe112, Trp84, Leu103, Phe127, Leu93, and Tyr92. These findings indicate that hydrogen bonding plays a dominant role in the ligand-protein association, which is likely responsible for the observed fluorescence quenching effects (Kalita et al., 2024).

Table 13 and Table 14 summarize the binding affinities, RMSD/upper bound (ub), and RMSD/lower bound (lb) values for docking of MF-HCl alone (single-ligand mode) and in the presence of caffeine (dual-ligand mode). In the dual-ligand case, critical residues of the AMPK active site, including Phe127, Leu93, Tyr92, Leu103, Val92, Phe112, and Trp84, participate in hydrogen bonding, hydrophobic, alkyl, and π-alkyl interactions with MF-HCl. A comparison of the data in Table 13 and Table 14 shows that MF-HCl exhibits generally stronger binding (more negative affinity values) when docked as a single ligand compared to the dual-ligand setup with CAF. The variation in the distance metrics between the optimal poses in the single- and dual-ligand dockings suggests that the presence of CAF modulates the binding mode and affinity of MF-HCl to the AMPK receptor. This competitive or allosteric influence implies that CAF may alter the pharmacological activity or binding efficacy of MF-HCl within the protein target.

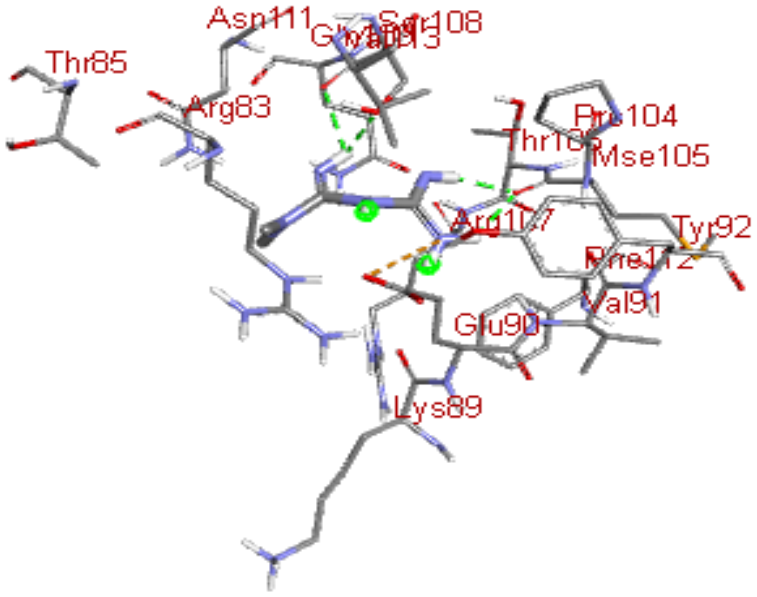

Figure 31: Three-dimensional visualization illustrating the binding conformations and interactions of metformin hydrochloride within the active site pocket of AMP-activated protein kinase (AMPK) (PDB ID: 1Z0N).

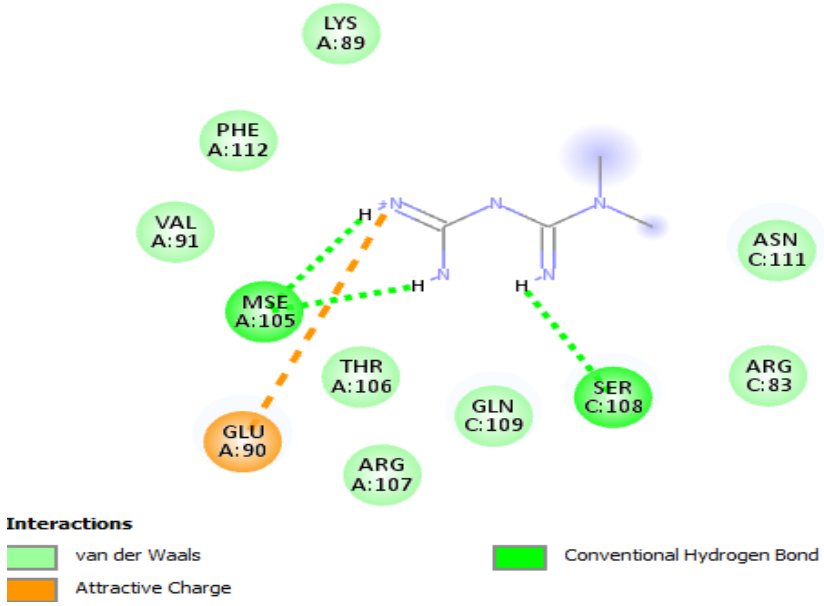

Figure 32: Two-dimensional diagram depicting the binding interactions and poses of metformin hydrochloride within the active site pocket of AMP-activated protein kinase (AMPK) (PDB ID: 1Z0N).

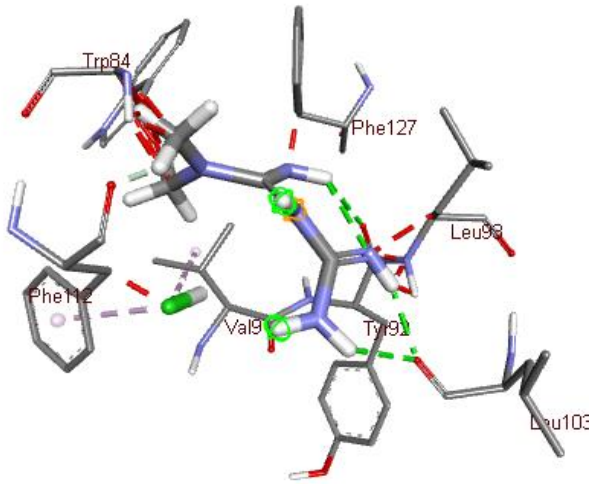

Figure 33: Three-dimensional visualization showing the binding conformations and interactions of metformin hydrochloride together with caffeine (dual-ligand docking) within the active site pocket of AMP-activated protein kinase (AMPK) (PDB ID: 1Z0N).

Table 113: Molecular docking affinities and distance from the best mode of MF-HCl against AMP-activated protein kinase (AMPK) (PDB ID: 1z0n)

Mode	Affinity (kcal/mol)	Distance from the best mode	
		RMSD/lb	RMSD/ub
1	-5	0	0
2	-4.7	2.127	3.071
3	-4	2.19	3.046
4	-3.9	26.971	28.176
5	-3.8	13.112	14.606
6	-3.8	15.509	16.458
7	-3.8	23.996	26.14
8	-3.8	27.707	28.821
9	-3.7	26.93	28.148

Table 124: Molecular docking affinities and distance from the best mode of MF-HCl plus CAF (two ligands) against AMP-activated protein kinase (AMPK) (PDB ID: 1z0n)

Ligand	Binding affinity (kcal/mol)	RMSD/ub	RMSD/lb
protein_caffeine_uff_E=351.80	-5.9	0	0
protein_caffeine_uff_E=351.80	-5.5	3.053	1.477
protein_caffeine_uff_E=351.80	-5.5	7.311	6.058
protein_caffeine_uff_E=351.80	-5.4	30.035	28.264
protein_caffeine_uff_E=351.80	-5.3	4.113	1.7
protein_caffeine_uff_E=351.80	-5.3	3.647	1.681
protein_caffeine_uff_E=351.80	-5.3	6.232	4.967
protein_caffeine_uff_E=351.80	-5.3	30.559	28.744
protein_caffeine_uff_E=351.80	-5.2	34.496	32.651
protein_met_uff_E=145.07	-5	0	0
protein_met_uff_E=145.07	-4.9	23.88	23.316
protein_met_uff_E=145.07	-4.8	21.407	20.373
protein_met_uff_E=145.07	-4.7	21.388	20.343
protein_met_uff_E=145.07	-4.7	23.952	23.511
protein_met_uff_E=145.07	-4.7	19.118	18.194
protein_met_uff_E=145.07	-4.5	22.653	22.169
protein_met_uff_E=145.07	-4.5	19.953	18.867
protein_met_uff_E=145.07	-4.5	22.015	21.034

5. Conclusion and Recommendations

5.1. Conclusion

This dissertation work provides a thorough exploration of the Solvatochromic behavior and photophysical characteristics of MF-HCl, as well as its molecular interactions with CAF, through an integrated approach combining advanced spectroscopic methods and computational modeling. The study successfully achieved its goals by clarifying how solvent polarity affects the spectral properties of MF-HCl, detailing the quenching of its fluorescence by CAF. Techniques such as UV-Vis absorption, fluorescence, FTIR spectroscopy, dynamic light scattering, and zeta potential analysis were paired with DFT simulations and molecular docking to yield robust insights.

Solvatochromic analyses demonstrated MF-HCl's strong dependence on solvent environment, with the excited-state dipole moment (μ_e) substantially larger than the ground-state value (μ_g). Application of Solvatochromic correlations; Lippert-Mataga ($\mu_e \approx 8.55$ D), Bakhshiev ($\mu_e \approx 8.34$ D), Kawski-Chamma-Viallet ($\mu_e \approx 6.08$ D), and Reichardt ($\mu_e \approx 6.40$ D) models highlighted enhanced polarizability and solute-solvent stabilization in the excited state, particularly impacting emission profiles. Supporting DFT results at the B3LYP level with varying basis sets produced ground-state dipole moments of 8.24–10.02 D and excited-state values of 10.87–18.74 D, along with HOMO-LUMO gaps around 5.51–5.70 eV, confirming the compound's electronic robustness and potential charge-transfer features.

Photophysical parameters of MF-HCl, encompassing quantum efficiencies, lifetimes, and rates of radiative versus non-radiative processes, showed clear modulation by solvent type and concentration, positioning it as a useful polarity-sensitive fluorescent marker. Interaction studies with CAF revealed static quenching via ground-state complexation, primarily driven by hydrogen bonding and van der Waals contributions. Förster resonance energy transfer calculations yielded a Förster distance (R_0) of approximately 1.81 nm and an effective donor-acceptor separation (r) of 1.55 nm, signifying highly efficient non-radiative transfer. Thermodynamic parameters indicated a spontaneous, enthalpy-driven process with favorable binding energetics. Supporting evidence from DLS (altered hydrodynamic sizes), zeta potential (shifted surface charges), and FTIR (perturbed vibrational modes) confirmed structural rearrangements upon complex formation.

Computational docking reinforced these observations, showing stable binding of MF-HCl and CAF individually and in combination to the AMP-activated protein kinase (AMPK) target (PDB ID: 1Z0N), consistent with quenching patterns and suggestive of relevance to metformin's

therapeutic activation of AMPK pathways. This multifaceted strategy yielded a comprehensive view of binding events, with potential ramifications for drug absorption, distribution, and effectiveness in caffeine-rich contexts.

Overall, the work enhances understanding of MF-HCl's solvent-responsive photo physics and intermolecular associations, offering valuable data for advancing pharmaceutical development and optimization. Although the research effectively merged empirical data with theoretical predictions, certain constraints, like continuum solvent approximations in computations and the absence of biological system testing, point to promising directions for subsequent investigations, such as in vitro/in vivo experiments and docking against diverse AMPK conformations. These outcomes enrich the domain of drug photochemistry and lay the groundwork for improved management of metabolic conditions using MF-HCl-based therapies.

5.2. Future Research and Recommendations

From an overall perspective, this research was constrained by limited funding and access to advanced instrumentation, preventing a comprehensive characterization of the metformin hydrochloride-caffeine interaction. Consequently, key aspects such as detailed changes in drug particle size, which directly influence therapeutic efficacy, along with cytotoxicity assays and cell imaging studies to evaluate membrane permeability during complexation, remain unexplored. Future investigations could prioritize these areas, including in vivo evaluations to assess real-world implications. The study demonstrated clear solvent-induced structural modifications in metformin hydrochloride, which can alter its pharmacokinetic profile and potentially contribute to toxicity. Pharmacologists are, therefore, encouraged to account for such Solvatochromic effects when designing or optimizing drug formulations. Furthermore, evidence of complex formation between the drug and caffeine suggests possible interference with absorption, distribution, and overall bioavailability. Given that many patients consume metformin alongside caffeine-rich beverages like tea or coffee, it is advisable to avoid simultaneous intake to minimize potential interactions. Additional research in this domain is strongly recommended to refine drug design strategies, enhance pharmacokinetic predictability, and ensure safer co-administration guidelines.

List of Publications

Articles from the Dissertation Work

- Asemare, S., Belay, A., Kebede, A. et al. Ground and Excited State Dipole Moments of Metformin Hydrochloride using Solvatochromic Effects and Density Functional Theory. J Fluoresc 34, 1207–1217 (2024). https://doi.org/10.1007/s10895-023-03355-4

- Asemare, S., Belay, A., Kebede, A. et al. Photophysical Properties, Fluorescence Quenching of Metformin Hydrochloride by Caffeine, and its Docking with the AMP-activated protein kinase receptor. J Fluoresc 35, 7927–7943 (2025). https://doi.org/10.1007/s10895-024-04128-3

Articles Not Included in the Dissertation

- ✓ Sherefedin, Umer, Abebe Belay, Kusse Gudishe, Alemu Kebede, Alemayehu Getahun Kumela, Tadesse Lemma Wakjira, Semahegn Asemare, T. Gurumurthi, and Dereje Gelanu. "Investigating the effects of solvent polarity and temperature on the molecular, photophysical, and thermodynamic properties of sinapic acid using DFT and TDDFT." *RSC advances* 14, no. 32 (2024): 23364-23377.
- ✓ Sherefedin, Umer, Abebe Belay, Kusse Gudishe, Alemu Kebede, Alemayehu Getahun Kumela, and Semahegn Asemare. "Photophysical properties of sinapic acid and ferulic acid and their binding mechanism with caffeine." *Journal of Fluorescence* 35, no. 4 (2025): 2379-2393.
- ✓ Feyisa, Tesfaye, Fekadu Tolessa, Abebe Belay, Semahegn Asemare, Gemechis Mathewos, and Jebel Haji. "Enhancing radiative cooling power using ultra-broadband near-unit spectrally selective thermal emitters based on metamaterial structure." *Journal of Optics* (2024): 1-13.
- ✓ Sherefedin, Umer, Abebe Belay, Kusse Gudishe, Alemu Kebede, Alemayehu Getahun Kumela, Tadesse Lemma Wakjira, Semahegn Asemare, and T. Gurumurthi. "Effects of temperature and solvent polarity on the thermodynamic and photophysical properties of ferulic acid using density functional theory (DFT)." *Journal of Molecular Liquids* 407 (2024): 125175.
- ✓ Sherefedin, Umer, Abebe Belay, Alemu Kebede, Semahegn Asemare, Kinfe Woldegiorges, Alemayehu Getahun Kumela, and Kusse Gudishe. "Determination of the ground and excited state dipole moments of ferulic and sinapic acids by solvatochromic effects and density function theory method." *AIP Advances* 13, no. 10 (2023).

List of Conference Participations

Conferences

The results of this study were disseminated through presentations at various national and international conferences. Valuable feedback and suggestions received during these sessions have been carefully integrated into the dissertation. The conferences attended are listed below.

- Ground and Excited State Dipole Moments of Metformin Hydrochloride using Solvatochromic Effects and Density Functional Theory was presented at the 2nd national conference on "Holistic research: fostering synergy across fields" held on May 25-26/2024, Mekdela Amba University, Ethiopia.
- Ground and Excited State Dipole Moments of Metformin Hydrochloride using Solvatochromic Effects and Density Functional Theory work was presented at the Ethiopian Physical Society (EPS) 18th annual national conference held on February 16-17/2024, Addis Ababa University, Ethiopia.
- Photophysical Properties, Fluorescence Quenching of Metformin Hydrochloride by Caffeine, and its Docking with the AMP-activated protein kinase receptor work was presented at the research conference on "Driving innovation: harnessing research in natural science, agriculture, and digital technology" held on February 22-23/2025, Mekdela Amba University, Ethiopia.

References

Agarwal, S., & Mehrotra, R. (2016). Mini Review_ An overview of Molecular Docking. *JSM Chemistry*, *4*(2), 1024–1028. https://www.researchgate.net/profile/Shweta-Agarwal-7/publication/303897563_Mini_Review_An_overview_of_Molecular_Docking/links/575b9fb108aed884620da00a/Mini-Review-An-overview-of-Molecular-Docking.pdf

Aljofan, M. (2019). *Anticancer activity of metformin : a systematic review of the literature*. *5*.

Alsaif, N. A., Wani, T. A., Bakheit, A. H., & Zargar, S. (2020). Multi-spectroscopic investigation, molecular docking and molecular dynamic simulation of competitive interactions between flavonoids (quercetin and rutin) and sorafenib for binding to human serum albumin. *International Journal of Biological Macromolecules*, *165*, 2451–2461. https://doi.org/10.1016/j.ijbiomac.2020.10.098

Ansari, M. J., Rajendran, R. R., Mohanto, S., & Agarwal, U. (2022). *Poly(N -isopropylacrylamide)-Based Hydrogels for Biomedical Applications: A Review of the State-of-the-Art*.

Arciniega, M. (2018). *olecular docking : current advances and challenges*. *21*, 65–87. https://doi.org/10.22201/fesz.23958723e.2018.0.143

Asemare, S., Belay, A., Kebede, A., & Sherfedin, U. (2023). Ground and Excited State Dipole Moments of Metformin Hydrochloride using Solvatochromic Effects and Density Functional Theory. *Journal of Fluorescence*, *0123456789*. https://doi.org/10.1007/s10895-023-03355-4

Asiri, A. M., Al-Amari, M. M., & Khan, S. A. (2022). Multistep Synthesis and Photophysical Investigation of Novel Pyrazoline, a Heterocyclic D-π-a Chromophore (PTPB) as a Fluorescent Chemosensor for the Detection of Fe3+ Metal Ion. *Polycyclic Aromatic Compounds*, *42*(4), 1186–1200. https://doi.org/10.1080/10406638.2020.1768563

Attia, M. S., El-naggar, H. A., Abdel-daim, M. M., & El-sayyad, G. S. (2021). *The potential impact of Octopus cyanea extracts to improve eggplant resistance against Fusarium -wilt disease : in vivo and in vitro studies*.

Bacilieri, M., & Moro, S. (2007). Ligand-Based Drug Design Methodologies in Drug Discovery Process: An Overview. *Current Drug Discovery Technologies*, *3*(3), 155–165. https://doi.org/10.2174/157016306780136781

Bailey, C. J. (2024). *Metformin : Therapeutic profile in the treatment of type 2 diabetes*. *26*(March), 3–19. https://doi.org/10.1111/dom.15663

Bakhshiev, N. ~G. (1964). Universal Intermolecular Interactions and Their Effect on the Position of the Electronic Spectra of Molecules in Two-Component Solutions. VII. Theory (General Case of an Isotropic Solution). *Optics and Spectroscopy*, *16*, 446.

Baldi, A. (2010). Computational approaches for drug design and discovery: An overview. *Systematic Reviews in Pharmacy*, *1*(1), 99–105. https://doi.org/10.4103/0975-8453.59519

Bassani, D., & Moro, S. (2023). Past, Present, and Future Perspectives on Computer-Aided Drug Design Methodologies. *Molecules*, *28*(9). https://doi.org/10.3390/molecules28093906

Batool, M., Ahmad, B., & Choi, S. (2019). A structure-based drug discovery paradigm. *International Journal of Molecular Sciences*, *20*(11). https://doi.org/10.3390/ijms20112783

Belay, A. (2010a). Measurement of integrated absorption cross-section, oscillator strength and number density of caffeine in coffee beans by integrated absorption coefficient technique. *Food Chemistry*, *121*(2), 585–590. https://doi.org/10.1016/j.foodchem.2009.12.052

Belay, A. (2010b). Measurement of integrated absorption cross-section, oscillator strength and number density of caffeine in coffee beans by integrated absorption coefficient technique. *Food Chemistry*, *121*(2), 585–590. https://doi.org/10.1016/j.foodchem.2009.12.052

Belay, A., & Gholap, A. V. (2009). *Characterization and determination of chlorogenic acids (CGA) in coffee beans by UV-Vis spectroscopy*. *3*(11), 234–240.

Belay, A., Kim, H. K., & Hwang, Y. H. (2016a). Binding of caffeine with caffeic acid and chlorogenic acid using fluorescence quenching, UV/vis and FTIR spectroscopic techniques. *Luminescence*, *31*(2), 565–572. https://doi.org/10.1002/bio.2996

Belay, A., Kim, H. K., & Hwang, Y. H. (2016b). Probing the interaction of caffeic acid with ZnO nanoparticles. *Luminescence*, *31*(3), 654–659. https://doi.org/10.1002/bio.3007

Belay, A., Kim, H. K., & Hwang, Y. H. (2017). Spectroscopic study of binding of chlorogenic acid with the surface of ZnO nanoparticles. *Russian Journal of Physical Chemistry A*, *91*(9), 1781–1790. https://doi.org/10.1134/S0036024417090023

Belayneh, A., & Molla, F. (2020). The Effect of Coffee on Pharmacokinetic Properties of Drugs: A Review. *BioMed Research International*, *2020*(Figure 1). https://doi.org/10.1155/2020/7909703

Bhattacharjee, S. (2016). NU SC. *Journal of Controlled Release*. https://doi.org/10.1016/j.jconrel.2016.06.017

Bjerregaard, T., Kim, S., Mette, B., & Hougaard, M. (2015). A Comprehensive Review of Drug – Drug Interactions with Metformin. *Clinical Pharmacokinetics*, *54*(8), 811–824.

https://doi.org/10.1007/s40262-015-0270-6

Bozkurt, E., Gül, H. I., & Tuğrak, M. (2017). Investigation of solvent effect on photophysical properties of some sulfonamides derivatives. *Turkish Journal of Chemistry*, *41*(2), 282–293. https://doi.org/10.3906/kim-1604-61

Camarasa, J., Pubill, D., & Escubedo, E. (2006). *Association of caffeine to MDMA does not increase antinociception but potentiates adverse effects of this recreational drug*. *11*(2005). https://doi.org/10.1016/j.brainres.2006.06.087

Capaz, R. B. (2014). Carsten A. Ullrich—Time-Dependent Density-Functional Theory: Concepts and Applications. *Brazilian Journal of Physics*, *44*(2–3), 286–288. https://doi.org/10.1007/s13538-014-0182-1

Cappelletti, S., Daria, P., Sani, G., & Aromatario, M. (2014). Caffeine: Cognitive and Physical Performance Enhancer or Psychoactive Drug? *Current Neuropharmacology*, *13*(1), 71–88. https://doi.org/10.2174/1570159x13666141210215655

Catala, J. (2009). *Toward a Generalized Treatment of the Solvent Effect Based on Four Empirical Scales : Dipolarity (SdP , a New Scale), Polarizability (SP), Acidity (SA), and Basicity (SB) of the*. 5951–5960.

Chamma, A., & Viallet, P. (1970). Determination du moment dipolaire d'une molecule dans un etat excite singulet. *CR Acad Sci Paris Ser C*, *270*, 1901–1904.

Chaudhary, K. K., & Mishra, N. (2016). Central Bringing Excellence in Open Access OPEN ACCESS A Review on Molecular Docking: Novel Tool for Drug Discovery. *A Review on Molecular Docking: Novel Tool for Drug Discovery. JSM Chem*, *4*(3), 1029. www.pdb.org.

Chen, Z., Conell, G. K. M. C., Michell, B. J., Snow, R. J., Canny, B. J., Kemp, B. E., Mcconell, G. K., Mich-, B. J., Snow, R. J., Canny, B. J., & Bruce, E. (2024). *rapid communication*. 1202–1206.

Chirasani, V. R., Pasek, D. A., & Meissner, G. (2021). Structural and functional interactions between the Ca 2 + - , ATP- , and caffeine-binding sites of skeletal muscle ryanodine receptor (RyR1). *Journal of Biological Chemistry*, *297*(3), 101040. https://doi.org/10.1016/j.jbc.2021.101040

Christina Pires Gonçalves, L. (2021). Photophysical properties and therapeutic use of natural photosensitizers. *Journal of Photochemistry and Photobiology*, *7*(June), 100052. https://doi.org/10.1016/j.jpap.2021.100052

Cramer, C. J. (2004). Essentials of Computational Chemistry Theories and Models Second Edition. In *John Wiley & Sons Ltd*.

http://scholar.google.com/scholar?hl=en&btnG=Search&q=intitle:Essentials+of+computational+chemistry#0

Dahlén, A. D., Dashi, G., Maslov, I., Attwood, M. M., Jonsson, J., Trukhan, V., & Schiöth, H. B. (2022). Trends in Antidiabetic Drug Discovery: FDA Approved Drugs, New Drugs in Clinical Trials and Global Sales. *Frontiers in Pharmacology*, *12*(January), 1–16. https://doi.org/10.3389/fphar.2021.807548

Dastmalchi, S., Hamzeh-Mivehroud, M., & Sokouti, B. (2016). Methods and algorithms for molecular docking-based drug design and discovery. In *IGI Global: Vol. i*.

DeRocco, A. G. (1967). Modern Quantum Chemistry. In *American Journal of Physics* (Vol. 35, Issue 11, pp. 1097–1097). https://doi.org/10.1119/1.1973756

Design, D. (2023). *Metformin : A Review of Potential Mechanism and Metformin : A Review of Potential Mechanism and Therapeutic Utility Beyond Diabetes*. https://doi.org/10.2147/DDDT.S409373

Domecq, J. P., Prutsky, G., Leppin, A., Sonbol, M. B., Altayar, O., Undavalli, C., Wang, Z., Elraiyah, T., Brito, J. P., Mauck, K. F., Lababidi, M. H., Prokop, L. J., Asi, N., Wei, J., Fidahussein, S., Montori, V. M., & Murad, M. H. (2015). Drugs commonly associated with weight change: A systematic review and meta-analysis. *Journal of Clinical Endocrinology and Metabolism*, *100*(2), 363–370. https://doi.org/10.1210/jc.2014-3421

Du, Y., Zhu, Y. J., Zhou, Y. X., Ding, J., & Liu, J. Y. (2022). Metformin in therapeutic applications in human diseases : its mechanism of action and clinical study. *Molecular Biomedicine*. https://doi.org/10.1186/s43556-022-00108-w

Dutta, S., Shah, R. B., & Singhal, S. (2023). *Metformin : A Review of Potential Mechanism and Therapeutic Utility Beyond Diabetes*. *June*, 1907–1932.

Eberhardt, J., Santos-martins, D., Tillack, A. F., & Forli, S. (2021). *AutoDock Vina 1.2.0: New Docking Methods, Expanded Force Field, and Python Bindings*. https://doi.org/10.1021/acs.jcim.1c00203

Faber, M. S., & Fuhr, U. (2004). Time response of cytochrome P450 1A2 activity on cessation of heavy smoking. *Clinical Pharmacology and Therapeutics*, *76*(2), 178–184. https://doi.org/10.1016/j.clpt.2004.04.003

Facciolo, L., Canton, M., Vedaldi, D., Dall, F., & Biologica, C. (2004). *Photophysical and Phototoxic Properties of the Antibacterial Fluoroquinolones Levofloxacin and Moxifloxacin techniques , including analysis of erythrocytes lysis and cytotoxicity in mammalian cells . 1*, 782–801.

Fahmy, H. M., Kandel, H. M., Al-shamiri, H. A. S., Negm, N. A., Elwahy, A. H. M., & Abou Kana, M. T. H. (2018). Spectroscopic Study of Solvent Polarity on the Optical and Photo-Physical Properties of Novel 9,10-bis(coumarinyl)anthracene. *Journal of Fluorescence*, *28*(6), 1421–1430. https://doi.org/10.1007/s10895-018-2317-1

Ferreira, L. G., Dos Santos, R. N., Oliva, G., & Andricopulo, A. D. (2015). Molecular docking and structure-based drug design strategies. In *Molecules* (Vol. 20, Issue 7). https://doi.org/10.3390/molecules200713384

Ferrie, R. P., Hewitt, G. E., & Anderson, B. D. (2017). *A Fluorescence Quenching Analysis of the Binding of Fluoroquinolones to Humic Acid*. https://doi.org/10.1177/0003702817715655

Foretz, M., Guigas, B., & Viollet, B. (2023). *Metformin : update on mechanisms of action and repurposing potential*. *19*(August). https://doi.org/10.1038/s41574-023-00833-4

Fryer, L. G. D., Parbu-patel, A., & Carling, D. (2002). The Anti-diabetic Drugs Rosiglitazone and Metformin Stimulate AMP-activated Protein Kinase through Distinct Signaling Pathways *. *Journal of Biological Chemistry*, *277*(28), 25226–25232. https://doi.org/10.1074/jbc.M202489200

Galetin, A., Brouwer, K. L. R., Tweedie, D., & Yoshida, K. (2024). *Membrane Transporters in Drug Development and as Determinants of Precision Medicine*. *23*(4), 255–280. https://doi.org/10.1038/s41573-023-00877-1.Membrane

Gemta, A. B. (2015). *Determination of self - associated 5- caffeoylquinic acid and its complexation with sodium hydroxide using UV- Vis spectroscopy*. *February 2010*.

Gey, E. (1995). Density-Functional Theory of Atoms and Molecules. In *Zeitschrift für Physikalische Chemie* (Vol. 191, Issue 2, pp. 277–278). https://doi.org/10.1524/zpch.1995.191.part_2.277a

Graham, G. G., Punt, J., Arora, M., Day, R. O., Doogue, M. P., Duong, J. K., Furlong, T. J., Greenfield, J. R., Greenup, L. C., Kirkpatrick, C. M., Ray, J. E., Timmins, P., & Williams, K. M. (2011). *Clinical Pharmacokinetics of Metformin*. *50*(2), 81–98.

Gülseven Sidir, Y., & Sidir, I. (2013). Solvent effect on the absorption and fluorescence spectra of 7-acetoxy-6-(2,3-dibromopropyl)-4,8-dimethylcoumarin: Determination of ground and excited state dipole moments. *Spectrochimica Acta - Part A: Molecular and Biomolecular Spectroscopy*, *102*, 286–296. https://doi.org/10.1016/j.saa.2012.10.018

Gunasekaran, S., Sankari, G., & Ponnusamy, S. (2005). Vibrational spectral investigation on xanthine and its derivatives - Theophylline, caffeine and theobromine. *Spectrochimica Acta - Part A: Molecular and Biomolecular Spectroscopy*, *61*(1–2), 117–127.

https://doi.org/10.1016/j.saa.2004.03.030

Hardie, D. G. (2004). *The AMP-activated protein kinase pathway – new players upstream and downstream*. https://doi.org/10.1242/jcs.01540

Hassan Baig, M., Ahmad, K., Roy, S., Mohammad Ashraf, J., Adil, M., Haris Siddiqui, M., Khan, S., Amjad Kamal, M., Provazník, I., & Choi, I. (2016). Send Orders for Reprints to reprints@benthamscience.ae Computer Aided Drug Design: Success and Limitations. *Current Pharmaceutical Design*, *22*, 572–581.

Henderson, J. N., Hazra, S., Dunkle, A. M., Salvucci, M. E., & Wachter, R. M. (2013). *Biochimica et Biophysica Acta Biophysical characterization of higher plant Rubisco activase*. *1834*, 87–97.

Hohnholt, M. C., Blumrich, E. M., Waagepetersen, H. S., & Dringen, R. (2017). The antidiabetic drug metformin decreases mitochondrial respiration and tricarboxylic acid cycle activity in cultured primary rat astrocytes. *Journal of Neuroscience Research*, *95*(11), 2307–2320. https://doi.org/10.1002/jnr.24050

Horiuchi, T., Sakata, N., Narumi, Y., Kimura, T., Hayashi, T., & Nagano, K. (2017). Metformin directly binds the alarmin HMGB1 and inhibits its proinflammatory activity. *Journal of Biological Chemistry*, *292*(20), 8436–8446. https://doi.org/10.1074/jbc.M116.769380

Hospital, A., Goñi, J. R., Orozco, M., & Gelpí, J. L. (2015). *Molecular dynamics simulations : advances and applications Molecular dynamics simulations : advances and applications*. *6949*. https://doi.org/10.2147/AABC.S70333

Iwaloye, O., Olamide, P., Olawale, F., Oyewole, O., Olalekan, O., Kikiowo, B., Emmanuel, A., Nnaemeka, H., Femi, C., Mary, I., Elizabeth, A., Orimoloye, M., & Amos, S. (2023). Informatics in Medicine Unlocked Computer-aided drug design in anti-cancer drug discovery : What have we learnt and what is the way forward ? *Informatics in Medicine Unlocked*, *41*(August), 101332. https://doi.org/10.1016/j.imu.2023.101332

Judeh, A. A. B. U., Sarief, A., Umar, Y., Ashwaq, O., & Haque, S. K. M. (2020). NH H 3 C. *J. Chil. Chem. Soc.*, *3*, 1–5.

Kalita, K., Phukan, S. J., Garai, S., & Sankaranarayanan, K. (2024). *Polyoxometalates Mediated Amyloid Fibrillation Dynamics and Restoration of Enzyme Activity of Hen Egg White Lysozyme Treated under Cold Atmospheric Pressure Plasma*. https://doi.org/10.1021/acsomega.3c06921

Kalliokoski, A., & Niemi, M. (2009). *Impact of OATP transporters on pharmacokinetics*. *1*, 693–705. https://doi.org/10.1111/j.1476-5381.2009.00430.x

Kapetanovic, I. M. (2008). Computer-aided drug discovery and development (CADDD): In silico-chemico-biological approach. *Chemico-Biological Interactions*, *171*(2), 165–176. https://doi.org/10.1016/j.cbi.2006.12.006

Kless, A. (1996). Computational chemistry using the PC. In *Zeitschrift für Physikalische Chemie* (Vol. 193, Issues 1–2, pp. 222–222). https://doi.org/10.1524/zpch.1996.193.part_1_2.222

Kokiashvili, N., Alexishvili, M., Gonashvili, M., Okujava, N., Titvinidze, G., & Rukhadze, M. (2012). Colloids and Surfaces A : Physicochemical and Engineering Aspects Revealing of pharmacokinetic peculiarities of surface active drug promethazine in its interaction with caffeine in rabbits. *Colloids and Surfaces A: Physicochemical and Engineering Aspects*, *413*, 169–173. https://doi.org/10.1016/j.colsurfa.2011.12.061

Koppal, V. V, Melavanki, R. M., Kusanur, R. A., Bhavya, P., & Patil, N. R. (2018). A role of solvent polarity on bimolecular quenching reactions of 3-acetyl-7-(diethylamino)-2H-chromen-2-one in binary solvent mixtures. *Journal of Molecular Liquids*, *260*, 221–228.

Kramar, J. A. (2021). *Dynamic light scattering distributions by any means*.

Krawczyk, P., Bratkowska, M., Wybranowski, T., Hołyńska-Iwan, I., Cysewski, P., & Jędrzejewska, B. (2020). Experimental and theoretical insight into spectroscopic properties and bioactivity of 4-(4-formylbenzylidene)-2-phenyloxazol-5(4H)-one dye for future applications in biochemistry. *Journal of Molecular Liquids*, *314*, 113632. https://doi.org/10.1016/j.molliq.2020.113632

Kumar, I., Kant, S., Singh, D., Kumar, P., & Ahir, P. (2024). *Volumetric , ultrasonic , conductometric and UV – visible analysis of molecular interactions between metformin hydrochloride and dulcitol in aqueous solutions Metformin Hydrochloride Dulcitol*. *396*(January).

Kwon, M., Jeon, J., Choi, M., & Song, I. (2020). *The Development and Validation of a Novel " Dual Cocktail " Probe for Cytochrome P450s and Transporter Functions to Evaluate Pharmacokinetic Drug-Drug and Herb-Drug Interactions*.

Lakowicz, J. R. (2000). Principles of Fluorescence Spectroscopy, Second ed. Joseph R. Lakowicz. In *Center for Fluorescence Spectroscopy* (3rd ed., Vol. 287, Issue 2). springer. https://doi.org/10.1006/abio.2000.4850

Lakowicz, J. R. (2006). Principles of fluorescence spectroscopy. In *Principles of Fluorescence Spectroscopy* (pp. 1–954). https://doi.org/10.1007/978-0-387-46312-4

Lakowicz, J. R. (2014). *Principles of Fluorescence Spectroscopy Third Edition*. *June*. https://doi.org/10.1007/978-0-387-46312-4

Lippert, E. (1955). Dipolmoment und Elektronenstruktur von angeregten Molekülen. *Zeitschrift Fur Naturforschung - Section A Journal of Physical Sciences*, *10*(7), 541–545. https://doi.org/10.1515/zna-1955-0707

Liptay, W. (1969). Electrochromism and solvatochromism. *Angewandte Chemie International Edition in English*, *8*(3), 177–188.

Madiraju, A. K., Erion, D. M., Rahimi, Y., Zhang, X. M., Braddock, D. T., Albright, R. A., Prigaro, B. J., Wood, J. L., Bhanot, S., MacDonald, M. J., Jurczak, M. J., Camporez, J. P., Lee, H. Y., Cline, G. W., Samuel, V. T., Kibbey, R. G., & Shulman, G. I. (2014). Metformin suppresses gluconeogenesis by inhibiting mitochondrial glycerophosphate dehydrogenase. *Nature*, *510*(7506), 542–546. https://doi.org/10.1038/nature13270

Mani, S., Supriya, T., Shankar, M., Kavya Lalitha, S., Dastgiri, J., & Niranjan Babu, M. (2016). a Over View on Molecular Docking American Journal of Biological and Pharmaceutical Research a Over View on Molecular Docking. *American Journal of Biological and Pharmaceutical Research*, *3*(2), 83–89. www.mcmed.us/journal/ajbpr

Manning, G. (2012). *The Protein Kinase Complement of the Human Genome*. *1912*(2002). https://doi.org/10.1126/science.1075762

Marcinek, K., Luzak, B., & Rozalski, M. (2024). The Effects of Caffeine on Blood Platelets and the Cardiovascular System through Adenosine Receptors. *International Journal of Molecular Sciences*, *25*(16). https://doi.org/10.3390/ijms25168905

Marsin, A., Bertrand, L., Rider, M. H., Deprez, J., Beauloye, C., Vincent, M. F., Berghe, G. Van Den, Carling, D., & Hue, L. (n.d.). *Phosphorylation and activation of heart PFK-2 by AMPK has a role in the stimulation of glycolysis during ischaemia*. 1247–1255.

May, M., & Schindler, C. (2016). Clinically and pharmacologically relevant interactions of antidiabetic drugs. *Therapeutic Advances in Endocrinology and Metabolism*, *7*(2), 69–83. https://doi.org/10.1177/2042018816638050

Meeting, I., Centre, P., Dundee, D. G. H., & Carling, D. (2003). *AMPK 2002 – 2nd International Meeting on AMP-activated Protein Kinase*. 162–168.

Melle, S., Calderón, O. G., Laurenti, M., Mendez-gonzalez, D., Egatz-, A., Lopez-cabarcos, E., Cabrera-granado, E., Diaz, E., Rubio-retama, J., Laurenti, M., Mendez-gonzalez, D., & Enrique, L. (2018). *FRET Distance Dependence from Upconverting Nanoparticles to Quantum Dots*. https://doi.org/10.1021/acs.jpcc.8b04908

Meneses, M. J., Silva, B. M., Sousa, M., Sá, R., Oliveira, P. F., & Alves, M. G. (2015). Send Orders for Reprints to reprints@benthamscience.ae Antidiabetic Drugs: Mechanisms of Action and Potential Outcomes on Cellular Metabolism. *Current Pharmaceutical Design*,

21, 3606–3620.

Milonni, P. W., & Eberly, J. H. (2010). *Laser physics*. John Wiley & Sons.

Miotke, M. M., & Józefowicz, M. (2017). *Solvatochromism of antiinflammatory drug – naproxen sodium*. *230*, 129–136.

Mohamed, N., Maideen, P., Jumale, A., & Balasubramaniam, R. (2017). Drug Interactions of Metformin Involving Drug Transporter Proteins. *Tabriz University of Medical Sciences*, *7*(4), 501–505. https://doi.org/10.15171/apb.2017.062

Mohd, A., Aslam, A., Khan, P., Bano, S., & Siddiqi, K. S. (2010). *Interaction and fluorescence quenching study of levofloxacin with divalent toxic metal ions*. *5*(2), 177–186.

Mokashi, V. V., Walekar, L. S., Anbhule, P. V., Lee, S. H., Patil, S. R., & Kolekar, G. B. (2014). Study of energy transfer between riboflavin (vitamin B2) and AgNPs. *Journal of Nanoparticle Research*, *16*(3), 2291. https://doi.org/10.1007/s11051-014-2291-8

Mrkalić, E., Jelić, R., Stojanović, S., & Sovrlić, M. (2021). Interaction between olanzapine and human serum albumin and effect of metal ions, caffeine and flavonoids on the binding: A spectroscopic study. *Spectrochimica Acta - Part A: Molecular and Biomolecular Spectroscopy*, *249*, 119295. https://doi.org/10.1016/j.saa.2020.119295

Mumin, A., Akhter, K. F., Abedin, Z., & Hossain, Z. (2014). *Determination and Characterization of Caffeine in Tea , Coffee and Soft Drinks by Solid Phase Extraction and High Performance Liquid Chromatography (SPE - Determination and Characterization of Caffeine in Tea , Coffee and Soft Drinks by Solid Phase Extraction and High Performance Liquid Chromatography (SPE – HPLC)*. *October*.

Nad, S., & Pal, H. (2001). Unusual Photophysical Properties of Coumarin-151. *Journal of Physical Chemistry A*, *105*(7), 1097–1106. https://doi.org/10.1021/jp003157m

Nagy, Á. (1998). Density functional. Theory and application to atoms and molecules. *Physics Report*, *298*(1), 1–79. https://doi.org/10.1016/S0370-1573(97)00083-5

Nigam, S., & Rutan, S. (2001). Principles and Principles and. *Applied Spectroscopy*, *55*(11), 362A.

Nivatya, H. K., Singh, A., Kumar, N., Sharma, L., Singh, V., & Mishra, R. (2025). *Assessing molecular docking tools : understanding drug discovery and design*.

Onyeachu, I. B., Abdel-azeim, S., Chauhan, D. S., & Quraishi, M. A. (2021). *Electrochemical and Computational Insights on the Application of Expired Metformin Drug as a Novel Inhibitor for the Sweet Corrosion of C1018 Steel*.

https://doi.org/10.1021/acsomega.0c03364

Oyola, R., Pin, L. E., Arce, R., & Silva, J. (2005). *Substitution and Solvent Effects on the Photophysical Properties of Several Series of 10-Alkylated Phenothiazine Derivatives Carmelo Garcı*. 3360–3371.

Painagoni, K. M., & Patil, H. D. (2013). Estimation of Ground and Excited State Dipole Moments of Some Laser Dyes. *Journal of Engineering Research and Applications Www.Ijera.Com*, *3*, 641–647. www.ijera.com

Panja, S. K. (2021). Dipolar state assisted aggregation induced optical behavior of push-pull Salen-type Schiff base (BIHyDE) in solution. *Journal of Molecular Structure*, *1234*, 130140. https://doi.org/10.1016/j.molstruc.2021.130140

Park, S. H., Gammon, S. R., Knippers, J. D., Paulsen, S. R., Rubink, D. S., Winder, W. W., Rubink, D. S., & Phosphoryla-, W. W. W. (2024). *Phosphorylation-activity relationships of AMPK and acetyl-CoA carboxylase in muscle*. *84602*, 2475–2482.

Patil A, N. R., Melavanki B, R. M., Chougala C, B. M., Shastri C And, L. A., & Sanningannavar, F. M. (2012). *Analysis of Two Fluorescent Molecules Properties Using Solvatochromic Shift Method*. *March 2017*.

Patil, V., Padalkar, V. S., Sekar, N., Patil, S. V., & Rajput, J. (2019). Synthesis of 2-methyl-5-(5-phenyl substituted-1,3,4 oxadiazole-2-yl) quinazolin-4-one fluorescent brightening agent: Computational and experimental comparison of photophysical structure. *Journal of Molecular Structure*, *1182*, 150–157. https://doi.org/10.1016/j.molstruc.2019.01.039

Polekhina, G., Gupta, A., Denderen, B. J. W. Van, Feil, S. C., Kemp, B. E., Stapleton, D., & Parker, M. W. (2005). *Structural Basis for Glycogen Recognition by AMP-Activated Protein Kinase*. *13*, 1453–1462. https://doi.org/10.1016/j.str.2005.07.008

Polyakova, E. B., Sabirzyanov, D. R., Prozorova, N. A., & Foteeva, A. V. (2022). *PHYSICOCHEMICAL PROPERTIES AND METHODS OF ANALYSIS OF VILDAGLIPTIN (REVIEW)*. *56*(1), 110–117. https://doi.org/10.1007/s11094-022-02606-1

Popovi, D. J. Ć., Laloševi, D. Ć., Miljkovi, D. Ć., Popovi, K. J. Ć., Apo, I. Č., & Popovi, J. K. Ć. (2018). *Caffeine induces metformin anticancer effect on fibrosarcoma in hamsters*. 2461–2467.

Ravi, M., Soujanya, T., Samanta, A., & Radhakrishnan, T. P. (1995). Excited-state dipole moments of some Coumarin dyes from a solvatochromic method using the solvent polarity parameter, E. *Journal of the Chemical Society, Faraday Transactions*, *91*(17), 2739–2742. https://doi.org/10.1039/FT9959102739

Reddy, V. S., Shiva, S., Manikantan, S., & Ramakrishna, S. (2024). Pharmacology of caffeine and its effects on the human body. *European Journal of Medicinal Chemistry Reports*, *10*(December 2023), 100138. https://doi.org/10.1016/j.ejmcr.2024.100138

Reichardt, C. (1994). Solvatochromic dyes as solvent polarity indicators. *Chemical Reviews*, *94*(8), 2319–2358. https://doi.org/10.1021/cr00032a005

Rena, G., Pearson, E. R., & Sakamoto, K. (2013). Molecular mechanism of action of metformin: Old or new insights? *Diabetologia*, *56*(9), 1898–1906. https://doi.org/10.1007/s00125-013-2991-0

Renfrew, A. K. (2014). Transition metal complexes with bioactive ligands: Mechanisms for selective ligand release and applications for drug delivery. *Metallomics*, *6*(8), 1324–1335. https://doi.org/10.1039/c4mt00069b

Sadigh, M. K., Zakerhamidi, M. S., Ahmadian, S. M. S., Johari-ahar, M., & Haghighi, L. Z. (2016). *Environment and solute-solvent interaction effects on photo-physical behaviors of Folic acid and Folinic acid drugs*. *1125*, 177–185.

Sahoo, S., Chakraborti, C. K., Behera, P. K., & Mishra, S. C. (2012). FTIR and Raman spectroscopic investigations of a norfloxacin/carbopol934 polymeric suspension. *Journal of Young Pharmacists*, *4*(3), 138–145. https://doi.org/10.4103/0975-1483.100017

Sánchez-lara, E., Treviño, S., Sánchez-gaytán, B. L., Sánchez-mora, E., Castro, M. E., Meléndez-bustamante, F. J., Méndez-rojas, M. A., & González-vergara, E. (2018). *Decavanadate Salts of Cytosine and Metformin : A Combined Experimental-Theoretical Study of Potential Metallodrugs Against Diabetes and Cancer*. *6*(October), 1–18. https://doi.org/10.3389/fchem.2018.00402

Sauer, M., Hofkens, J., & Enderlein, J. (2011). *Basic Principles of Fluorescence Spectroscopy Handbook of Fluorescence Spectroscopy and Imaging*. WILEY-VCH Verlag GmbH & Co. KGaA, Boschstr. 12, 69469 Weinheim, Germany.

Sayantan Mondal, Rudra N. Samajdar, Saumyak Mukherjee, A. J. B. and, & Bagchi*, B. (2018). Unique Features of Metformin : A Combined Experimental , Theoretical and Simulation Study of its Structure , Dynamics and Interaction Energetics with DNA Grooves. *The Journal of Physical Chemistry*. https://doi.org/10.1021/acs.jpcb.7b11928

Setiawan, D., Kazaryan, A., Martoprawiro, M. A., & Filatov, M. (2010). A first principles study of fluorescence quenching in rhodamine B dimers: How can quenching occur in dimeric species? *Physical Chemistry Chemical Physics*, *12*(37), 11238–11244. https://doi.org/10.1039/c004573j

Sherefedin, U., Belay, A., Gudishe, K., Kebede, A., & Getahun, A. (2025). Photophysical

Properties of Sinapic Acid and Ferulic Acid and Their Binding Mechanism with Caffeine. *Journal of Fluorescence*, *35*(4), 2379–2393. https://doi.org/10.1007/s10895-024-03689-7

Sherefedin, U., Belay, A., Kebede, A., Asemare, S., Woldegiorges, K., Kumela, A. G., & Gudishe, K. (2023). *Determination of the ground and excited state dipole moments of ferulic and sinapic acids by solvatochromic effects and density function theory method*. https://doi.org/10.1063/5.0160608

Shi, X., Xue, W., Liang, S., Zhao, J., & Zhang, X. (2016). Acute caffeine ingestion reduces insulin sensitivity in healthy subjects: a systematic review and meta-analysis. *Nutrition Journal*, *15*(1), 1–8. https://doi.org/10.1186/s12937-016-0220-7

Sina, A., Masoomeh, S., & Dehghan;Gholamreza. (2021). *RESEARCH ARTICLE A rapid , simple and ultrasensitive spectrofluorimetric method for the direct detection of metformin in real samples based on a nanoquenching approach*. *October 2020*, 658–667. https://doi.org/10.1002/bio.3982

Sıdır, Y. G. (2015). *Spectrochimica Acta Part A : Molecular and Biomolecular Spectroscopy Estimation of ground and excited state dipole moments of Oil Red O by solvatochromic shift methods*. *135*, 560–567. https://doi.org/10.1016/j.saa.2014.07.049

Skoromnik, O. D., Feranchuk, I. D., Leonau, A. U., & Keitel, C. H. (2017). Analytic model of a multi-electron atom. *Journal of Physics B: Atomic, Molecular and Optical Physics*, *50*(24), 1–11. https://doi.org/10.1088/1361-6455/aa92e6

Sliwoski, G., Kothiwale, S., Meiler, J., & Lowe, E. W. (2014). Computational methods in drug discovery. *Pharmacological Reviews*, *66*(1), 334–395. https://doi.org/10.1124/pr.112.007336

Šola, I., & Vujˇ, V. (2024). *Phytochemical Composition and Functional Properties of Brassicaceae Microgreens : Impact of In Vitro Digestion*.

Somogyi, A., & Muirhead, M. (1987). *Pharmacokinetic Interactions of Cimetidine 1987*. *366*, 321–366.

Song, Y., Zhu, S., Xiang, S., Zhao, X., Zhang, J., Zhang, H., Fu, Y., & Yang, B. (2014). *Investigation into the fluorescence quenching behaviors and applications of carbon dots †*. https://doi.org/10.1039/c4nr00029c

Sousa, S. F., Ribeiro, A. J. M., Coimbra, J. T. S., Neves, R. P. P., Martins, S. A., Moorthy, N. S. H. N., Fernandes, P. A., & Ramos, M. J. (2013). Protein-Ligand Docking in the New Millennium – A Retrospective of 10 Years in the Field. *Current Medicinal Chemistry*, *20*(18), 2296–2314. https://doi.org/10.2174/0929867311320180002

Strickler, S. J., & Berg, R. A. (1962). Relationship between absorption intensity and fluorescence lifetime of molecules. *The Journal of Chemical Physics*, *37*(4), 814–822. https://doi.org/10.1063/1.1733166

Suhina, T. (2017). *Fluorescent molecular rotors From working principles to visualization of mechanical contacts*.

Suman Mallick, Kaushik Pal, F. C. and A. L. K. (2016). Photophysical and Acid-Base Properties of an Antimalaria Drug Quinine. *Physical Chemistry Chemical Physics*. https://doi.org/10.1039/C6CP04931A

Tanwir, A., Jahan, R., Quadir, M. A., Kaisar, M. A., & Hossain, K. (2012). *Spectroscopic Studies of the Interaction between Metformin Hydrochloride and Bovine Serum Albumin*. *88029661900*(1), 45–49.

Taylor, P., Rahnama, E., Mahmoodian-moghaddam, M., Khorsand-ahmadi, S., Saberi, R., & Chamani, J. (2014). *Binding site identification of metformin to human serum albumin and glycated human serum albumin by spectroscopic and molecular modeling techniques : a comparison study*. *October*, 37–41. https://doi.org/10.1080/07391102.2014.893540

Thomas J. Hitchings, a School Project Students, b Angela Shepherd, b M. A., *a, a and P. J. S., & Received. (2025). *As featured in :* https://doi.org/10.1039/d5ce00711a

Thorn, C. F., Aklillu, E., McDonagh, E. M., Klein, T. E., & Altman, R. B. (2012). PharmGKB summary: Caffeine pathway. *Pharmacogenetics and Genomics*, *22*(5), 389–395. https://doi.org/10.1097/FPC.0b013e3283505d5e

Thorne, A. P. (1988). Laser spectroscopy. In *Spectrophysics* (pp. 202–226). Springer.

Trott, O., & Olson, A. J. (2009). *Software News and Update AutoDock Vina : Improving the Speed and Accuracy of Docking with a New Scoring Function , Efficient Optimization , and Multithreading*. https://doi.org/10.1002/jcc

Truong, J., Abu-Suriya, N., Tory, D., Bahho, R., Ismaiel, A., Nguyen, T., Mansour, A., Nand, V., Saponja, J., Dua, K., De Rubis, G., & Parisi, D. (2025). An Exploration of the Interplay Between Caffeine and Antidepressants Through the Lens of Pharmacokinetics and Pharmacodynamics. *European Journal of Drug Metabolism and Pharmacokinetics*, *50*(1), 1–15. https://doi.org/10.1007/s13318-024-00928-x

Ullah, N., Amin, A., Alamoudi, R. A., Rasheed, S. A., Alamoudi, R. A., Nawaz, A., Raza, M., Nawaz, T., Ishtiaq, S., & Abbas, S. S. (2022). *Fabrication and Optimization of Essential-Oil-Loaded Nanoemulsion Using Box – Behnken Design against Staphylococos aureus and Staphylococos epidermidis Isolated from Oral Cavity*.

Valeur, B. (2003). Absorption of UV–Visible Light. *Molecular Fluorescence*, *8*, 20–33. https://doi.org/10.1002/3527600248.ch2

Viola, G., Salvador, A., Cecconet, L., Basso, G., Vedaldi, D., Dall'Acqua, F., Aloisi, G. G., Amelia, M., Barbafina, A., Latterini, L., & Elisei, F. (2007). Photophysical properties and photobiological behavior of amodiaquine, primaquine and chloroquine. *Photochemistry and Photobiology*, *83*(6), 1415–1427. https://doi.org/10.1111/j.1751-1097.2007.00181.x

Weiser, T., & Weigmann, H. (2019). Effect of Caffeine on the Bioavailability and Pharmacokinetics of an Acetylsalicylic Acid-Paracetamol Combination: Results of a Phase I Study. *Advances in Therapy*, *36*(3), 597–607. https://doi.org/10.1007/s12325-019-0891-5

Welton, C. R. and T. (2011). *Solvents and Solvent Effects in Organic Chemistry* (C. R. and T. Welton (ed.); 4th ed.). WILEY-VCH Verlag GmbH & Co. KGaA, Weinheim.

Welton, T. (2011). *Christian Reichardt and Thomas Welton Solvents and Solvent Effects in Organic Chemistry* (C. R. and T. Welton (ed.); 4th ed.). WILEY-VCH Verlag GmbH & Co. KGaA, Weinheim.

Woldegiorges, K., Belay, A., & Kebede, A. (2022). Photophysical properties of levofloxacin and norfloxacin drugs and their fluorescence quenching mechanism with caffeine. *Spectroscopy Letters*, *55*(8), 500–513. https://doi.org/10.1080/00387010.2022.2110596

Woldegiorges, K., Belay, A., Kebede, A., & Abebe, T. (2021). Estimating the Ground and Excited State Dipole Moments of Levofloxacin and Norfloxacin Drugs Using Solvatochromic Effects and Computational Work. *Journal of Spectroscopy*, *2021*. https://doi.org/10.1155/2021/7214182

Wu, Z., Chen, S., Wang, Y., Li, F., & Xu, H. (2023). *Current perspectives and trend of computer-aided drug design : a review and bibliometric analysis*.

Xi, X., Han, J., & Zhang, J. (2001). Stimulation of Glucose Transport by AMP-activated Protein Kinase via Activation of p38 Mitogen-activated Protein Kinase *. *Journal of Biological Chemistry*, *276*(44), 41029–41034. https://doi.org/10.1074/jbc.M102824200

Yartsev, A., & Peisah, C. (2021). Caffeine-clozapine interaction associated with severe toxicity and multiorgan system failure: a case report. *BMC Psychiatry*, *21*(1), 1–5. https://doi.org/10.1186/s12888-021-03199-x

Zhou, G., Myers, R., Li, Y., Chen, Y., Shen, X., Fenyk-Melody, J., Wu, M., Ventre, J., Doebber, T., Fujii, N., Musi, N., Hirshman, M. F., Goodyear, L. J., & Moller, D. E. (2001). Role of AMP-activated protein kinase in mechanism of metformin action. *Journal of Clinical Investigation*, *108*(8), 1167–1174. https://doi.org/10.1172/JCI13505

Zhou, S., Lv, P., Li, M., Chen, Z., Xin, H., Reilly, S., & Zhang, X. (2023). SARS-CoV-2 E protein: Pathogenesis and potential therapeutic development. *Biomedicine and Pharmacotherapy*, *159*(October 2022), 114242. https://doi.org/10.1016/j.biopha.2023.114242

Appendix: Declaration

I hereby declare that this PhD Dissertation is my original work and has not been presented for a degree from any other university, and all sources of material used for this dissertation have been duly acknowledged.

Name: Semahegn Asemare Bitew

Signature: _____

This PhD dissertation has been submitted for examination with my approval.

Supervisor.

Name: _____

Signature: _____

Date of submission